EPSC2017

TP4 abstracts

EPSC Abstracts
Vol. 11, EPSC2017-40, 2017
European Planetary Science Congress 2017

Limitation on the height of the highest mountain of Mars and the Earth

C. X. Chen
CAS Key Laboratory of Geospace Environment, Department of Geophysics and Planetary Sciences, School of Earth and Space Sciences, University of Science and Technology of China, Hefei, Anhui, China (chuxin@ustc.edu.cn)

Abstract

Mars Global Surveyor did precise topographic survey using the laser and drawn the Mars' topographic map which use Mars geoid (Areoid) as a benchmark. The study found that the highest point is on Mount Olympus (21,229 meter). In addition, other volcanoes on Mars are also much higher than the highest mountain on the Earth. The radius of Mars is half of that of Earth, the volume and mass of Mars are much smaller than those of Earth. To explain the reason why the height of Olympus is much higher than that of the Everest, we set up a stress model of a mountain. We find the main factor that affects the highest mountains' height is the gravitational acceleration. The depth of the deepest trench on the Earth is also estimated using the same method.

EPSC Abstracts
Vol. 11, EPSC2017-99, 2017
European Planetary Science Congress 2017

Mars Trek: An Interactive Web Portal for Current and Future Missions to Mars

E. Law (1), B. Day (2)
(1) Jet Propulsion Laboratory, California Institute of Technology. M/S 168-200. 4800 Oak Grove Dr. Pasadena, CA, USA 91109. (Emily.S.Law@jpl.nasa.gov, +01-818-354-6208)
(2) NASA Solar System Exploration Research Virtual Institute. NASA Ames Research Center. M/S 17-1. Moffett Field, CA, USA. 94035. (Brian.H.Day@nasa.gov, +01-650-604-2605

Abstract

NASA's Mars Trek (https://marstrek.jpl.nasa.gov) provides a web-based Portal and a suite of interactive visualization and analysis tools to enable mission planners, lunar scientists, and engineers to access mapped data products from past and current missions to Mars. During the past year, the capabilities and data served by Mars Trek have been significantly expanded beyond its original design as a public outreach tool. At the request of NASA's Science Mission Directorate and Human Exploration Operations Mission Directorate, Mars Trek's technology and capabilities are now being extended to support site selection and analysis activities for the first human missions to Mars.

1. Introduction

This presentation will provide an overview of the uses and capabilities of NASA's Mars Trek online mapping and modeling portal, a web based suite of data visualization and analysis tools designed to support mission planning, scientific research, and education/outreach.

2. A Comprehensive Online Web Portal

Mars Trek integrates a suite of interactive tools incorporating observations from past and current missions. The online web portal allows anyone with access to a computer to search through and view a vast number of coregistered images and other digital products. As a web-based application, Mars Trek does not require users to purchase or install any software beyond current web browsers. The portal provides easy-to-use tools for browsing, data layering, and feature search. Current tools include distance measurement, elevation profiling, and calculating Sun angles. Data sets include photographic, spectrometric, mineralogy, thermal, and landform data, as well as DEMs generated from stereo imagery and laser altimetry.

Originally released in June, 2015 as a public outreach tool, Mars Trek is currently being enhanced to support site selection and analysis for upcoming human and robotic missions to Mars. Many new data products are being added, with emphasis on providing detailed information for proposed exploration zones. New tools will include lighting analysis, slope mapping, crater detection, boulder detection, and traverse planning. Users will be able to download data products from Mars Trek and access metadata for each product. Web services and APIs will allow other clients to access data from Mars Trek's servers. A new interface for Mars Trek will provide consistency with the range of NASA Trek platforms including portals for the Moon, Vesta, Phobos, and more. This interface provides for advanced 3D visualization and navigation. Standard keyboard gaming controls allow the user to maneuver a first-person visualization of "flying" across the surface of the Moon. User-specified bounding boxes can be used to generate STL and/or OBJ files to create physical models of surface features with 3D printers.

Mars Trek is also a powerful tool for education and outreach, as is exemplified by its being designated as key supporting infrastructure for NASA Science Mission Directorate's STEM Activation Initiative, and its serving of data to a growing community of digital planetariums.

As private industry and space agencies of a growing number of nations plan new missions to Mars, detailed maps and models of Mars' surface and climate will be essential for mission planning. Mars Trek's generalized suite of tools are being designed to meet the needs of this new generation of missions.

The portal will also provide an outstanding means of dissemination of data from these missions. Layering and blending many different data products and putting individual products in the context of many others will facilitate mining of information going far beyond what individual products can provide separately. In addition to mission planning and planetary science, Mars Trek will continue supporting the essential task of engaging the public in this great adventure.

Mars Trek is developed at NASA's Jet Propulsion Laboratory (JPL) and managed as a project of NASA's Solar System Exploration Research Virtual Institute (SSERVI) at NASA Ames Research Center.

3. Extension to Phobos

At the request of the Planetary Science Division of NASA's Science Mission Directorate, we are extending the technologies of our existing Trek platforms to create a new portal for Mars' largest moon, Phobos. In this effort, we are working with the International Phobos/Deimos Landing Site Working Group and with JAXA, with JAXA's MMX mission as a primary driver.

4. Summary and Conclusions

Mars Trek's new features make it especially useful for the planning of a new generation of Mars exploration missions, conducting a wide range of Mars planetary science research, and facilitating exciting visualizations and exploration in the realms of education and outreach. The user community is invited to provide suggestions and requests as the development team continues to expand the capabilities of Mars Trek, its related products, and the range of data and tools that it provides. As the EPSC community looks forward to a new generation of surface and orbital robotic activities at Mars, as well as preparation for the first human missions to Mars, tools such as Mars Trek will become increasingly essential.

Acknowledgements

The authors would like to thank the Planetary Science Division of NASA's Science Mission Directorate and the Advanced Explorations Systems Program of NASA's Human Exploration Operations Directorate and for their support and guidance in the development of Moon Trek.

EPSC Abstracts
Vol. 11, EPSC2017-107-1, 2017
European Planetary Science Congress 2017

Kilometer-sized cones on Mars: igneous or mud volcanoes?

P. Brož (1), P. Fawdon (2,3), and O. Čadek (4)
(1) Institute of Geophysics of the Czech Academy of Science (**Petr.broz@ig.cas.cz**), (2) Birkbeck, University of London, Malet St, London WC1E 7HX, (3) Open University, Milton Keynes MK7 6AA, United Kingdom (4) Faculty of Mathematics and Physics, Department of Geophysics, Charles University in Prague, Czech Republic.

Abstract

Here we present our project about the investigation of kilometer-sized cones on Mars in the attempt to reveal if such cones had been formed by igneous or mud volcanoes based on detailed investigation of their morphometries, morphologies, and spatial distributions.

1. Introduction

There is an ongoing debate within scientific community about the formation process of kilometer-sized cones reported from several regions on Mars (e.g., [1-8]). Two of the main mechanisms considered as possible explanations, are (1) small scale igneous volcanism (e.g., [1,4-7]) and (2) mud volcanism (e.g., [2,8,10]). It is important to differentiate between these two processes because of the very different implications these processes have for the Martian crust and near surface environment. Both processes involve key factors of environmental habitability meaning that understanding the origin of these features is important in our understanding of recent habitability of Mars.

On Earth small volcanoes and mud volcanism form of morphologically similar landforms (Fig. 1). Both processes form cones with relatively steep flanks and central craters on their tops; often additionally associated with flow-like units spreading around those cones. Consequently, because of this convergence of form, is not readily apparent how to distinguish between these two processes using satellite images. As a consequence, on Mars (Fig. 2) both processes (e.g, [2] vs. [7], [8] vs. [9]) have been invoked to explain the observed cones and this introduces an element of ambiguity where the geological context dose not substantially favours only one process over the other. However, examples exist with a clear geological setting indicating a parsimonious explanation. Two examples of this are the cones on the flanks of Pavonis Mons [1] and at Ulysses Colles which is situated on heavily fractured crust inside the Tharsis. In these contexts, the cones are interpreted to be parasitic igneous volcanoes and a field of volcanic scoria cones [6, 9] respectively. Here these interpretations are possible because of the dominantly volcano-tectonic setting and lack of large centre of sedimentary deposition, necessary for mud volcanism.

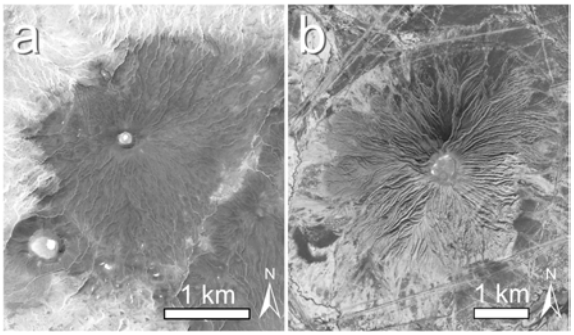

Figure 1: An example of terrestrial igneous (a) and mud (b) volcano showing striking similarities in their morphologies. (a) Volcano in Libya (centered 17.30°E , 26.142°N, © CNES/SPOT) (b) Mud volcano in Azerbaijan (centereted 49.29°E, 40.163°N, © ImageGlobe). Images obtained from GoogleEarth™.

2. Project aim

The aim of this study is compare the morphologies and morphometries of Martian putative scoria cones and mud volcanoes to explore differences and/or similarities in their shapes and hence to investigate if we can distinguee between causal mechanisms. This work builds on the work done by [7] by investigating an additional cone field in Chryse Planitia where the putative mud volcanoes have previously been described [9]. To do this we use topographic data derived from HiRISE (~30 cm/pixel, [12]) and CTX (5–6 m/pixel; [13]) stereo images. New high-resolution DEM were computed for 8 HiRISE stereo pairs (Fig. 2) using the methods described in [14]. From these several basic morphometrical parameters are measured for each cone, including the average,

the maximum slope of the cone's flanks and delineation of the volcano shape. This is done in plan view by numerical tracing where the slope exceeds 1°, following the method used in [9]. To analyse the spatial distribution of these edifices, we applied the Poisson Nearest Neighbor (PNN) analysis in similar way as applied in [15].

3. Preliminary results

We previously showed [9] that cones within three regions of different geological context (Ulysses Colles, Hydraotes Colles and the Coprates cones) show striking similarities in their morphologies. However the minor differences that are seen in their morphometries can be explained by variations in atmospheric pressure and gravity between the two fields. The shape of the cones can be reconstructed numerically by tracking the ballistic trajectories of ejected particles and recording the cumulative deposition of repeatedly ejected particles using this method concluded [9] that these cones represent small-scale igneous volcanoes, i.e. scoria cones.

When we compared cones from Chryse Planitia with those previously investigated cones, we found that although the edifices show some similarities in shapes, investigation of their morphologies and morphometries together show a number of important variations. While cones attributed as putative Martian scoria cones are often clustered, have multiple central craters, are superposed on elevated flow-like units and variations in their shapes can be explained by simple numerical model, the putative mud volcanoes are characteristic by freestanding edifices with one central crater (if even present) which may be breached. If so the breached section covered a substantial portion of the craters circumference. Putative mud volcanoes also show a wide variety in shapes (three different types) within the field suggesting a more complex scenario for their formation more susceptible to environmental conditions.

Therefore, our preliminary results suggest previous notion by [10] that cones in Chryse Planitia may represent Martian mud volcanoes as these cones actually show much wider variations in their general shapes, distributions and appearance than those investigated by [9] which have been interpreted as Martian putative scoria cones.

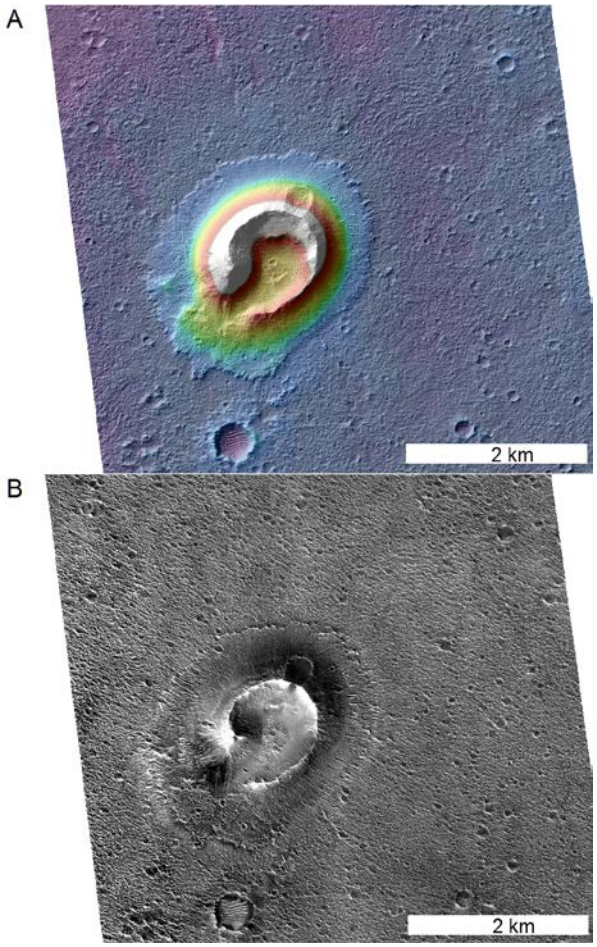

Figure 2: A comparison between (A) a HiRISE DTM overlain on a hillshade model and (B) the HiRSE image of the same cone in Chryse Planitia. This shows the detail available for the morphometric analysis.

References

[1] Bleacher et al., 2007, JGR 112 [2] Skinner and Tanaka, 2007, Icarus 186 [3] Harrison and Chapman, 2008, Icarus 198 [4] Meresse et al., 2008, Icarus 194 [5] Lanz et al., 2010, JGR 115, E12019 [6] Brož and Hauber, 2012, Icarus 218 [7] Brož and Hauber, 2013, JGR 118 [8] Okubo, 2016, Icarus 269 [9] Brož et al., 2015, JGR 120 [10] Komatsu et al., 2016, Icarus 268 [11] Brož et al., EPSL, under review (2017) [12] McEwen et al., 2007, JGR 112, E05S02 [13] Malin et al., 2007, JGR 112, E05S04 [14] Moratto et al. (2010), LPSC, XLI, Abstract #2364 [15] Corvec et al., 2013, Earth-Science Reviews, 124.

EPSC Abstracts
Vol. 11, EPSC2017-118-5, 2017
European Planetary Science Congress 2017

Mars Express Science Ground Segment overview: A study about the mission's evolution, new challenges and future perspectives

J. Marín-Yaseli de la Parra, A. Cardesín Moinelo, D. Merritt, M. Breitfellner, M. Castillo, E. Grotheer, D. Titov and P. Martin,
ESA European Space Astronomy Centre (ESAC), Camino bajo del Castillo s/n, Urb. Villafranca del Castillo, P.O. Box 78, 28691 Villanueva de la Cañada, Madrid, Spain (jmarin@sciops.esa.int / T: +34-91-8131577)

Abstract

We present an overview of more than 13 years of mission operations from the perspective of the Science Ground Segment (SGS), including the evolution of the mission planning system and summarizing the new challenges ahead for the years remaining until the end of the mission. In addition, we will emphasize the planning for the solar conjunction season during the Summer of 2017. In comparison with the SGS planning for the Rosetta mission, we will present some observation statistics and we will conclude with the planned system improvements and future mission perspectives.

1. Introduction

Mars Express remains one of ESA's most scientifically productive missions and has fully accomplished its objectives. The mission provides a unique enabling capability for Mars climate evolution research and complex process understanding [9].

The Mars Express (MEX) Science Ground Segment team is composed of 6 scientist-engineers who are responsible for the definition and maintenance of the overall scientific plan in cooperation with the Project Scientist (PS) [13].Their duties include:

- coordinating the candidate orbit selection process between the Instrument teams and the relevant Mission Operation Center (MOC) teams,
- supporting the planning activities of the MEX Principal Investigators (PI) in the preparation of science operations for their instruments and shielding MOC from the details of this iterative process,
- producing a set of consolidated instrument payload operations requests and pointing timeline requests based on the Long Term Plan (LTP) and the output of the medium term planning (MTP) exercise, and transferring these to the MOC,
- iterating the instrument payload requests with the MOC and possibly the PIs to resolve inconsistencies,
- coordinating software patching for instruments,
- participating in the Resource Allocation Board (RAB) which convenes during the MTP and STP phases,
- participating in Mission Review Boards (MRBs) which investigate instrument anomalies.

2. New challenges: the case of the 2017 solar conjunction

Dealing with a long-term mission in an operational phase, there are constant challenges, such as adjusting the planning for Mars seasons and the evolution of the spacecraft systems. We will present the improvements and new methodologies created for the science scheduling challenges faced during the Summer 2017 conjunction season.[3]

3. MEX - Other planetary missions science planning system comparison

SGS personnel is based at the ESAC ESA centre where the operations engineers are involved across the various planetary missions. This provides an important know-how transfer among similar but technically different ground segments. We will show an overview of the differences that exist between some other newer missions as Rosetta and Mars Express SGS systems.

4. Some planning statistics

We will provide some downlink observation statistics for the overall MEX mission science as well as a useful analysis of SGS planning in comparison with other ESA planetary missions.[4,5 and 6]

5. Future of the mission and system improvements

Finally, we will summarize the future objectives for the mission planning up to 2020 and the general status of the spacecraft, instruments and manpower.[1,2]

6. Summary and conclusions

Flexibility is key for science missions in comparison with Earth Observation planning tools for which automation is vital for their development. Unfortunately, this implies manual processes and requires qualified operators, both engineers and scientists to achieve the PIs goals. In order to improve SGS systems across planetary missions, it is vital to maintain accurate reporting and documentation for long-term missions such as MEX and for an optimized transfer of know-how to future, potentially more complex planetary missions.

Acknowledgements

We are particularly grateful for the assistance given by the MOC to SGS during the past years of mission operations. Without their excellent and constant collaboration in the science planning process the Mars Express mission would not have obtained such prolific scientific results.

References

[1] Titov, D., Cardesin, A., Martin, P., Mars Express: Mission Status, Recent Findings and Future Plans, The Sixth International Workshop on “the Mars Atmosphere: Modelling and observation”, held on 17-20 January 2017.

[2] Titov, D., Bibring, J. -P., Cardesin, A., Mars Express: status and recent findings, EGU General Assembly, where and when, 2016.

[3] Mars Express MEOR: Science Case, presented at the Mission Extensions Operations Review (MEOR), ESTEC-ESOC-ESAC, 30 May 2016.

[4] Gondet, B., Bibring, J. -P., Montmessin, F., The Mars Express limbs observations database, EGU General Assembly 2015, held in Vienna, Austria, id.3824,12-17 April 2015.

[5] Mars Express Master Science Plan Overview Documentation (MEX-EST-PL-11912, Issue 1.5,, November 2004.

[6] Mars Express: The scientific payload, ESA publications SP-1240, ISBN 92-9092-556-6, August 2004.

[7] Mars Express continues on reduced solar power Refocus, Volume 4, Issue 6, November–December 2003, Pages 9, January 2004.

[8] Hechler, M., Yañez, A., Mars express orbit design, Acta Astronautica, Volume 53, Issues 4–10, pages 497-507, August–November 2003.

[9] R. Schmidt, Mars Express - ESA's first mission to planet Mars, Acta Astronautica, Volume 52, Issues 2–6, pages 197-202, January–March 2003.

[10] Whitcomb, G.P, The ESA approach to low-cost planetary missions, Acta Astronautica, Volume 52, Issues 2–6, pages 79-86, January–March 2003.

[11] P. Moulinier, F. Faye, J.C. Lair, E. Maliet., Mars Express spacecraft: design and development solutions for affordable planetary missions, Acta Astronautica, Volume 52, Issues 2–6, pages 203-209, January–March 2003.

[12] Dieter Kolbe, Mars Express: Evolution towards an affordable European Mars Mission (Ref. A-5, (082)), Acta Astronautica, Volume 45, Issues 4–9, pages 285-292, August–November 1999.

[13] Mars Express Science Management Plan, ESA/SPC(97)40, October 1997.

EPSC Abstracts
Vol. 11, EPSC2017-164, 2017
European Planetary Science Congress 2017

What stable nitrogen-bearing minerals could be stored in the surface during early Noachian Mars and what are the constraints in terms of temperature and pH?

I. van de Burgt (1,2), E. Sefton-Nash (2), I.L. ten Kate (1)
(1) Utrecht University, Utrecht, the Netherlands, (2) ESA ESTEC, Noordwijk, the Netherlands, (vdburgt.i@gmail.com)

Early Noachian Mars, nitrogen adsorption, habitability, ExoMars Rover mission

Abstract

Nitrogen plays an important role in many biomolecules and is significant in biological activity on Earth. While nitrogen remains the dominant component in Earth's atmosphere, the nitrogen content of the early Mars atmosphere is ill-constrained, yet fundamental to understanding the habitability of early Mars [16]. The objective of this study is to determine the feasibility and role of nitrogen fixation in clays in conditions that may have prevailed on early Mars. We model fixation as well as loss rates of the nitrogen in phyllosilicates within temperature and pH bounds plausible for ancient Mars surface conditions. We find that ~0.3 – 2.3 teragram (Tg, 10^{12} gram) of nitrogen per Myr may be fixed into the clay phases that are observed on Mars' surface, and that only ~3% of this would be released back to non-fixed reservoirs (aqueous, atmospheric).

1. Introduction

The atmosphere of early Mars contained more than ten times the amounts of free nitrogen than it does today [9, 10]. Before Mars' early and dense atmosphere was lost, this nitrogen was free for interaction with surface minerals and liquids. This study aims to shed light on processes involved fixation of nitrogen into the clays of Mars and what major constraints were involved in this process. Mars' abundant clay minerals may have served as a nitrogen sink due to their excellent capacity of storing cations in their negatively charged interlayers [10].

2. Methods

2.1 Model description

We present a nitrogen box model, as in [17], but with four reservoirs (Figure 1). N_2 (first reservoir) reduces to NO (second reservoir) by lightning [7, 12]. A second flux describes the reduction of NO to ammonium (NH_4^+, third reservoir) by FeS [18]. NH_4^+ (aqueous) may then be adsorbed into clays (fourth reservoir). We used montmorillonite and nontronite as these are the two widely occurring clays on Mars [2, 5]. Their layered structure allows inorganic cations, e.g., NH_4^+ or K^+, to be fixed in the negatively charged interlayers [10].

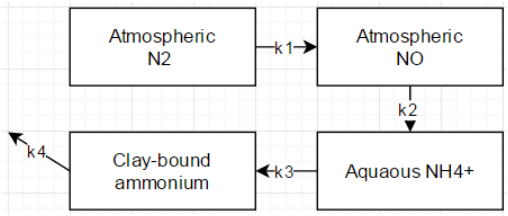

Figure 1. Schematic of the box model. Fluxes are described in the text. The initial reservoir size of N_2 was $8x10^5$ TgN.

This model was run for a time-span of 2 Myr for maximum and minimum bounds of input parameters to produce a plausible envelope of nitrogen fixation.

2.2 Calculations

The adsorption of NH_4^+ into clay minerals was calculated after the work of Boatman and Murray, 1982 [1]:

$$N_{clay} = a_{NH4+} / \left(\left(\frac{1}{K_{ads}} + a_{NH4+}\right) * \Gamma * M_N\right) \quad (1)$$

a_{NH4+} is the activity of NH_4^+. This is the multiplication of the molar concentration by the activity coefficient of 0.57 for seawater [6, 17]. M_N is the molar mass of nitrogen (14.01 g/mol). K_{ads} is the adsorption constant (12 and 11.7 for nontronite and montmorillonite [1], respectively), and Γ is the cation exchange capacity (0.94 mmol/g and 0.69 mmol/g for nontronite and montmorillonite [1, 14], respectively).

To calculate temperature dependence, the Arrhenius equation (2) was used:

$$\frac{v1}{v2} = \exp(10b * (T_1 - T_2)/(T_1 * T_2)) \quad (2)$$

v_1/v_2 is the rate of reaction for a new temperature (T_2) versus the rate of reaction of the reference temperature (T_1). The constant b is the product of the activation energy and the gas constant and equals 6352 K [14]. Upper and lower temperature bounds for the model are set 263 K and 283 K informed by warm and wet early Mars assumptions of previous studies [4, 11].

pH dependence of the loss rate from adsorbed NH_4^+ to volatile NH_3 was calculated using equation (3) and the equilibrium constant $K_{NH3} = 10^{-9.25}$ [17]:

$$pH: (NH_3) = ((NH_4) * K_{NH3})/H^+ \quad (3)$$

The stability field of both phyllosilicate minerals are weakly acidic to alkaline [3]. The pH boundaries in this model are set to 6 - 9.

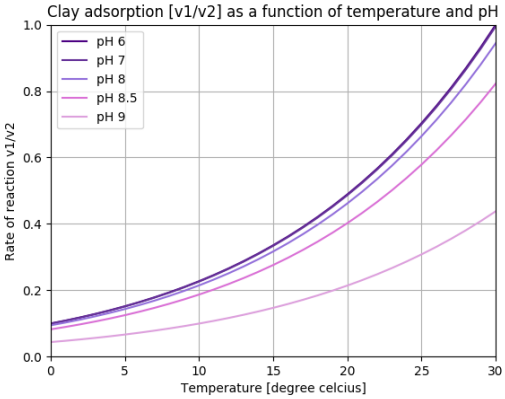

Figure 2: The v_1/v_2 dependence of pH as a function of temperature.

3. Results

The calculation of ammonium adsorption into phyllosilicates without any constraints, pH < 6 and temperature = 303 K, is equivalent to fixing 10.25×10^{12} g N/Myr.

However, pH and temperature both have an effect on the rate of adsorption of nitrogen into different phyllosilicates (Figure 2). For the upper boundary (pH 6 and temperature 283 K) we calculate a v_1/v_2 of 0.23. For the lower boundary (pH 9 and temperature 263 K) a v_1/v_2 of 0.034. Consequently, provided that reactions are not supply-limited we estimate that plausible rates of N fixation in nontronite and montmorillonite lie in the range of ~0.3 – 2.3 Tg N/Myr.

4. Summary and Conclusions

Given the current knowledge about surface conditions and atmospheric composition on early Noachian Mars, we use constraints in pH and temperature and a hypothetical box model to gain a better understanding of nitrogen fixation with respect to phyllosilicates thought to have formed on early Mars. We find that pH is only a meaningful constraint when very alkaline conditions prevail, but a decline in temperature results in a strong decline of nitrogen fixation. Nonetheless, even at the lowest rates of fixation it is possible to lock a large amount of nitrogen in clay minerals that are prevalent on the surface of Mars today. Clues to Mars' ancient atmospheric inventory, and the consequence for early habitability, may therefore lie in rocks that will be targeted by ESA's upcoming ExoMars Rover, which is intended to sample Noachian-aged clay-bearing rocks.

Acknowledgements

I would like to thank the University of Utrecht for providing funds. I further thank my co-workers for constructive criticism.

References

[1] Boatman, C. D., and J. W. Murray. Limnology and Oceanography 27.1 (1982): 99-110. **[2]** Carter, J., et al. Icarus 248 (2015): 373-382. **[3]** Chevrier, V., F. Poulet, and J.-P. Bibring, Nature 448.7149 (2007): 60-63. **[4]** Craddock, R. A., and A. D. Howard. Journal of Geophysical Research: Planets 107.E11 (2002). **[5]** Ehlmann, B. L., and C. S. Edwards. Annual Review of Earth and Planetary Sciences 42 (2014): 291-315. **[6]** Fairén, A. G., et al. Nature 431.7007 (2004): 423-426. **[7]** Kasting, J. F., and J. C. G. Walker. Journal of Geophysical Research: Oceans 86.C2 (1981): 1147-1158. **[8]** Mancinelli, R. L., and A. Banin. International Journal of Astrobiology 2.03 (2003): 217-225. **[9]** Manning, C. V., C. P. McKay, and K. J. Zahnle. Icarus 197.1 (2008): 60-64. **[10]** McBride, M. B. (1994). **[11]** McKay, C. P., and W. L. Davis. Icarus 90.2 (1991): 214-221. **[12]** Navarro-González., R., M. J. Molina, and L. T. Molina. Geophysical Research Letters 25.16 (1998): 3123-3126. **[13]** Rodrigo, A., et al. Ecological Modelling 102.2 (1997): 325-339. **[14]** Sayles, F. L., and P. C. Mangelsdorf.. Geochimica et Cosmochimica Acta 41.7 (1977): 951-960. **[15]** Squyres, S., and J. F. Kasting. Science 265.5173 (1994): 744-749. **[16]** Stern, J. C., et al. Proceedings of the National Academy of Sciences 112.14 (2015): 4245-4250. **[17]** Stüeken, E. E. Astrobiology16.9 (2016): 730-735. **[18]** Summers, D. P., et al. b Astrobiology 12.2 (2012): 107-114.

EPSC Abstracts
Vol. 11, EPSC2017-207-1, 2017
European Planetary Science Congress 2017

Fault Populations on Alba Mons, Mars, and their Age Relationships to Volcanic, Fluvial, and Glacial Processes

R. Karimova (1), E. Hauber (1), D. Crown (2), T. Platz (2, 3), D. Berman (2), S. Scheidt (4), and C. Weitz (2)
(1) German Aerospace Center (DLR), Institute of Planetary Research, Berlin, Germany (Ernst.Hauber@dlr.de), (2) Planetary Science Institute, Tucson, USA, (3) Max Planck Institute for Solar System Research, Göttingen, Germany. (4) Univ. Arizona, Tucson, USA.

Abstract

We map the cross-cutting relationships between faults, valley networks, and (volcanic) flows on Alba Mons to infer the temporal sequences of the major processes that influenced the area. Preliminary mapping on the northwestern flank suggests that lava flows predate the valley networks, and the faults postdate both the flows and the fluvial valleys. We also mapped individual fault segments for future quantitative fault population analysis.

1. Introduction

Alba Mons is a large, low-relief volcano with a planform extent of 1015 km × 1150 km exceeding that of Olympus Mons but with only ~6 km relief and extremely low flanks slopes (~1°) [1]. Alba Mons has a summit caldera complex, extensive lava flow fields on its flanks and in the surrounding plains [2], and prominent sets of graben (e.g., Tantalus and Alba Fossae) that extend from south of the volcano around its flanks and into the northern plains [3,4]. A series of dendritic valley networks [5] is found on Alba Mons' flanks; coupled with the volcano's low relief, the valley networks have been interpreted to indicate pyroclastic deposits at the base of the volcano, suggesting that Alba Mons may be a transitional form from the ancient highland paterae to the prominent shield volcanoes of the Tharsis region [6].

This study is part of a larger project that will result in two formal USGS geologic maps of Alba Mons` summit region and its western flank [7]. Here we focus on two specific questions: 1) What are the quantitative properties of the fault populations such as their length distribution and the displacement-length ratio? 2) What are the relative ages of lava flows, channels, and tectonic features (e.g., graben, ridges, and pit crater chains) on the upper flanks of Alba Mons?

2. Methods and data

Images with ~5m/pixel resolution taken by the Context Camera (CTX) on the Mars Reconnaissance Orbiter (MRO) were used for the mapping, and images (~0.5m/pixel resolution) of a few selected sites from the High Resolution Imaging Science Experiment (HiRISE) were used for cross-evaluation of small-scale features. The test mapping area is located on the northwestern flank of Alba Mons extending over 44.5-46.5°N and 112-114°W. It was selected due to the presence of all three features of interest, i.e., valley networks, faults, and lava flows. Figure 1 shows some examples of identified cross-cutting relationships where the contact points are marked accordingly.

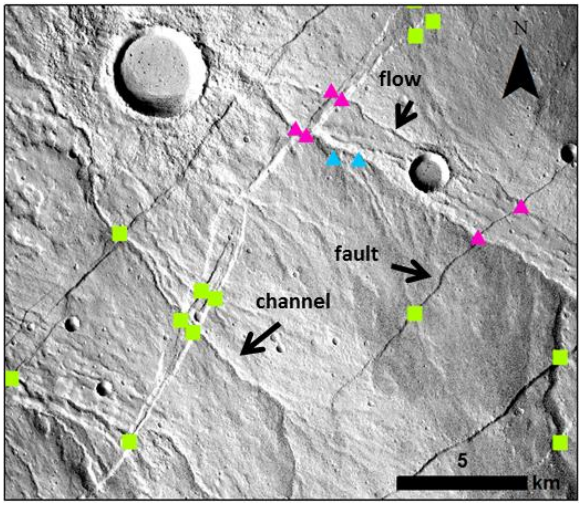

Figure 1: CTX image showing examples of mapped cross-cutting relationships. See Fig. 2 for legend.

3. Preliminary results

The numerous faults in the test area are part of the larger concentric graben sets surrounding the summit region and appear to be the youngest of the three

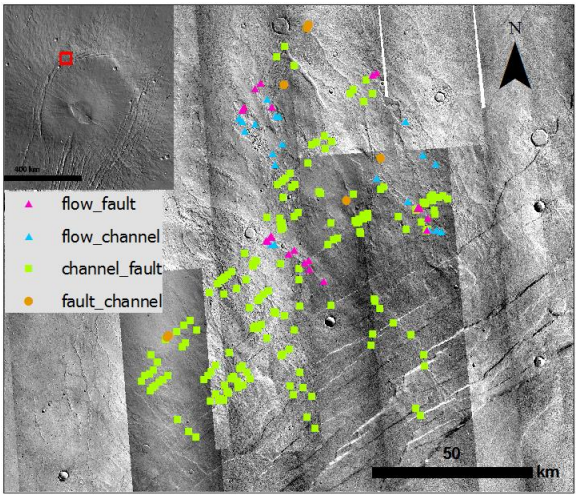

Figure 2: Cross-cutting relationships mapped in the test area. * The first item in the legend name is older, e.g. flow_fault = the flow is older than the fault.

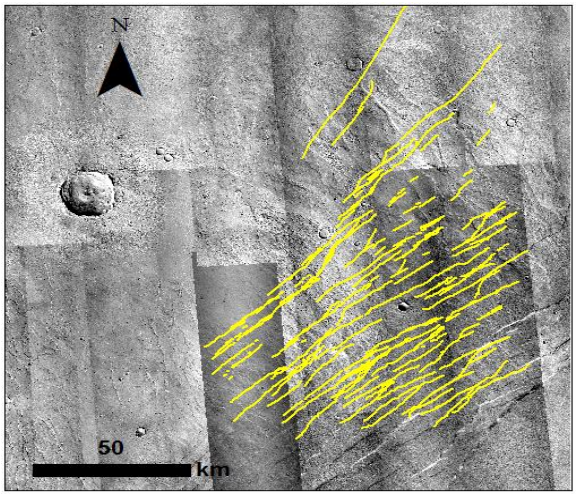

Fig. 3: Individual fault segments, often in en echelon patterns. Base map is same CTX image mosaic as in Fig. 2.

types of landforms. Numerous channels predate faults. Lava flows are less abundant, but where unambiguously identified, they appear older than both faults and valley networks (Fig. 2). This result agrees with previous mapping [2, 8]. Identification of the relationships was in some cases complicated by crater ejecta, as well as what we assume to be the ice-rich latitude-dependent mantle that is known to be ubiquitous in mid-latitudes [e.g., 9]. HiRISE images show that the topographic expression of geomorphological features is somewhat subdued, especially when observed at very small scale, which resembles "blanketing" by an extensive mantle deposit. In some cases it is hard to distinguish the type of flows, which may be either lava or debris flows.

4. Discussion and conclusions

Preliminary results from one test region suggest that the volcanic activity ceased on this part of Alba Mons before the onset of the extensive fluvial activity. This along with the preferential formation of channels on the northern flank of Alba Mons are suggested by [2] to be evidence for the accumulation of friable ice-rich material during high obliquity periods. As to the pyroclastic origin of the deposits proposed by [6], this age sequence would require a late pyroclastic activity that might have occurred after the effusive flows were emplaced. Mapping of a larger area where more lava flows are present is planned before we can conclusively confirm the sequence of geological processes.

The young relative age of the mapped faults suggests that the majority of them correspond to the stage III faulting event [10], which is part of a complex sequence of tectonic activity that lasted from Noachian to Late Amazonian. The faults appear extremely pristine and well-preserved when compared to other faults on Mars, supporting the notion of a relatively recent formation. We plan to extend the detailed mapping of the faults at small scales to obtain a representative sample of quantitative fault length distribution. This can be useful for estimating the strains acting on the area to constrain formation models of the prominent graben systems surrounding Alba Mons.

References

[1] Plescia, J.: J. Geophys. Res., 109, E03003, doi:10.1029/2002JE002031, 2004. [2] Ivanov, M. and Head, J.: J. Geophys. Res., 111, E09003, doi:10.1029/2005JE002469, 2006. [3] Gulick, V., Baker, V.: J. Geophys. Res., 95, 14,325-14,344, 1990. [4] Cailleau, B., et al.: J. Geophys. Res., 108 (E12), 5141, doi: 10.1029/2003JE002135, 2003. [5] Öhman, T., McGovern, P.: Icarus, 233, 114-125, doi: 10.1016/j.icarus.2014.01.043, 2014. [6] Mouginis-Mark, P., et al.: Bull. Volc., 50, 361-379, 1988. [7] Crown, D., et al.: Lunar Planet. Sci. Conf. XLVII, abstract #2383, 2016. [8] Chowdhury, D.: M.Sc. Thesis, Univ. of Calif., Los Angeles, USA, 2013. [9] Kostama, V.-P., et al.: Geophys. Res. Lett., 33, L11201, 2006. [10] Tanaka, K. L.: Lunar Planet. Sci. Conf. Proc. Vol. 20, 1990.

EPSC Abstracts
Vol. 11, EPSC2017-208, 2017
European Planetary Science Congress 2017

On the structure of the lithosphere of Mars: New insights from crustal composition and rheology of the upper mantle

Alberto Jiménez-Díaz (1), Isabel Egea-González (2,3), Laura M. Parro (1), Miki Tasaka (4) and Javier Ruiz (1)
(1) Departamento de Geodinámica, Facultad de Ciencias Geológicas, Universidad Complutense de Madrid. 28040 Madrid, Spain (aljimene@ucm.es), (2) Departamento de Física Aplicada. Universidad Politécnica de Cartagena. 30202 Cartagena, Spain, (3) Departamento de Física Aplicada. Escuela Politécnica Superior de Algeciras, Universidad de Cádiz, 11202 Algeciras, Cádiz, Spain, (4) Department of Geoscience, Interdisciplinary Graduate School of Science and Engineering, Shimane University, 1060 Nishikawatsu-cho, Matsue-shi, Shimane 690-8504, Japan

Abstract

We conduct an in-depth study of the thermal structure and rheology of the lithosphere of Mars, focusing on the effects of crust composition, creep behaviour of olivine (the main mineral in the lithosphere mantle), and the abundance of iron and water in the mantle.

1. Introduction

An adequate knowledge of the thermal and rheological properties of crust and mantle is fundamental for deciphering and understanding the thermal state and interior evolution of a planetary body. Previously, indirect methods have been used to calculate heat flows for Mars. A commonly used indirect method is based on the relation between the thermal state of lithospheric rocks and their mechanical strength, usually related through the effective elastic thickness of the lithosphere or from the depth to the brittle–ductile transition beneath large thrust faults. The so-obtained heat flows are valid for the time when the lithosphere was loaded or faulted, and therefore when deduced from regions deformed in different ages provides information on the thermal evolution of Mars [1, 2]. Thus, heat flow estimates based on lithosphere strength indicators are strongly dependent on the assumed compositions, the choice of predominant deformation mechanisms, and other thermal and mechanical parameters.

2. The role of the crust

As mentioned previously, Ruiz et al. [1] and Ruiz [2] calculated in a consistent manner upper and lower limits for the surface heat flows derived from the effective elastic thickness of the lithosphere or from faulting depth beneath large thrust faults. In these works the crustal density was assumed to be 2900 kg m^{-3}, which is suitable for a basaltic crust (see below), the thermal conductivity of the crust was assumed to be 2 W m^{-1} K^{-1}, a value appropriate for basalts (see e.g., [3]), and for creep parameters of the Martian crust, it had taken into account the constants for the flow law of diabase [4]. The use of a wet diabase law is appropriate for a basaltic Martian crust and is consistent with extensive evidence for water-related geological activity in early Mars (e.g., [5, 6]).

A crustal density of 2900 kg m^{-3} can be consistent with a basaltic crust somewhat fractured, or consistent with a basaltic crust including a felsic component. Indeed, some recent works suggest that the Martian crust could contain a substantial amount of felsic rocks [7-10], although other works consider as non-solids the orbital-based evidences for a felsic component (see [11]). Moreover, Baratoux et al. [9] proposed a high density (>3200 kg m^{-3}) for the Martian basalts, although a crust so dense is incompatible with geophysical studies [9], maybe favouring the presence of a felsic component.

3. The role of the lithospheric mantle

On the other hand, in these works [1, 2] the ductile strength of the lithospheric mantle was calculated for dry olivine dislocation creep rheology (a flow law obtained for artificially dried dunites; [12]), which gives a generous upper limit to the surface heat flow obtained from lithospheric strength [1, 2]. For wet olivine, the flow law of the Anita Bay dunite [12] was commonly used. This flow law places a lower limit on the strength of wet olivine due to its relative

weakness (compared with other wet dunites, such as Aheim dunite), which gives a lower limit to the surface heat flow.

However, Zhao et al. [13] have reported that anhydrous olivine is considerably weaker when it is proportionally iron-rich, as expected for the Martian mantle (for a review see [14]), which would reduce mantle strength and hence the obtained heat flows. Likewise, recent careful examinations of the creep behaviour of olivine under hydrous conditions as a function of iron content suggest that the viscosity of the Martian mantle will be a factor of ~20 lower than the viscosity of Earth's mantle [15]. Also, the behaviour of the upper lithospheric mantle is in turn largely controlled by low-temperature plasticity of olivine-rich rocks, resulting in a rheology significantly weaker than that usually used for the upper mantle (see e.g., [16] for discussion under anhydrous conditions).

4. First steps & Future work

All of these issues motivate us to explore to what extent the composition of the crust or the creep behaviour of olivine could affect the thermal and mechanical structure of the lithosphere of Mars, and hence on the heat flow estimates based on lithosphere strength indicators.

In a first step, we carefully and systematically explore the effects of composition of the crust on the thermal and mechanical structure of the Martian lithosphere (see [17]). To make this, we use suitable parameters (appropriated for, respectively, mafic and felsic materials), in order to evaluate the case of an end-member felsic crust, and its influence on the thermal and mechanical properties of the crust and lithosphere. Also, we identify the parameters that have a major impact on the thermal state and mechanical behaviour of the lithosphere. Finally, we extend our analysis to specific case scenarios and discuss the implications of our results for the thermal state, structure and evolution of Mars (see e.g., [18, 19]).

In a subsequent step, we intend to analyse in detail the influence of the creep behaviour of olivine and the effects of the abundance of iron and water in the mantle on the mechanical behaviour of the lithosphere.

Taken together, these two main lines will provide an integrated overview of the role of the crust and lithospheric mantle within the framework of the thermal and mechanical structure of the lithosphere of Mars. Our first results will be presented in the European Planetary Science Congress 2017.

Acknowledgements

The work by L.M.P. was supported by a FPU2014 grant from the Ministerio de Educación, Cultura y Deporte of Spain. This work has received funding from the European Union's Horizon 2020 Programme (H2020-Compet-08-2014) under grant agreement UPWARDS-633127, and from the Spanish Ministry of Economy and Competitiveness Project CGL2014-59363-P (AMARTE).

References

[1] Ruiz, J. et al., Icarus 215, 508-517, 2011. [2] Ruiz, J., Sci. Rep. 4, 4338, 2014. [3] Beardsmore, G.R. and Cull, J.P., Cambridge University Press, Cambridge, 324 pp., 2001. [4] Caristan, Y., J. Geophys. Res. 87, 6781-6790, 1982. [5] Head, J.W. et al., Space Sci. Rev. 96, 263-292, 2001. [6] Dohm, J.M. et al., Planetary and Space Science 57, 664-684, 2009. [7] Carter, J. and Poulet, F., Nature Geosci. 6, 1008–1012, 2013. [8] Wray, J. et al., Nature Geosci. 6, 1013–1017, 2013. [9] Baratoux, D. et al., J. Geophys. Res. Planets 119, 1707-1727, 2014. [10] Sautter, V. et al., Nature Geosci. 8, 605–609, 2015. [11] Rogers, A.D. and Nekvasil, H., Geophys. Res. Lett. 42, 2619-2626, 2015. [12] Chopra, P.N. and Paterson, M.S., J. Geophys. Res. 89, 7861-7876, 1984. [13] Zhao, Y.-H., Zimmerman, M.E. and Kohlstedt, D.L., Earth Planet. Sci. Lett. 287, 229-240, 2009. [14] Kohlstedt, D.L. and Mackwell, S.J., in Planetary Tectonics, eds. T.R. Watters and R.A. Schultz, Cambridge University, pp 397-456, 2010. [15] Tasaka, M., Zimmerman, M.E. and Kohlstedt, D.L., J. Geophys. Res. Solid Earth, 120, 6039–6057, 2015. [16] Mei, S. et al., J. Geophys. Res. 115, B08204, 2010. [17] Jiménez-Díaz, A. et al., 48th Lunar and Planetary Science Conference, LPI Contribution No. 1964, id.1453, 2017. [18] Egea-González, I. et al., Icarus 288, 53–68, 2017. [19] Parro, L.M. et al., Scientific Reports 7, 45629, 2017.

EPSC Abstracts
Vol. 11, EPSC2017-224-6, 2017
European Planetary Science Congress 2017

Observations of south polar landforms, Mars: a case study in Angustus Labyrinthus.

J. Hao (1), G.G. Michael (1), R. Jaumann (1,2), S. Adeli (2)
(1) Freie Universität Berlin, Inst. of Geological Sciences, Planetary Sciences and Remote Sensing Group, Malteserstr. 74-100, 12249 Berlin, Germany (J.Hao@fu-berlin.de), (2) German Aerospace Centre (DLR), Institute of Planetary Research, Rutherfordstraße 2, 12489 Berlin, Germany.

1. Introduction

Araneiform terrain (informally called "spiders"), usually characterized by central depressions and radially branched troughs carved into the substrate, is an enigmatic features of the Martian south polar area with no terrestrial analogies (Fig.1). They are thought to result from CO2 sublimation driven seasonal erosion [1-3].

The High Resolution Imaging Science Experiment (HiRISE) onboard NASA's Mars Reconnaissance Orbiter (MRO) spacecraft, together with the High Resolution Stereo Camera (HRSC) images onboard Mars Express, have repeatedly imaged Angustus Labyrinthus, informally known as the Inca City (-81ºN, 296ºE), which is characterized by rectilinear intersecting ridges and an active area for spring sublimation and jet activities and thus host a considerable concentration of spiders [2].

We mapped the spiders´ spatial distribution in the Inca City and classified them into four species according to their morphological features including two undescribed types. Our goal is to investigate the formation mechanisms and distribution characteristics of the spiders. We also evaluate whether the morphometry bears information about the homogeneity or heterogeneity of the surface material and supports gas-venting or other channel-erosion models.

2. Method

Inca City is characterized by rectilinear intersecting ridges (Fig.1). Its interior regions are active areas for spring sublimation and jet activities, and they host a considerable concentration of spiders [3]. We systematically scrutinized and mapped all spiders in the Inca City (Fig.1) using 100 HiRISE images.

HiRISE can return 25cm per pixel surface images with high signal to noise ratio [7,8]. HRSC provides a large and continuous coverage of the Martian surface with intermediate resolution 12.5m per pixel [9]. Both of them enable us to identify spiders including their troughs under low light conditions (Fig.1).

3. Result

We made a detailed mapping of the spider distribution and location in Inca city by investigating 100 HiRISE (Fig.1). In total we found 3618±34 spiders. Some of them are connected by troughs and it is not easy to determine whether this is a single spider.

Adding to the two types of spiders already described - fat and thin spiders [3], we identified two new types spiders which we termed 'elongated' and 'half' spiders (Fig.2).

Thin spiders usually with rough and large centres and thin and long troughs have much more complex and interlinked troughs net and irregular central depression shapes. They have large diversity in sizes and very distinctive characteristics making them easy to distinguish and identify (Fig.2b). Fat spiders have relatively larger centre depressions with wide and short troughs emanating radially from centre depressions (Fig.2a). Their troughs have very few branches and become narrow quickly increasing with distance from centre depressions (Fig.2a).

Half spiders only show one half of the typical spider features but the troughs nevertheless radiate from main depression (Fig.2d). They are found along the boundary with ridges or steep slopes and are relatively rare. Elongated spiders are characterized by linear central depressions and much thinner

branching troughs (Fig.2c). The troughs are short compared with the linear central depressions. A large fraction of the troughs emanates directly from the central depressions with branches or bifurcations (Fig.2c).

4. Future Work

We mapped the distributions of spiders in the Inca City and classified key morphometric features as well as subtler characteristics. Thus we intend to study the spatial growth trend of the spiders' troughs and to understand the implications for the surface properties and processes involved. We will focus on investigating how far and in which way spiders are controlled and affected by environmental parameters.

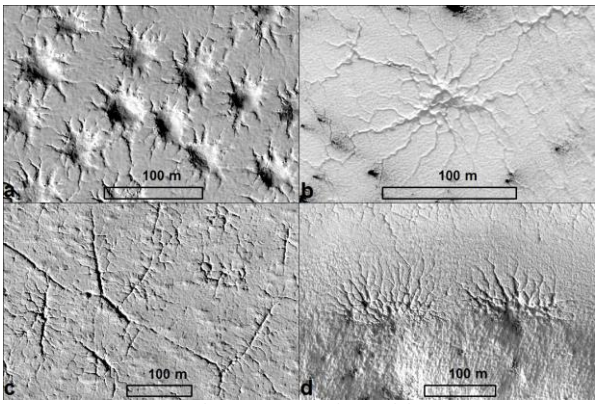

Figure 2. Four types of spiders. (a)A field of fat spiders, centered approximately at -81.62ºN, 296.395ºE. HiRISE image PSP_005993_0985 was acquired at Ls=342 with 50cm/pixel. (b) A field of thin spiders, centered approximately at -81.441ºN, 295.92ºE. HiRISE image PSP_003928_0815 was acquired at Ls=247 with 25cm/pixel. (c) A field of elongated spiders, centered approximately at -81.768ºN, 296.02ºE. HiRISE image PSP_006204_0985 was acquired at Ls=351 with 50cm/pixel. (d) A field of half spiders, centered approximately at -81.562ºN, 295.806ºE. HiRISE image PSP_006204_0985 was acquired at Ls=351, with 50cm/pixel.

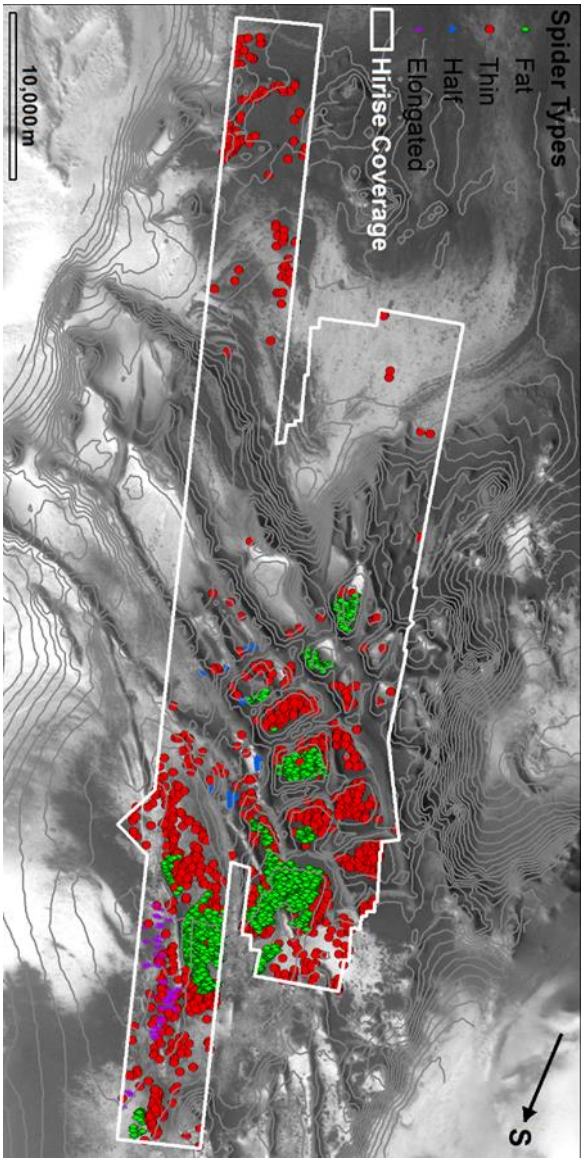

Figure 1. HiRISE coverage on Inca City superposed upon the spatial mapping of spiders and HRSC image and a contour map of 50m derived from the Mars Orbiter Laser Altimeter (MOLA). The white polygon indicates the area covered by HiRISE images.

References

[1]Kieffer et al., (2007) Nature 442, 793-796. [2]Piqueux et al., (2003) JGR, 108 (E8), 5084. [3]Hansen et al. (2010) Icarus 205(1), 283-295.[4]Portyankina, G., et al. (2013) 2013 EPSC (Abstract 2013-410). [5]Leighton, R.B. and Murray, B.C. (1966) Science 153, 136–144. [6]Portyankina, G., et al. (2016) Icarus 282, 93-103. [7]McEwen, A. S., et al. (2007a) JGR, 112, E05S02. [8]McEwen, A. S., et al. (2010) Icarus, 205, 2-37. [9]Jaumann, R., et al. (2007) Planet. Space Sci., 55 (7–8), 928–952.

EPSC Abstracts
Vol. 11, EPSC2017-228, 2017
European Planetary Science Congress 2017

Penetration of Solar Radiation into Solid Carbon Dioxide

H. E. Chinnery, A. Hagermann, E. Kaufmann, S. R. Lewis, M. M. Grady.
School of Physical Sciences, The Open University, Milton Keynes, UK. (Hannah.chinnery@open.ac.uk)

Abstract

The e-folding scale, otherwise known as the absorption scale length, has been determined by laboratory measurements for carbon dioxide slab ice, granular ice and snow. This can give insights into thermal gradients within snow packs or ice covered regolith on Mars, where surface CO_2 ice is naturally occurring. With long-term ice coverage, localised perturbations in subsurface heat flow could occur. This also has implications for the radiative budget of CO_2 ice covered surfaces, as well as physical processes, such as the formation of so-called spider formations in the 'cryptic region' near the Martian south pole.

1. Introduction

Solid carbon dioxide ice exists both on the surface, and in the subsurface of Mars [1]. CO_2 clouds and accumulations of CO_2 ice in snowfall up to 1.5 m deep at the seasonal northern cap have been observed by the Thermal Emission Spectrometer [2] and the Mars Orbiter Laser Altimeter [3], and CO_2 snowfall was modelled to be able to occur in particular locations at high latitudes [4]. The permanent northern polar cap is predominantly water ice, whereas in the south there is a much higher proportion of CO_2 ice, and the seasonal extension of the ice caps in both hemispheres is due to the condensation of CO_2 as slab ice. It is likely that the seasonal ice caps are formed by both direct condensation to the surface, and from snowfall, which anneals to form solid ice [4].

2. Background

It is the current consensus that low albedo slab ice forms during the autumn and winter months outwards from the poles. Of particular interest is the cryptic region, where so-called spider formations are observed during spring time. Work has been done in modelling these observations [5], and has now been successfully recreated experimentally in the laboratory, under particular temperature and pressure conditions [6]. This involved measuring temperature profiles through CO_2 ice with embedded dust particles [7]. However, the optical properties of pure carbon dioxide ice under broad spectrum visible wavelengths are poorly understood.

In this work, we intend on measuring the e-folding scale of each different polymorph of CO_2 ice likely on Mars, which includes slab ice as part of the seasonal polar caps, CO_2 snow, and granular CO_2. The latter is possibly formed in cracks and faults in the slab ice. The thermal expansion coefficient for CO_2 ice is almost twice that of water ice, and so with day to night time temperature variations experienced in these regions on the surface of Mars, it is quite possible that thermal expansion during the day could lead to expansion and buckling of the ice sheet, later contracting overnight and leaving regions of granular ice debris. We measure the e-folding scale of a range of discreet grain size ranges, as small grains of around 500 µm could yield very different results than 5 mm sized grains.

3. Theory

The Solid State Greenhouse Effect is a result of ices being translucent in the visible electromagnetic spectrum but opaque in the infra-red, which means that light can penetrate through a surface ice layer and be absorbed by the underlying regolith [8], [9]; [6]. The extent of this effect is, in part, reliant upon the e-folding scale of the overlying ice. The e-folding scale is defined as the depth through a medium over which intensity is reduced by 1/e of the original intensity, which means it can be compared directly to other materials, such as water ice.

4. Laboratory Experiments

CO_2 snow and ice is made in the lab and used as soon as possible. This minimises water frost contamination or physical alterations, such as sintering of snow particles or excessive thermal cracking in the ice

blocks. Figure 1 shows a simplified diagram of the experimental set up.

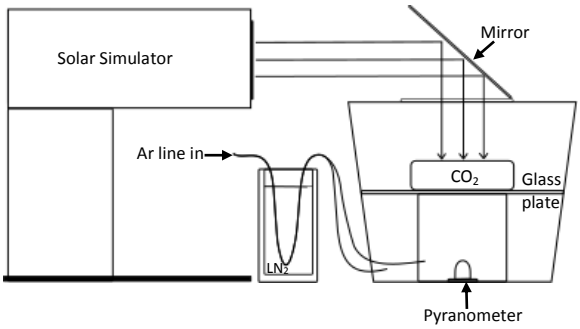

Figure 1 Schematic of experimental set up for the e-folding scale measurements.

CO_2 snow is made using an Air Liquide Snowpack. Translucent slab ice is made using a pressure vessel cooled by liquid nitrogen from the base, as described by Kaufmann & Hagermann [6]. Experimental protocol for measurements for CO_2 snow is based on that used by Kaufmann & Hagermann [7] for water snow experiments.

5. Summary

Results from the measurements of the e-folding scale of CO_2 slab ice, granular ice and snow will be discussed and compared to measurements of other materials available in the literature. The implications of these results will then be discussed in terms of heat-flow and surface processes.

Acknowledgements

This research is funded via an STFC PhD Studentship to HEC.

References

[1] Phillips, R.J., Davis, B.J., Tanaka, K.L., Byrne, S., Mellon, M.T., Putzig, N.E., Haberle, R.M., Kahre, M.A., Campbell, B.A., Carter, L.M., Smith, I.B., Holt, J.W., Smrekar, S.E., Nunes, D.C., Plaut, J.J., Egan, A.F., Titus, T.N. and Seu, R., 2011. Massive CO2 Ice Deposits Sequestered in the South Polar Layered Deposits of Mars. Science, 332: 838-841.

[2] Kieffer, H., Titus, T. 2001. TES Mapping of Mars' North Seasonal Cap. Icarus, 154(1): 162-180.

[3] Smith, D.E., Zuber, M.T. and Neumann, G.A., 2001. Seasonal Variations of Snow Depth on Mars. Science, 294: 2141 – 2146.

[4] Kuroda, T., Medvedev, A.S., Kasaba, Y. and Hartogh, P., 2013. Carbon dioxide ice clouds, Snowfalls, and Baroclinic Waves in the Northern Winter Polar Atmosphere of Mars. Geophysical Research Letters, 40(8): 1484-1488.

[5] Pilorget, C., Forget, F., Millour, E., Vincendon, M. and Madeleine, J.B., 2011. Dark spots and cold jets in the polar regions of Mars: New clues from a thermal model of surface CO2 ice. Icarus, 213(1): 131-149.

[6] Kaufmann, E. and Hagermann, A., 2017. Experimental investigation of insolation-driven dust ejection from Mars' CO2 ice caps. Icarus, 282: 118-126

[7] Kaufmann, E. and Hagermann, A., 2015. Penetration of Solar Radiation into Pure and Mars-Dust Contaminated Snow. Icarus, 252: 144-149

[8] Brown, B.H. and Matson, D.L., 1987. Thermal Effects of Insolation Propagation into the Regoliths of Airless Bodies. Icarus, 72: 84-94.

[9] Fanale, F.P., Salvail, J.R., Matson, D.L. and Brown, B.H., 1990. The Effect of Volume Phase Changes, Mass Transport, Sunlight Penetration, and Densification on the Thermal Regime of Icy Regoliths. Icarus, 88: 193-204.

EPSC Abstracts
Vol. 11, EPSC2017-231, 2017
European Planetary Science Congress 2017

Evolution studies of the Niger Vallis outflow channel, Mars: Preliminary results based on CTX and HiRISE data

S. Kukkonen (1,2) and V.-P. Kostama (1)
(1) Astronomy Research Unit, P. O. Box 3000, FI-90014 University of Oulu, Finland (soile.kukkonen@oulu.fi, petri.kostama@gmail.com) (2) Arctic Planetary Science Institute, Rovaniemi, Finland.

Abstract

Niger Vallis is one of the four major outflow channels which cut the volcanic and sedimentary emplacements of the eastern Hellas rim region of Mars. As it is assumed that the channels were carved by water and later resurfaced by ice-related deposits, the channels represent a significant stage in both the fluvial and glacial history of Mars.

In this work we present our preliminary mapping and crater count dating results measured for the Niger Vallis outflow channel.

1. Introduction

The eastern rim region of the Hellas basin of Mars is characterized by the large outflow channel systems Dao, Niger, Harmakhis, and Reull Valles. The channels likely formed during the Hesperian period when the subsurface volatiles in their source regions were mobilized and released due to activation of the nearby volcanoes (e.g. [1–4]).

The Dao, Harmakhis, and Reull channels have been the subject of numerous studies at various scales (e.g. [4–8]). Dao's tributary Niger Vallis, however, has received less attention. In this work we present our preliminary results concerning the mapping and crater count dating of the floor units of Niger Vallis. The purpose of the study is to outline the role of Niger Vallis in the formation of the eastern Hellas outflow channels and in the Martian climate history.

2. Data and methods

This work is based on MRO's CTX (~5 m/pixel) and HiRISE (~0.3–0.5 m/pixel) datasets. All the image data were imported onto a GIS environment, where the floor units of Niger Vallis were mapped. In crater count dating, the established crater count methods [9–11] and the Craterstat software were used [12].

3. Geology of Niger Vallis

Niger Vallis differs from the other eastern Hellas outflow channels by being a clearly shallower, but also branched and discontinuous channel (Figure 1). The system begins at the topographic level of ~ –4 km, ~1.5 km higher than Dao and Harmakhis Valles [4]. Based on its morphology, Niger can be divided into two parts. The upper part consists of two branches that both begin from the well-defined and closed depressions Peraea and Ausonia Cavi, which apparently represent the source areas of the Niger system [4]. The branches themselves, however, are poor in their morphology. Their surface has sunk indicating that the branches have been modified mainly by subsurface activity. In places, the branches are characterized by circular depressions which may be a collapsed surface or ancient impact craters that the channels have utilized to run towards the lower topography. The depressions are covered by the lineated valley fills (e.g. [13]) which originate from the depression walls. When the northern and southern branches finally connect, the northern branch seems to cut the southern one thus postdating its formation.

While upper Niger has a very featureless appearance, lower Niger is deep and steep-sided; ergo modified by on-surface activity. Lower Niger is, however, also very fragmented. It consists of separate collapse basins, which are connected by narrower channels. The surface is mainly covered by lineated valley fills, although uncovered parts can also be observed. On other nearby outflow channels, similar uncovered floor has been typically interpreted as an original channel surface [6–8]. In the case of Niger Vallis, however, the uncovered units are clearly more extensive and their texture radically differs from that found on Harmakhis and Reull Valles, for example. In contrast to the very plain units of Harmakhis and Reull, the material on Niger Vallis seems to be more hummocky. On Niger, the uncovered units also have

ridges which indicate that they have been modified by compressional folding and faulting (e.g. [14], (Figure 2). In addition, some of the units show evidence of ice-sublimation, implying that the units may, however, contain ice. We measured an age of ~3.5 Ga and several resurfacing ages for the uncovered units (Figure 1). The oldest age corresponds with the ages measured for Ausonia (~3.9 Ga) and Peraea (~3.4 Ga) Cavi [5]. The lineated valley fill deposits, in turn, show ages of <200 Ma. Due to the strong modification the units have experienced because of their ice-related nature, the ages are, however, just younger deadlines for the formation of the deposits. The older deadlines may be related to the time range of 210–440 Ma when the uncovered units resurfaced. This time scale is also consistent with the formation of lineated valley fills on Dao and Harmakhis Valles [7–8].

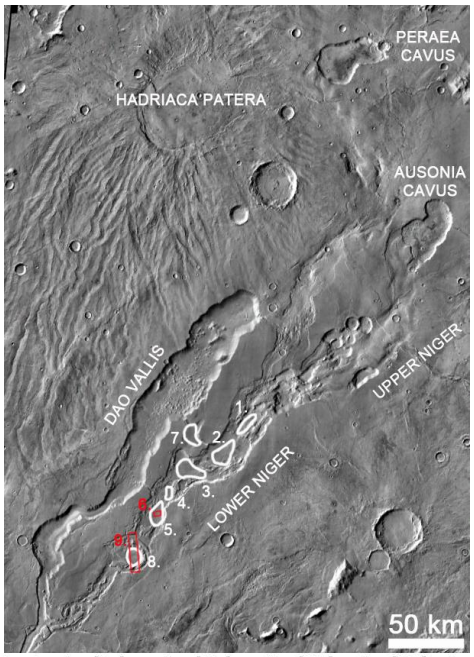

No	Dataset	Age [Ga]	Age [Ma]	Age [Ma]	Age [Ma]	Age [Ma]
1	CTX		370 (± 100)		42 (± 9)	12 (± 2)
2	CTX	3.5 (+0.1/-1)	440 (± 100)	140 (± 30)	65 (± 10)	17 (± 2)
3	CTX	1.1 (± 0.2)	210 (± 30)		38 (± 3)	11 (± 0.6)
4	CTX	3.2	250 (± 70)		53 (± 8)	10 (± 0.9)
5	CTX		310 (± 60)			
6	HiRISE		300 (± 90)		21 (± 5)	5.8 (± 0.5)
7	CTX		220 (± 60)	68 (± 10)	30 (± 4)	
8	CTX			60 (± 20)	40 (± 8)	12 (± 1)
9	HiRISE					12 (± 3)

Figure 1: Preliminary crater count results for Niger Vallis. Areas 1–6 represent the uncovered, possibly original floor of the channel, whereas the areas 7–9 are covered by lineated valley fills. The CTX-scale counting areas are outlined in white and the HiRISE-scale areas in red.

4. Conclusion

The formation of Niger seems to have started from Ausonia Cavus, when the southern branch of Niger was carved due to the subsurface activity. This was followed by the formation of the northern branch from Peraea Cavus. The main activity on the lower Niger ended ~3.5 Ga ago, after which the channel probably resurfaced ~1.1 Ma ago. The next significant resurfacing phase ended ~210–440 Ma ago. The resurfacing event may be also related to the formation of ice-rich lineated valley fill deposits, which cover now the major parts of lower Niger.

Acknowledgements

S.K. is sincerely grateful to Academy of Finland for funding this study.

References

[1] Baker, V., University of Texas Press, 1982. [2] Squyres, S. et al., Icarus, 70, 385–408, 1987. [4] Price, K., USGS Map I–2557, 1998. [3] Kostama, V.-P. et al., EPSL, 294, 321–331, 2010. [4] Bleamaster, L. and Crown, D., USGS Map I–3096, 2010. [5] Musiol, S. et al., JGR, 116, E08001, 2011. [6] Kostama, V.-P. et al., PSS, in press, 2017. [7] Korteniemi, J. and Kukkonen, S., 44th LPSC, #2815, 2013. [8] Kukkonen, S. and Kostama V.-P., DPS meeting #48, id.426.09. [9] CATWG, Icarus, 37, 467–474, 1979. [10] Ivanov B., Space Sci. Rev. 96, 87–104, 2001. [11] Hartmann W. K. and Neukum G., Space Sci. Rev. 96, 165–194, 2001. [12] Michael G. and Neukum G., EPSL, 294, 223–229, 2010. [13] Morgan G.A. et al., Icarus, 202(1), 22–38, 2009. [14] Golombek M.P. et al., JGR, 106, 23811–23821, 2001.

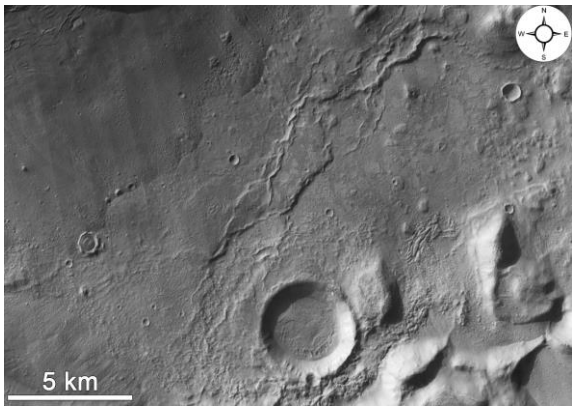

Figure 2: CTX detail of smooth but ridged deposits on the Niger Vallis floor. The deposits may be remnants of the original Niger surface.

EPSC Abstracts
Vol. 11, EPSC2017-249, 2017
European Planetary Science Congress 2017

Laboratory hyperspectral studies of ice/regolith associations. Application to icy surfaces on Mars.

Z. Yoldi, A. Pommerol, O. Poch, R. Cerubini and N. Thomas.
Physikalisches Inst., University of Bern, Sidlerstrasse 5, CH-3012 Bern, Switzerland (zurine.yoldi@space.unibe.ch)

1. Context

Ices are ubiquitously present on Mars. Whether it is in the form of H_2O or CO_2, they are found at almost all latitudes over the atmosphere and surface of the red planet. Depending on the surface and atmospheric conditions −temperature, pressure and humidity, ice will appear under various forms and will therefore interact in different ways with the substrate, i.e the regolith. From stable and seasonal polar caps to low latitude diurnal-cycled frosts [1, 2] through high-latitude covered permafrost [3]. When it comes to its detection and quantification, this variety is also a challenge. Spectral or colour imaging and reflectance spectrometry stand out as the techniques needed to *i)* detect the ice on the surface, *ii)* characterize its association mode with the regolith (grains, frost, slab…) and *iii)* determine the ice concentration. Both global and local coverages are important; on one hand, near-global coverage such as the one provided by the OMEGA spectrometer [4] and the stereo camera HRSC [5] are key to understand the big picture and to identify scientific targets. On the other hand, the higher resolution provided by the spectrometer CRISM [6] and colour cameras HiRISE and CaSSIS [7, 8], is crucial to study local phenomena. Currently inserted into Mars orbit and about to start the aerobraking phase, the ESA's Trace Gas Orbiter (TGO) transports the Colour and Stereo Surface Imaging System (CaSSIS), with four colour bands (475nm (BLUE), 650nm (PAN), 850 nm (NIR) and 950nm (IR)). CaSSIS will complement the data of other cameras thanks to the non-Sun-synchronous orbit of TGO around Mars and the high signal-to-noise ratio of the instrument, which will allow us to observe in good conditions not only seasonal phenomena but also diurnal ones, such as H_2O and CO_2 frosts.

Laboratory measurements are essential for the interpretation of these data. We study whether visible and near-infrared spectro-photometric signatures can help us identifying water frost from orbit or for example, distinguishing between water adsorption by the regolith and frost deposition on it. Through hyperspectral imaging we analyze the spectra and colour of well-known and characterized samples, which allows us to recognize signatures associated to different ice-soil association modes, for instance intimate or areal mixtures. We have carried out a campaign of measurements covering a wide range of parameters of interest (ice/soil ratio, association mode, H_2O/CO_2 ice) and analyzed their spectra to identify key features. At the same time, we simulate the colours of our samples as would be seen by CaSSIS, characterizing their different signatures depending on their nature. This enables us, among others, to assess the filter combinations that will be more efficient to use for different CaSSIS targets, that is, which filters should be used when it comes to detect and characterize ice, minerals, etc.

2. Samples and experiments

The measurements have been carried out in the LOSSy at the University of Bern, using our simulation chamber SCITEAS [9] and according to the various ice production methods that we have developed through time [9, 10]. We have produced samples with particulate water ice of different grain sizes, mixed with different ratios Mars soil analogues and ices, deposited water frost over Mars analogue surfaces (JSC Mars-1, [11]) as well as studied CO_2 ice signatures. Hyperspectral imagery implies that for every pixel imaged, a full spectrum between 0.38 and 2.4 μm is available. For each experiment, a color analysis is also carried out (Fig 2).

We will present the results of our campaign. Average spectra will be shown, such as the example in Fig 1, where we can see the spectra of CO_2 ice for different particle sizes and how our samples are contaminated with water frost depending on their size. Also colour simulations such as Fig 2, where CaSSIS filters are combined to obtain the best combination to discern water ice from JSC Mars-1. A series of spectral and colour analyses will be presented along with the consequences for ice detection from orbit.

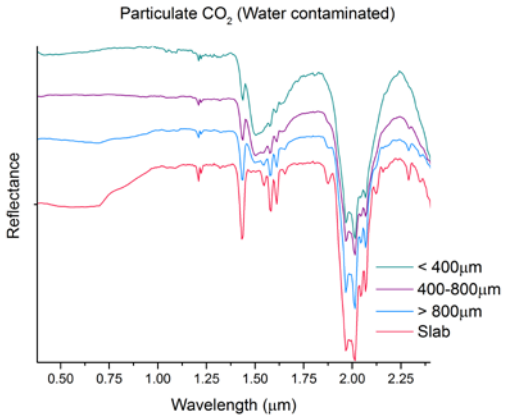

Figure 1. Slab and particulate CO_2 ice contaminated by H_2O. Smaller CO_2 particles have cold-trapped water from the atmosphere. The slopes between 0.7 and 1.0 μm on the >800μm and slab spectra are measurement artefacts.

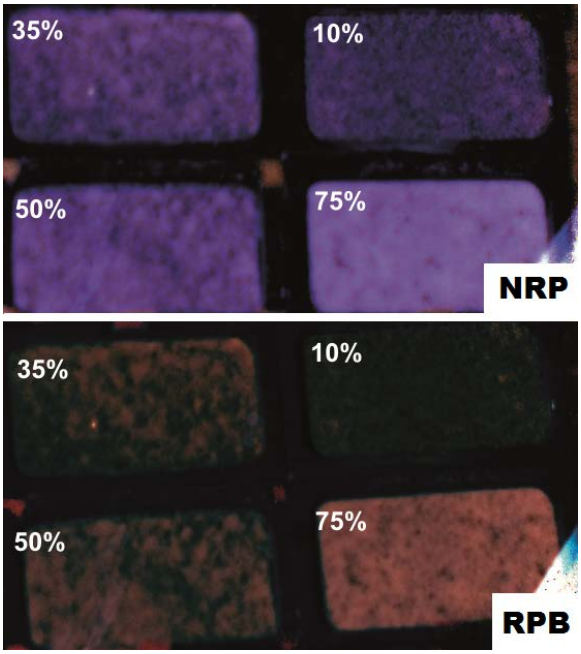

Figure 2. Different weight % of ice (marked next to each sample). RGB composites of CaSSIS Near-Red-Pan filters (on top) and Red-Pan-Blue (on bottom).

Acknowledgements

The team from the University of Bern is supported through the Swiss National Science Foundation and through the NCCR PlanetS.

References

[1] Piqueux, S., et al, 2016. Discovery of a widespread low-latitude diurnal CO2 frost cycle on Mars, J. Geophys. Res. Planets, 121, 1174–1189, doi:10.1002/ 2016JE005034.

[2] Smith, P. H. et al., 2009. H2O at the Phoenix Landing Site. Science Vol 325

[3] Mangold, N., P. et al 2002, Experimental and theoretical deformation of ice– rock mixtures: Implications on rheology and ice content of Martian permafrost, Planet. Space Sci., 50, 385– 401, doi:10.1016/S0032-0633(02)00005-3.

[4] Bibring, J.-P., et al. 2004, OMEGA: Observatoire pour la Minéralogie, l'Eau, les Glaces et l'Activité, in Mars Express: the Scientific Payload, edited by A. Wilson and A. Chicarro, ESA Spec. Publ., ESA SP‐1240, 37–49.

[5] Jaumann. R., et al. (2006) The high-resolution sterei camera (HRSC) experiment on Mars Express: Instrument aspects and experiment conduct from interplanetary cruise through the nominal mission. Planetary and Space Science. https://doi.org/10.1016/j.pss.2006.12.003.

[6] Murchie. S, et al. 2007. Compact Reconnaissance Imaging Spectrometer for Mars (CRISM) on Mars Reconnaissance Orbiter (MRO). Journal of Geophysical Research. doi:10.1029/2006JE002682.

[7] McEwen S. A., et al. 2007. Mars Reconnaissance Orbiter's High Resolution Imaging Science Experiment (HiRISE). Journal of Geophysical Research. doi:10.1029/2005JE002605.

[8] Thomas, N. et al, 2016. The colour and stereo surface imaging system for ESA's trace gas orbiter. LPSC 47.

[9] Pommerol., A. et al., 2015a. The SCITEAS experiment: Optical characterizations of sublimating icy planetary analogues. Planetary and Space Science, http://dx.doi.org/10.1016/j.pss.2015.02.004i

[10] Poch, O. et al., 2016. Sublimation of ice–tholins mixtures: A morphological and spectrophotometric study.Icarus, http://dx.doi.org/10.1016/j.icarus.2015.11.006

[11] Allen C.C., et al., 1998. JSC MARS-1: A Martian Soil Simulant. Space, 469–476. DOI:10.1061/9780784403396

EPSC Abstracts
Vol. 11, EPSC2017-260, 2017
European Planetary Science Congress 2017

Formation of recurring slope lineae on Mars by rarefied gas-triggered granular flows

F. Schmidt (1), F. Andrieu (1), F. Costard (1), M. Kocifaj (2,3) and A. G. Meresescu (1)
(1) GEOPS, Univ. Paris-Sud, CNRS, Université Paris-Saclay, Rue du Belvédère, Bât. 504-509, 91405 Orsay, France (2) ICA, Slovak Academy of Sciences, Dubravska Road 9, 845 03 Bratislava, Slovak Republic (3) Faculty of Mathematics, Physics, and Informatics, Comenius University, Mlynska dolina, 842 48 Bratislava, Slovak Republic (frederic.schmidt@@u-psud.fr)

Abstract

Recurring Slope Linae or RSL are seasonal dark features appearing when the soil reaches its maximum temperature. They appear on various slopes at the equator of Mars, in orientation depending on the season. Today, liquid water related processes have been promoted, such as deliquescence of salts. Nevertheless external atmospheric source of water is inconsistent with the observations. Internal source is also very unlikely. We take into consideration here the force occurring when the sun illuminates granular soil in rarefied gas conditions to produce a Knudsen pump. This process significantly lowers the angle of repose of sandy material. Hence, relatively low slope could start to flow. RSL seems to originate from rough terrains and boulders. We propose that the local shadows due to boulders over the soil, is the triggering phenomena. In this case, the Knudsen pump is magnified and could lead to flow. This new exotic dry process involving neither water nor CO2 and is consistent with the seasonal and facet's orientation appearance of RSL.

1. Introduction

The temperature and solar irradiation dependence has been recognized very early, and has been mainly interpreted as an effect of humidity [1, 2]. Indeed, RSL activity occurs in the closest point to liquid water in the phase diagram, at present time on Mars [3]. Various sources of liquid water have been discussed: subsurface aquifers, melting of subsurface ice, deliquescence of salt recharged by atmospheric water [4].

Nevertheless, the location of RSL is near the equator where atmospheric water vapor is at the lowest [5]. Also, the surface condensation of atmospheric water ice rarely occurs and subsurface ice is not stable. The source of water seems still a mystery because an internal source, such as a subsurface aquifer, has also been excluded near the crater rim [3]. In addition, the actual amount of atmospheric water required to re-charge the RSL's source each year seems not sufficient. The precise thermal calculations using THEMIS measurement instrument show no evidence of liquid water [6] and there is no direct evidence of liquid water from CRISM, but only indirect detection [4].

We propose here a re-interpretation of the RSL features and a new process to explain the RSL activity without involving any volatiles. This process aims to reconcile all available data. We put forward that the photophoretic effect, triggered by the sun radiation, modifies seasonally the angle of repose of the granular material. Since the slopes of granular material are stable near 30°, even a minor change in the angle of repose due to the air flux in the porous space of the soil could significantly change the stability.

2. Method

Knowing the direct solar flux, the one scattered by the atmosphere, and the thermal infrared flux from the Mars Climate Database [7], we estimate the incoming energy fluxes on various facet. By using these values as boundary conditions on a precise thermal surface balance model [8,9], we aim at estimating the Knudsen pump effects on one particular RSL site: Garni crater. Each facet is computed for a slope of 30° and different orientation, throughout all the seasons.

3. Results

Figure 1 shows the angle of repose of a granular material, modified by the natural pump. Without this pumping effect, the angle of repose remains constant though time with a values ~30°. With regular pumping effect, there is only very few changes in the angle of repose.

Figure 2 shows the same for an enhanced pump due to the shadowing of a boulder. Here we show that the switch off of direct solar irradiation considerably lowers the angle of repose, but also varies along the solar cycle. Figure 2 also superposes the activity observed in Garni carter [3]. Flows activity occurs always in period of low repose angle. The proposed mechanism has a good agreement between activity and low period of angle of repose.

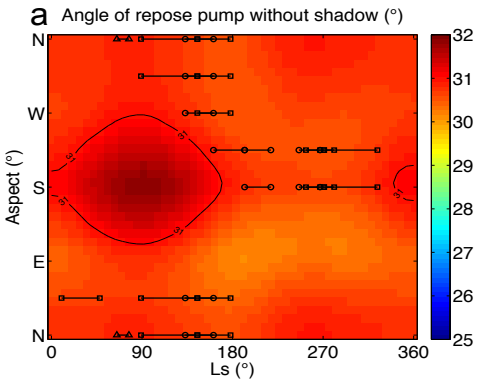

Figure 1: Angle of repose, modified by the Knudsen pump effect, as a function of slope aspect and season for the regular pump. Black lines represents the RSL activity observed at Garni crater. Each activity is encompassed by two images: before and after.

4. Conclusion

We propose an original mechanism for RSL as a result of a dry natural pump within the granular soil [10]. This mechanism is exotic and can't occur on Earth due to high-pressure level. On Mars, our model suggests that the Knudsen pump is efficient enough to trigger a flow in accordance with observed seasonality of RSL. Since the equator of Mars is most probably volatiles depleted, this mechanism should be considered as good candidate to explain RSL features. In this case, liquid water may not be present on Mars at present time.

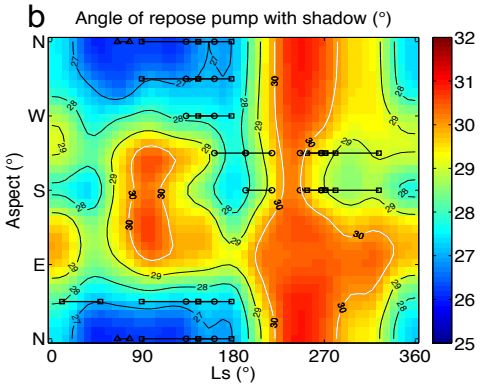

Figure 2: Idem figure 1, expect for the enhanced pump.

References

[1] McEwen, A. S., et al. (2011), Science, 333, 740-743 [2] McEwen, A. S., et al. (2014), Nature Geoscience, 7, 53-58 [3] Chojnacki, M., et al. (2016), Journal of Geophysical Research: Planets, 121, 1204-1231 [4] Ojha, L., et al. (2015), Nature Geoscience, 8, 829-832 [5] Smith, M. D. (2002), JGR, 107, 5115- [6] Edwards, C. S. & Piqueux, S. (2016), GRL, 43, 8912-8919 [7] Lewis, S. R., et al. (1999), JGR, 104, 24177-24194 [8] Kocifaj, M., et al. (2010), Monthly Notices of the Royal Astronomical Society [9] Kocifaj, M., et al. (2011), Icarus, 211, 832-838 [10] Schmidt., F. et al. (2017), Nature Geoscience, 10, 270-273

EPSC Abstracts
Vol. 11, EPSC2017-279, 2017
European Planetary Science Congress 2017

Evolution of organic molecules under Mars-like UV radiation conditions in space and laboratory

Rouquette, L. laura.rouquette@lisa.u-pec.fr (1), Stalport F. fabien.stalport@lisa.u-pec.fr (1), Cottin H. herve.cottin@lisa.u-pec.fr (1), Coll P. patrice.coll@lisa.u-pec.fr (1), Szopa C. cyril.szopa@latmos.ipsl.fr (2,3), Saiagh K. kafila.saiagh@lisa.u-pec.fr (1), Poch O. olivier.poch@csh.unibe.ch (1), Khalaf D. diana.khalaf@gmail.com (1), Chaput D. didier.chaput@cnes.fr (4), Grira K. katia.grira@lisa.u-pec.fr (1), Dequaire T. tristan.dequaire@lisa.u-pec.fr (1)
(1) Laboratoire Interuniversitaire des Systèmes Atmosphériques (LISA) CNRS-Univ Paris Diderot and Paris Est Créteil, Créteil France. (2) Laboratoire Atmosphère, Milieux, Observations Spatiales (LATMOS) CNRS-Univ Pierre et Marie Curie and Versailles Saint-Quentin-en-Yvelines (3) Institut Universitaire de France (4) Centre National d'Etudes Spatiales (CNES)

Abstract

The detection and identification of organic molecules at Mars are of prime importance, as some of these molecules are life precursors and components. While *in situ* planetary missions are searching for them, it is essential to understand how organic molecules evolve and are preserved at the surface of Mars. Indeed the harsh conditions of the environment of Mars such as ultraviolet (UV) radiation or oxidative processes could explain the low abundance and diversity of organic molecules detected by now [1].

In order to get a better understanding of the evolution of organic matter at the surface of Mars, we exposed organic molecules under a Mars-like UV radiation environment. Similar organic samples were exposed to the Sun radiation, outside the International Space Station (ISS), and under a UV lamp (martian pressure and temperature conditions) in the laboratory.

1. The EXPOSE R2 experiment

The EXPOSE R2 facility has been placed in low Earth orbit (LEO) under Solar radiation, outside the International Space Station (ISS) in 2014. One of the EXPOSE R2 experiment, called PSS (Photochemistry on the Space Station), is dedicated to astrobiology- and astrochemistry-related studies. Part of PSS samples have been dedicated to the study of the evolution of organic molecules under Mars-like surface radiation conditions. Organic samples have been exposed directly to the Sun under KBr filters (UV transmission >200 nm) from November 2014 to February 2016, mimicking the UV radiation conditions of the surface of Mars. Four types of samples were exposed in the form of thin layers of solid molecules: adenine, adenine with nontronite (a clay mineral detected on Mars), chrysene and glycine with nontronite.

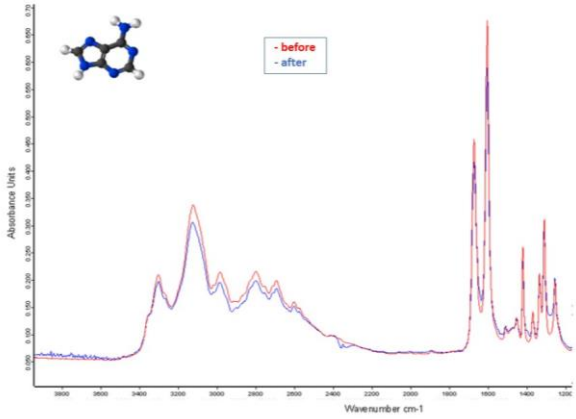

Figure 1: IR spectrum of a thin film of adenine before (in red) and after (in blue) being exposed on the International Space Station.

To characterize the evolution of our samples under irradiation, analyses by infrared spectroscopy (IRTF) were performed, before the launch of EXPOSE R2 to the ISS in 2014, and after the exposure in space and the return on Earth, this year (see figure 1). These analyses allowed determining whether each molecule is preserved or photodegraded, and if so, its photolysis rate. The effect of nontronite on organic molecules preservation has been investigated as well. We also compared these results from LEO with laboratory data.

2. The MOMIE lab experiment

The MOMIE (Mars Organic Matter Irradiation and Evolution) experiment has been set up to study the evolution or organic matter under martian radiation within the laboratory [2] [3]. Organic samples, under the form of thin films, are in this case exposed under a UV lamp (200-400 nm). Adenine, adenine with nontronite, chrysene and glycine were also studied in this experiment, allowing us to compare their evolution with the results in LEO, followed by other molecules such as uracil.

To characterize the evolution of our samples, analyses by infrared spectroscopy (IRTF) are also performed all along the irradiation. Thus, we are able to follow the sample photodegradation and the possible formation of new products at any time.

3. Conclusions

Concerning the search for organic molecules at Mars, mimicking martian radiation conditions in space and in the laboratory has been the best way to understand and interpret *in situ* results so far. In both experiments, organic molecules tend to photodegrade under Mars-like UV radiation. Minerals, depending on their nature, can protect or accelerate the degradation of organic molecules. For some molecules, new products, possibly photoresistant, seem to be produced. Finally, experimenting in space allow us to get close to *in situ* conditions and to validate our laboratory experiment while the laboratory experiment is essential to study the evolution of a large amount and diversity of organic molecules.

References

[1] Patel, M.R., Zarnecki, J.C., and Catling, D.C. (2002) Ultraviolet radiation on the surface of Mars and the Beagle 2 UV sensor. *Planet Space Sci* 50:915–927.

[2] Poch O., Noblet A., Stalport F., Correia J. J., Grand N., Szopa C., Coll P., Chemical evolution of organic molecules under Mars-like UV radiation conditions simulated in the laboratory with the "Mars Organic Molecules Irradiation and Evolution" (MOMIE) setup, *Planetary and Space Science*, 85, 188-197, 2013.

[3] Poch O., Kasi S., Stalport F., Szopa C., Coll P., Laboratory insights into the chemical and kinetic evolution of several organic molecules under simulated Mars surface UV radiation, *Icarus*, 242, 50-63, 2014.

EPSC Abstracts
Vol. 11, EPSC2017-300-1, 2017
European Planetary Science Congress 2017

A global permittivity map of the Martian surface from SHARAD and some geological correlations

J. Gurgurewicz (1,2), L. Castaldo (1), D. Mège (2,3), R. Orosei (4) and G. Alberti (5)
(1) Institute of Geological Sciences, Polish Academy of Sciences, Research Centre in Wrocław, Poland, (2) Space Research Centre, Polish Academy of Sciences, Warsaw, Poland, (3) Laboratoire de Planétologie et Géodynamique, CNRS UMR 6112, Université de Nantes, France, (4) Istituto di Radioastronomia, Istituto Nazionale di Astrofisica, Bologna, Italy, (5) Consorzio di Ricerca sui Sistemi di Telesensori Avanzati, CO.RI.S.T.A., Napoli, Italy (jgur@cbk.waw.pl / Fax: +48228403131)

Introduction

We present the first global SHARAD permittivity map of the Martian surface and discussion on geological correlations. The SHARAD synthetic-aperture, orbital sounding radar carried by NASA's Mars Reconnaissance Orbiter, is capable of detecting dielectric discontinuities in the subsurface caused by compositional and/or structural changes. It can inform on the average permittivity over a thickness up to 15 meters below the surface, depending on the material being sounded. The signal is strongly affected by the presence of intersticial water, and, more generally, can help discriminate between rock types. SHARAD data are therefore helpful to constrain the geology of a given area when complementing other datasets.

SHARAD permittivity map

A model has been developed to estimate the effect of surface roughness on echo power, depending on statistical parameters such as RMS height and topothesy. The model is based on the assumption that topography can be characterized as a self-affine fractal, and its use makes possible to estimate the dielectric properties of the first metres of the Martian soil. Methodological details are described in [1].

The SHARAD global permittivity map of Mars after RMS height correction is presented on Figure 1. Figure 2 gives the absolute error based on the dispersion of estimates within the same map resolution cell [1]. The permittivity of non-porous CO_2 ice is 2.1, that of non-porous water ice is 3.1, while that of igneous rocks, such as those found on the Martian surface, ranges between 4 and 10, depending both on composition and porosity [4].

Geological correlations

Regions where the SHARAD permittivity map is especially helpful in constraining geology when checked against other datasets (visible imagery, gamma-ray spectroscopy, MARSIS/MEx permittivity map) include, for instance, the dichotomy boundary, lava flows associated with the huge Elysium Mons volcanic shield, and ice-filled craters in the Martian arctic [1].

Results and conclusion

The dichotomy boundary is accurately followed by SHARAD permittivity contrasts, with higher permittivity south of the boundary. The latitudinal banding observed on GRS hydrogen abundance data is not reproduced, suggesting that the ice-rich 1 m thick surface layer might not be representative of deeper ice distribution. The permittivity boundary does not either follow the permittivity boundary of MARSIS, which gives permittivity averaged over tens of meters, suggesting the dichotomy boundary is not a clear vertical plane, or that MARSIS might not image the same feature (Figure 1).

Although SHARAD does frequently not give exploitable results on the major shield volcanoes, in some instances lava flows can be distinguished, perhaps due to different thickness or alteration.

The permittivity of Korolev and Dokka, two large high-latitude ice-filled impact craters, is significantly higher than the permafrost-rich surrounding lowlands, which could be related to the existence of snow dunes in these craters.

These examples illustrate how permittivity derived from SHARAD can be used to constrain the subsurface geology inferred from other data sources.

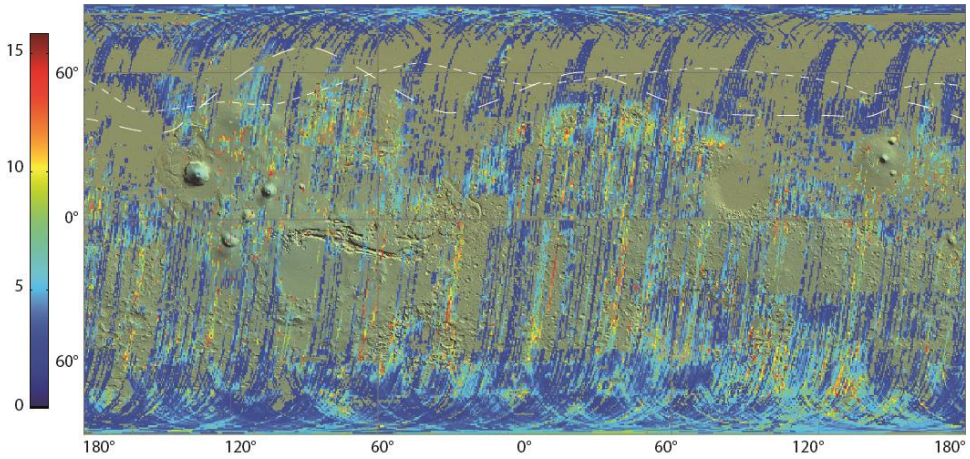

Figure 1: SHARAD global permittivity map of Mars after RMS height correction [1]. The line with long dashes indicates the MARSIS dielectric boundary (6-7) between the highlands and lowlands [2]. The line with short dashes indicates the boundary between mid-latitude areas in the northern hemisphere having equivalent hydrogen abundance < 8% (south) and > 8% (north) after GRS [3].

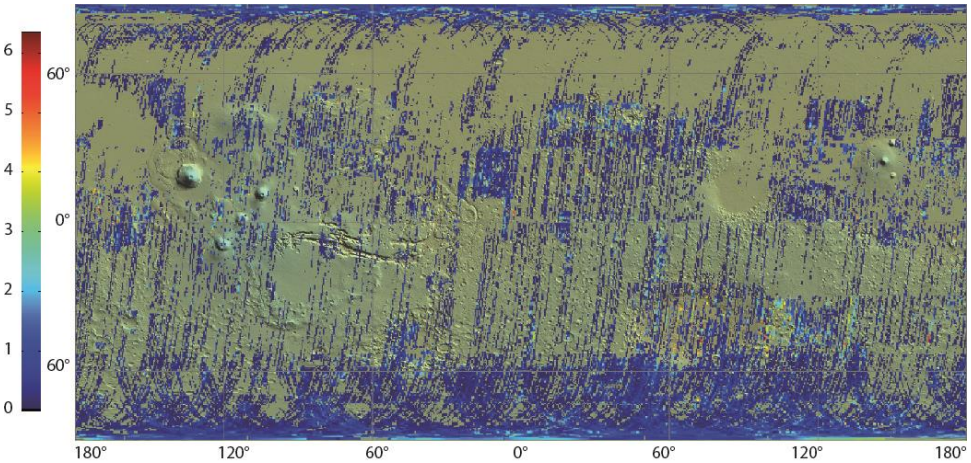

Figure 2: Permittivity standard deviation after RMS height correction [1].

Acknowledgements

This work was supported by the TEAM programme of the Foundation for Polish Science (project TEAM/2011-7/9), co-financed by the European Union within the framework of the European Regional Development Fund.

References

[1] Castaldo, L., Mège, D., Gurgurewicz, J., Orosei, R., and Alberti, G.: Global permittivity mapping of the Martian surface from SHARAD, Earth Planet. Sci. Lett., Vol. 462, pp. 55-65, 2017.

[2] Mouginot, J., Pommerol, A., Kofman, W., Beck, P., Schmitt, B., Hérique, A., Grima, C., and Safaeinili, A.: The 3–5 MHz global reflectivity map of Mars by MARSIS/Mars Express: implications for the current inventory of subsurface H2O, Icarus, Vol. 210, pp. 612–625, 2010.

[3] Feldman, W.C., Prettyman, T.H., Maurice, S., Plaut, J.J., Bish, D.L., Vaniman, D.T., Mellon, M.T., Metzger, A.E., Squyres, S.W., Karunatillake, S., Boynton, W.V., Elphic, R.C., Funsten, H.O., Lawrence, D.J., and Tokar, R.L.: Global distribution of near-surface hydrogen on Mars, J. Geophys. Res., Vol. 109, E09006, 2004.

[4] Rust, A.C., Russell, J.K., and Knight, R.J.: Dielectric constant as a predictor of porosity in dry volcanic rocks, J. Volcanol. Geotherm. Res., Vol. 91, pp. 79–96, 1999.

EPSC Abstracts
Vol. 11, EPSC2017-333, 2017
European Planetary Science Congress 2017

Mars polar cliffs: stressed out and falling apart

S. Byrne (1), M.M. Sori (1), P. Russell (2), A. Pathare (3), P. Becerra (4), J. Molaro (5), S. Sutton (1), M.T. Mellon (6) and the HiRISE Team (1). (1) University of Arizona, Tucson, AZ, USA. (shane@lpl.arizona.edu) (2) UCLA, Los Angeles, CA, USA. (3) Planetary Science Institute, Tucson, AZ, USA. (4) Physikalisches Institut, Universität Bern, Bern, Switzerland. (5) Jet Propulsion Laboratory, Pasadena, CA, USA. (6) Southwest Research Institute, Boulder, CO, USA.

Abstract

Steep, icy, north polar cliffs are actively retreating through fracturing and blockfalls and are scoured clean of dust by avalanches each spring. We explain this activity through thermoelastic stresses.

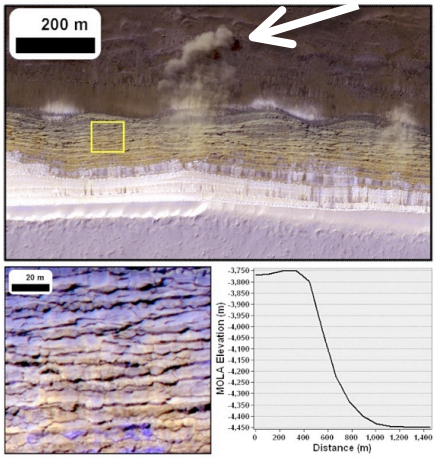

Figure 1. HiRISE image (PSP_007338_2640, L_s 34) of 70° scarp (MOLA topography at bottom right) at 84°N 235°E with avalanche (arrow) in progress [10]. Box shows location of scarp texture in bottom left.

1. Introduction

The martian North Polar Layered Deposits (NPLD) are a stack of contiguous layers of dusty water ice that record paleoclimate [1,2]. Dust content varies from layer to layer, but is minor overall [3,4].

Strong local effects on erosion and deposition patterns can be seen. Poleward-migrating spiraling troughs pervade the NPLD interior [5]. At the NPLD boundaries, steep scarps up to 800m in relief and 70° in slope (Figure 1) exist. These scarps typically overlie exposures of a sandy basal unit [6,7] and removal of this friable material may be undermining the NPLD and leading to their steepness. Their steep equatorward-facing orientation mean these cliffs defrost early and receive intense summertime insolation with a strong diurnal cycle and low incidence angles. In contrast to troughs in the NPLD-interior, steep scarps appear heavily fractured with jagged slab-like fragments (Figure 1) and lack the usual thick slumping dust covers [9].

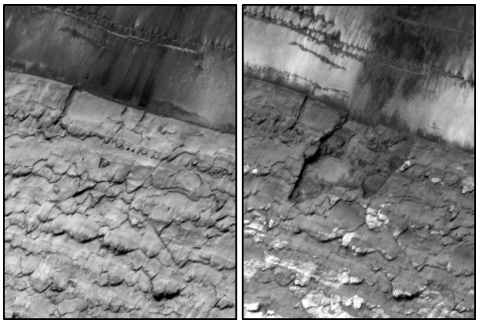

Figure 2. HiRISE images ESP_016292_2640 (left) and ESP_024639_2640 (right) show collapse of a 70m wide slab during MY30.

Fresh basal debris [8] is common and exfoliation of large slabs (Figure 2) indicates the prevalence of active sheeting joints in addition to surface-normal fractures. HiRISE observations show springtime (L_s 0–50°) dust/frost avalanches (Figure 1) are frequent [10]. The geometry of these icy scarps, and the absence of a thick dust cover suggest they are likely subject to high ablation rates. Springtime avalanches may scour these scarps of any thin dust lags acquired the previous summer. However, HiRISE color data show enough dust exists to darken their surfaces.

2. Thermo-mechanical Model

We simulated temperatures of the steep scarps with a standard 1D semi-implicit thermal diffusion model with radiative boundary conditions at the top surface and negligible heat flow from beneath. The steepness of these slopes means that they exchange reflected and emitted radiation with surrounding flat terrain as well as open sky. To account for this, we separately simulated the temperatures of the surrounding terrain

(assumed to be dark sand, albedo 0.15, thermal inertia [TI, MKS units] 225) to calculate the upwelling fluxes onto the scarp face. The thermophysical properties of the scarp itself were taken to be those of water ice at 200 K (TI 2130) overlain by a thin dust cover (albedo 0.25, TI 85). The thickness of this dust cover is a crucial controlling factor on the thermal behavior of the ice and also strongly affects the season at which the scarp losses its CO_2 frost cover. HiRISE shows a defrosted scarp at L_s 350°, so dust provides negligible insulation, although still affects albedo.

We follow the approach of [11] to solve for the time varying stress in a viscoelastic solid. No lateral strain can occur, so surface-parallel thermal expansion and contraction at each depth is opposed by elastic stresses on short timescales that viscously decay over longer timescales. Viscous strain rate is grain-size dependent, we use the Zenner pinning approach of [12] with NPLD dust abundances [3] to constrain ice grain sizes to be 10–1000 μm. Large summertime diurnal temperature oscillations cause surface stresses to vary by several MPa and alternate between extensional and compressive (Figure 3). Compressional stresses occur during warmer periods and are thus more effectively viscously relaxed than extensional stresses. Colder ice in winter allows for greater extensional stress.

3. Discussion

The tensile strength of water ice ranges from 1–2 MPa. Peak extensional stress at the surface exceeds this by an order of magnitude (Figure 3). Thus, these steep scarps cannot remain unfractured and cracks are expected to depths of 5–10 m. Opening of cracks can reduce extensional stress and the fracture spacing should decrease until all points on the scarp face are near enough to a crack to avoid further fracturing.

In addition, surface-parallel compression in concert with surface curvature can generate extensional stresses below (and normal to) the surface [13]. It is believed that this effect is responsible for large surface-parallel sheeting joints forming on terrestrial granitic domes. High compressional stresses on these martian scarps are relatively easy to generate, so only modest surface curvature is required to overcome the increasing pressure with depth [13]. Peak compressive stresses (Figure 3) occur in the upper few meters in spring, coinciding with the seasonality of (and potentially triggering) avalanche activity.

Fast viscous relaxation of these scarps is expected [14], but blockfalls (Figure 2) provide competition. A self-perpetuating cycle of dust-free steep cliffs causing thermoelastic fractures that drive avalanches and blockfalls has been established in these locales.

References

[1] Thomas et al., Mars, Univ. AZ Press, 1992. [2] Byrne, Ann. Rev. Earth & Planet. Sci., 2009. [3] Grima et al., GRL, 2009. [4] Lalich et al., GRL, 2017.[5] Smith et al., Nature, 2010. [6] Byrne & Murray, JGR, 2002. [7] Fishbaugh & Head, Icarus, 2005. [8] Fanara et al., 6th Intl. Mars Polar Conf., 2016. [9] Herkenhoff et al., Science, 2007. [10] Russell et al., GRL, 2008. [11] Mellon, JGR, 1997. [12] Durand et al., JGR, 2006. [13] Martel, GRL, 2011. [14] Sori et al., GRL, 2016.

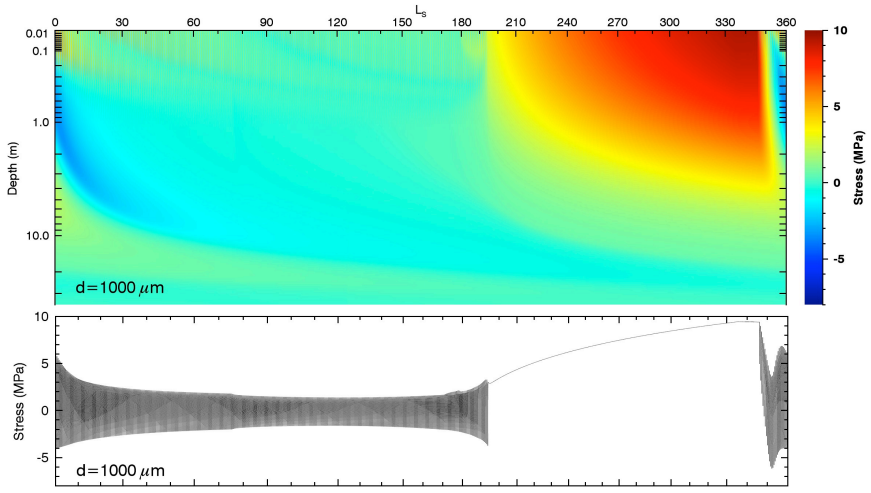

Figure 3. (Top) Thermoelastic stresses (positive is extension) on a southwest facing 70° slope as a function of depth and season. (Bottom) Stresses at the surface. Results shown for an ice grain size of 1mm. Stresses are similar for grains of 100 microns and a factor of several lower for grains of 10 microns.

EPSC Abstracts
Vol. 11, EPSC2017-372, 2017
European Planetary Science Congress 2017

Global Martian volcanism as a new interpretation of geological past of terrestrial bodies and moons in the Solar System

N. Zalewska (1,2)
(1) The Institute of Aviation, Warsaw, Poland (2) Space Research Center PAS, Poland (natalia.zalewska@ilot.edu.pl).

1. Introduction

Many papers and articles have been telling us for years about the (Late) Heavy Bombardment of Earth-type planets including our Moon. Numerous craters on these planets are considered traces of collisions with smaller celestial bodies. This theory has been around for years, since the exploration of space began. Besides, Jupiter's moons have such traces and even characteristic crater chains interpreted exclusively as traces of serial impacts of asteroids after fragmentation above the surface. But when we look at the volcanic cones and the various other volcanic forms on Earth, we also notice that craters, especially those that are inactive for millions of years, are strikingly similar to the conically formed domes and caldera craters on Mars [1] and terrestrial planets, additionally including moons of Jupiter and moons of other large planets as well as our Moon.

2. Comparison, analogues

The primary basaltic volcanism of hundreds of millions of years ago could produce very broad calderas because of very low viscosity (low Si content of ultramafic rocks: <5% assuming ~ 100 μm grains) [2], which bottom part collapsed in time after cooling, creating something that resembles a crater. Also, the center of volcanic crater, which stagnated last and after solidification formed a cone, which could have been interpreted as the central peak of the impact crater. Ring material from the caldera, instead of being interpreted as the edges of lava flows, is interpreted as ejecta-material thrown during the impact. Forms that we can compare them to on Earth are, for example: Lake Myvatn with its pseudo-craters located in volcanic active part of Iceland, underwater volcanoes in Hudson Bay, Pinacate Peaks in Mexico (Fig.1,3), Atlantic volcanism, Aleutian maars (large calderas), Hawaiian volcanoes, Pacific plate volcanoes in San Francisco and Crater Lake in Oregon. Volcanic forms we can observe are: pseudo-craters, scoria cones, maars, tuyas, guyots and lava domes. Many of these form under ice cover or at the bottom of the ocean. Similar forms are recognizable on Mars especially on its northern hemisphere. Isidis Planitia (Fig.2), Acidalia Planitia, Utopia Planitia and Amazonis Planitia (Fig.4) are densely dotted with cones and calderas. Latest study of LCP/HCP (low and high calcium pyroxene) from dust-free Mars sites show a relatively recent volcanism on Mars [3], [4].

3. Conclusions

The difference between the impact crater and the volcanic crater on terrestrial bodies can be very difficult to recognize because of close similarity between them, especially in morphology as well as the geometric distortion of images made by spectrometers in the nadir. In this case, the geochemistry and the degree of melting or lack there at the moment of impact must be taken into account. Whether krystobalite, trydymite, stiszovite, shocked varieties of quartz are found in the crater or not, will tell us which phenomenon occurred. This would require precise on site research using rovers.

References

[1] Greeley, R. and Spudis. P.: Volcanism on Mars, Reviews of Geophysics and Space Physics, Vol. 19, pp. 13-41, 1981.

[2] Sen, G.: Petrology, Introduction to Igneous Rocks, Springer, pp 19-49, 2014.

[3] Mangold N. et al. : Mineralogy of recent volcanic plains in the Tharsis region, Mars, and implications for platy-ridged flow composition, Earth and Planetary Science Letters Vol. 294, pp. 440-450, 2010.

[4] Trigo-Rodriguez, J, Rietmeijer, F., Llorca, J., Janches, D.: Advances in Meteoroid and Meteor Science, Springer, 2008.

Figure 1: Pinacate Mexico, image 2x2 km. The beginning of eruption 4 million years ago. Characteristic double caldera is in the center of the image. 31.756338 N, 113.496827 W

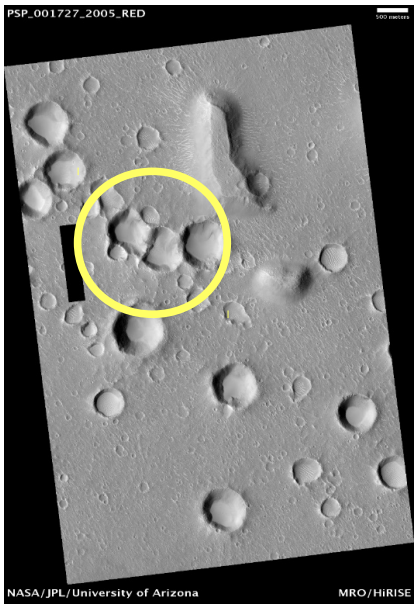

Figure 2: HiRISE PSP 001727_2005, Lat: 20.5° Long: 94.8°. Northern part of Isidis. Characteristic double calderas are in the center of the image. Calderas in the form of a maars on Isidis are probably not the result of an impact but of extensive volcanism.

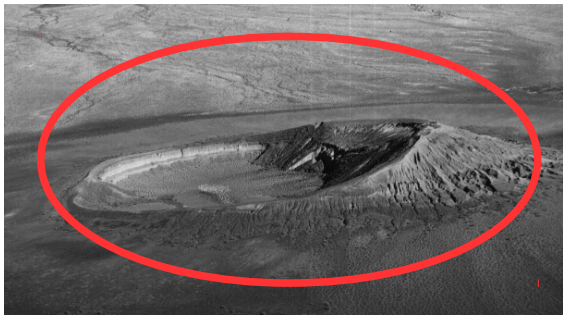

Figure 3: Cerro Colorado volcano Pinacate Crater in Mexico-irregular caldera, diameter 975 m, 31.916360 N, 113.299865 W

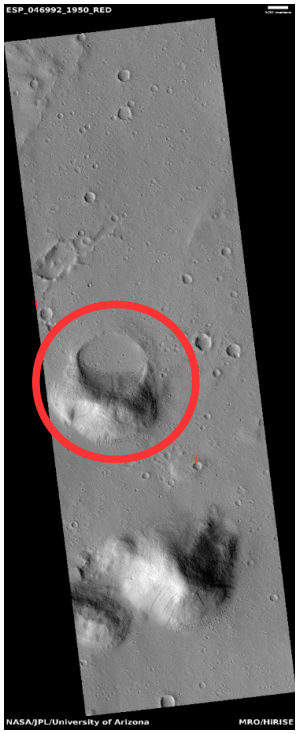

Figure 4: HiRISE ESP 046992_1950, Lat: 15° Long: 192.1°, Amazonis Planitia. In the middle of the image an irregular caldera is visible. The calderas are covered with dust. Forms are probably of volcanic origin.

EPSC Abstracts
Vol. 11, EPSC2017-378, 2017
European Planetary Science Congress 2017

Survival of perennial carbon dioxide ice caps on Mars

S. Byrne (1), P.O. Hayne (2), P. Becerra (3).

(1) University of Arizona, Tucson, AZ, USA. (shane@lpl.arizona.edu) (2) Jet Propulsion Laboratory, Pasadena, CA, USA. (3) Physikalisches Institut, Universität Bern, Bern, Switzerland.

1. Introduction

The southern residual ice cap (SRC) of Mars is composed in-part of high-albedo solid CO_2 [1]. It buffers the current atmosphere and probably stabilizes a buried CO_2 reservoir [2] at least 20 times its size. Yet this critical deposit is apparently being eroded at a prodigious rate calling into question the stability of the current martian climate [3]. Here, we tie observations of the SRC surface and overlying atmosphere by Mars Reconnaissance Orbiter (MRO) together with landscape evolution models that predict, not a stable cap, but rather one that waxes and wanes over timescales of ~10^2 years. Our results imply large dust storms provide a mechanism that allows regrowth of the cap and so play a crucial role in stabilizing the current climate.

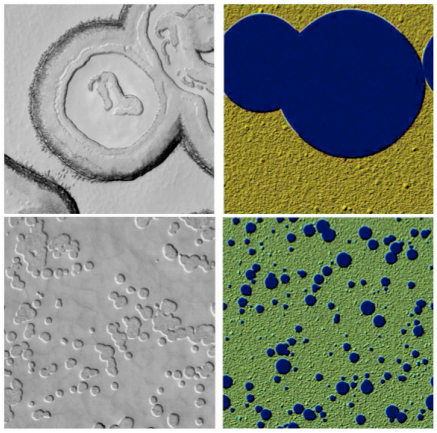

Figure 1. All panels are 1 km^2 and illuminated from the right. (Left) Two examples of SRC terrain with pit densities of ~1 and ~100 km^{-2}. (Right) DTMs (elevation scale in Fig. 2) of model results for higher (top) and lower (bottom) smoothing efficiencies.

CO_2 ice slabs within the SRC vary from 2-10 m thick [4-5]. The SRC has areas at its margins and in its interior where underlying water ice shows through [4-7]. It contains abundant flat-floored, quasi-circular pits (Figure 1) with a wide range of spatial densities [8]. The inclined walls of these pits retreat by several meters each year [3,5,9] leading [3] to suggest that the SRC is in the process of disappearing. However, a changing climate is unexpected as the orbit of Mars changes on much longer timescales. In contrast, other sections of the SRC lack these pits and show little change, but may be accumulating or ablating vertically. Only small changes in SRC extent have occurred in recent decades [10].

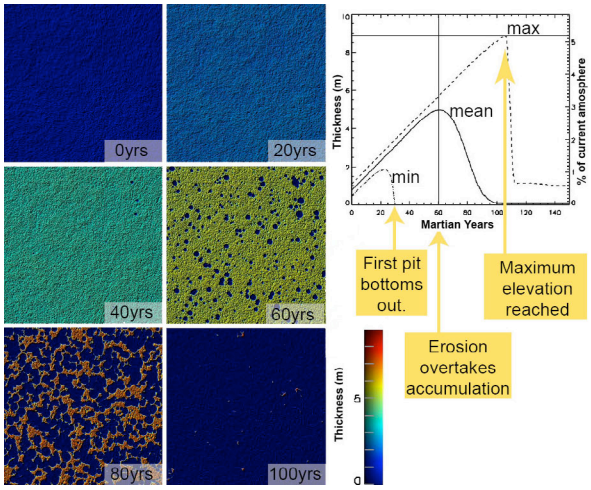

Figure 2. DTMs at times indicated of a typical model run of a CO_2 landscape. (Right) minimum, mean and maximum CO_2 ice thicknesses as a function of time.

2. Observations and Model Results

In our landscape evolution model CO_2 ice elevation falls or rises via ablation or condensation due to imbalances in surface energy budgets. In a typical model run (Figure 2), ice accumulation begins on a low-roughness surface; however, roughness increases with time. After about 30 years, pits begin to form and grow down to the water-ice basement. Over the following decades these pits expand laterally (by a few m/yr as observed [9]) even while the intervening flat surfaces continue to accumulate mass vertically. As the accumulation area (mesa-tops) shrinks, and the ablation areas (pit perimeters) grow, the landscape as a whole passes from a net-accumulation

to a net-ablation regime (Figure 2). Many SRC locales are close to the final state shown, where only isolated (and shrinking) mesas remain. This overall behavior is an inevitable consequence of starting with a surface that is not perfectly flat; CO_2 ice caps can never be stable indefinitely. Summertime exposure of the underlying water ice results in heat-storage and an inability for a perennial cap to recondense [11].

Understanding that surface roughness governs pit-initiation resolves how differing pit concentrations (Figure 1) occur. CO_2 snowfall up to a few tenths of the total seasonal surface CO_2 has been detected here by the Mars Climate Sounder [12]. In our model, recently-condensed surficial CO_2 ice can be mobilized by wind and is capable of infilling small-scale roughness (treated mathematically as diffusion). Some parts of the SRC are windier leading to more smoothing and larger pit-spacing (Figure 1).

To allow a new SRC to form, interannual variability (specifically additional CO_2 condensation or snowfall) is required. We have observed refrosting of dark SRC areas after the MY28 summer global dust storm [13]. A similar, more-extreme, refrosting was observed by Mariner 9 and Viking after the Mars Year 9 global storm. We suggest atmospheric dust drives enhanced snowfall the winter following a large storm, both by providing condensation nuclei to a sub-saturated atmosphere and cooling the atmosphere (dust is a much more effective emitter of heat than CO_2 gas).

Additional surface CO_2 ice can offset heat stored in subsurface water ice and allow perennial CO_2 to begin growing again. This new perennial cap will accumulate and be in-turn destroyed by expanding pits in a cyclic process. Each cap differs in exact form, but has identical overall behavior (Figure 3).

3. Summary and Conclusions

No climate change is necessary to explain the current erosion of the SRC; expanding pits exist at all phases of its life cycle. As different parts of the cap are at different stages of this cycle no systematic atmospheric pressure changes are predicted. Interannual variability in the form of winters with above-average condensation/snowfall is required to explain a recurring SRC. Historical and MRO data suggest that these winters are preceded by large dust storms.

References

[1] Kieffer, JGR, 1979. [2] Phillips et al., Science, 2011 [3] Malin et al., Science, 2001. [4] Byrne & Ingersoll, Science, 2003. [5] Thomas et al., Icarus, 2005. [6] Titus et al., Science, 2003. [7] Bibring et al., Nature, 2004. [8] Thomas et al., Nature, 2000. [9] Thomas et al., Icarus, 2009. [10] Piqueux & Christensen, JGR, 2008. [11] Jakosky and Haberle, JGR, 1990. [12] Hayne et al., Icarus, 2014. [13] Becerra et al., Icarus, 2015.

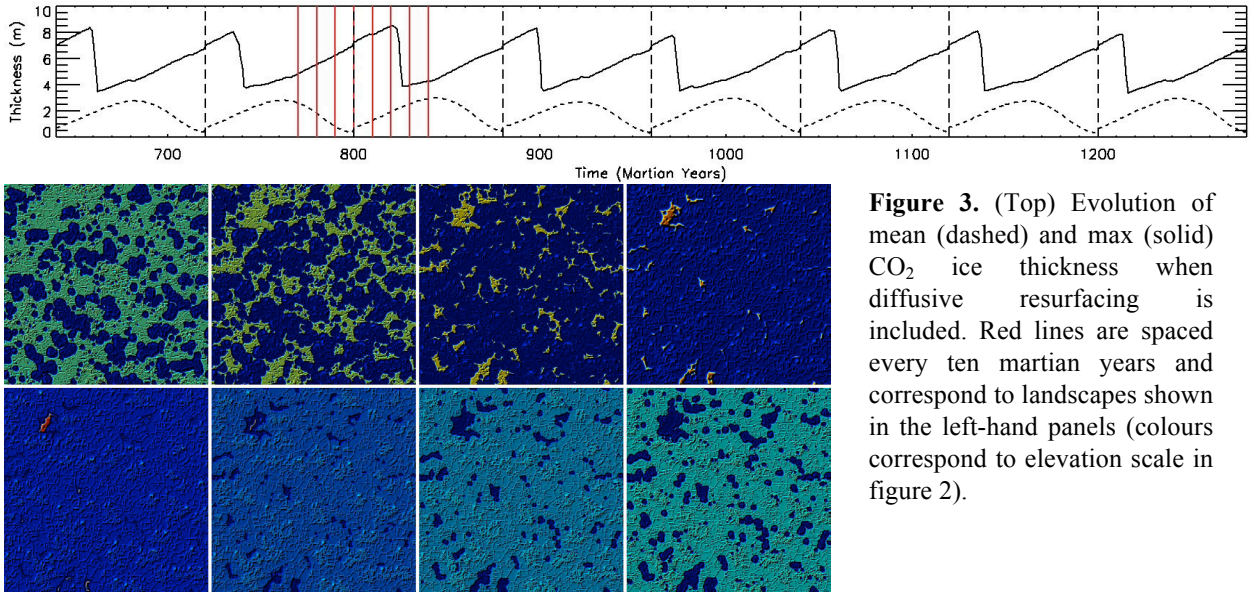

Figure 3. (Top) Evolution of mean (dashed) and max (solid) CO_2 ice thickness when diffusive resurfacing is included. Red lines are spaced every ten martian years and correspond to landscapes shown in the left-hand panels (colours correspond to elevation scale in figure 2).

EPSC Abstracts
Vol. 11, EPSC2017-382, 2017
European Planetary Science Congress 2017

Present-day flow rates of mid-latitude glaciers on Mars

M.M. Sori, S. Byrne, and A.M. Bramson
University of Arizona, Tucson, USA (sori@lpl.arizona.edu)

1. Introduction

Water ice is abundant on Mars. A combination of radar data and image analysis has shown that a large volume of that ice (on the order of 10^5 km^3) exists in the form of mid-latitude glacial landforms [1]. These glaciers are important to characterize and understand because they hold promise for elucidating Martian paleoclimate and may be important in landscape evolution.

To better understand mid-latitude glacial evolution on Mars, we estimate flow rates of viscously deforming icy features. We select a flow feature that has fine-scale topographic data available from a HiRISE-derived digital elevation model (DEM). We estimate the geometry of the feature and use it as input into a finite element method (FEM) numerical flow model to estimate deformation rates under current and past Martian conditions. We discuss the implications of our results for glacial history and the prospects of observing active flow.

2. Image Analysis

The HiRISE camera [2] aboard the Mars Reconnaissance Orbiter has obtained image coverage of ~3% of the Martian surface at resolutions of ~25 cm/pxl. Stereo images allow for construction of DEMs with vertical precision of ~1 m. Previous work [e.g., 3] that estimated stresses and strain rates associated with mid-latitude flow features was limited by Mars Orbiter Laser Altimeter (MOLA) resolution and coverage. HiRISE-derived DEMs allow superior measurement of relevant physical parameters, such as surface slope and flow thickness.

Here, we analyze a viscous flow feature in the Deuteronilus Mensae region on Mars (Fig. 1), which has an associated HiRISE-derived DEM. The feature contains downslope lineations characteristic of flow and superposes lineated valley fill (LVF), which are thought to represent glacial deposits [e.g., 4]. By extracting topographic profiles from the DEM, we find that this flow feature has an approximately poleward-facing surface slope of ~2° and a thickness of <100 m.

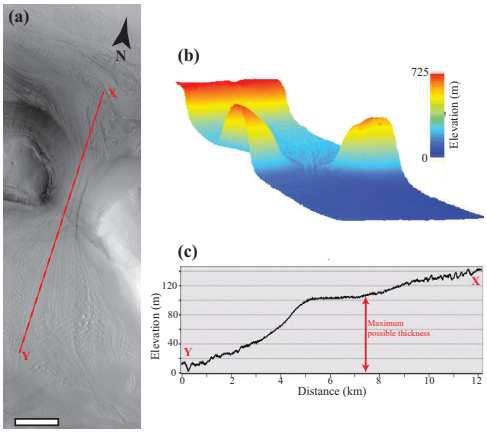

Figure 1. (a) HiRISE image PSP_007795_2175 of a flow feature at 37°N, 25°E. (b) Projected DEM of the image in (a) with 5× vertical exaggeration, constructed using another HiRISE image, PSP_009588_2175, as a stereo pair. (c) Topographic profile of the flow feature parallel to its downslope direction, represented by a red dashed line in (a).

3. Flow Model

We use the FEM software Elmer/Ice [5] to solve the Stokes equations for conservation of mass and momentum and estimate flow velocities. We approximate the flow feature (Fig. 1) as a 2D mass under Martian gravity, with a free surface boundary condition at the top of the feature and no sliding at the base (i.e., cold-based glaciation). We use a rheology that separates strain rate into various deformation mechanisms [6] and considers the effects of intermixed dust or debris [7]. The rheology is grain-size dependent; we choose a

nominal grain size of 1 mm. We have previously applied this methodology to quantify viscous flow of icy material at Mars' north pole [8] and on Ceres [9].

Ice rheology is highly sensitive to temperature. We estimate temperature in mid-latitude Martian ice using a 1D semi-implicit thermal model [10] that simulates energy balance at the surface between direct insolation, blackbody radiation, and thermal conduction into the subsurface. We assume the feature is pure ice of thermal inertia ~2100 J m^{-2} $s^{-0.5}$ K^{-1} superposed by 1-m-thick regolith with albedo 0.25 and thermal inertia ~250 J m^{-2} $s^{-0.5}$ K^{-1}. With these parameters, and under current orbital conditions, the annual-average temperature of our feature is 215.3 K.

For this feature, we find relatively low velocities. Under current conditions, we show that the feature is expected to viscously deform at rates of order 10^{-4} m/yr (Fig. 2). We nominally assume that the feature is pure ice; although radar analysis has not been conducted for this particular feature, it has confirmed such an interpretation for other similar features [11, 12]. However, we also ran cases of non-zero dust contents.

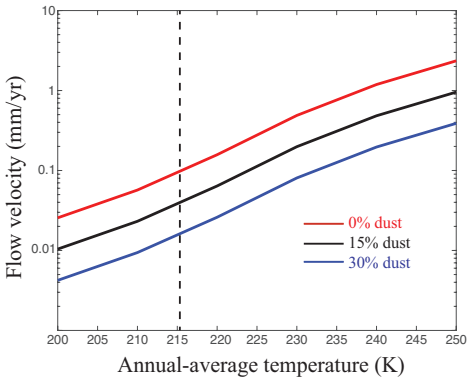

Figure 2. Flow model results for the feature in Figure 1 for various dust contents. Dashed vertical line represents the annual-average temperature in current conditions from our thermal model.

4. Conclusions

The viscous flow feature contained within this HiRISE DEM is insufficiently thick or steep to undergo significant deformation on timescales less than Myrs under current conditions. It has previously been hypothesized [e.g., 8] that active viscous flow may be possible to observe in HiRISE images over the lifetime of the instrument. However, our results show viscous flow features similar to this one are not good candidates to conduct such searches, because they require ~kyrs to flow a distance comparable to a HiRISE pixel.

We will report on the application of our methodology to other viscous flow features at the mid-latitudes of Mars in order to understand how representative the results presented here are of other glacial landforms. Additional areas of study include flow features superposing lobate debris aprons and concentric crater fill. We expect simulations of other viscous flow features will result in significantly higher velocities due to greater surface slopes [3]. We are also refining our methodology to conduct 3D flow simulations.

References

[1] Levy, J.S., Fassett, C.I., Head, J.W., Schwartz, C., and Watter, J.L., J. Geophys. Res. Planets 119, pp. 2188–2196, 2014. [2] McEwen, A.S., et al., J. Geophys. Res. 112, E05S02, 2007. [3] Milliken, R.E., Mustard, J.F., and Goldsby, D.L., J. Geophys. Res. 108, E65057, 2003. [4] Head, J.W., Marchant, D.R., Agnew, M.C., Fassett, C.I., and Kreslavsky, M.A., Earth Planet. Sci. Lett. 241, pp. 663–671, 2006. [5] Gagliardini, O., et al., Geosci. Model Dev. 6, pp. 1299–1318, 2013. [6] Goldsby, D.L. and Kohlstedt, D.L., J. Geophys. Res. 106, pp. 11017–11030, 2001. [7] Durham, W.B. and Stern, L.A., Annu. Rev. Earth Planet. Sci. 29, pp.295–330, 2001. [8] Sori, M.M., Byrne, S., Hamilton, C.W., and Landis, M.E., Geophys. Res. Lett. 43, pp. 541–549, 2016. [9] Sori, M.M., et al., Geophys. Res. Lett. 44, pp.1243–1250, 2017. [10] Bramson, A.B., Byrne, S., and Bapst, J., 48th LPSC, 20–24 March 2017, The Woodlands, TX, USA, 2017. [11] Holt, J.W., et al, Science 322, pp.1235–1238, 2008. [12] Plaut, J.J., et al., Geophys. Res. Lett. 36, L02203, 2009.

EPSC Abstracts
Vol. 11, EPSC2017-390, 2017
European Planetary Science Congress 2017

The maximum size of inflated flood lavas: implications for the origin and evolution of Athabasca Valles, Mars

M.M. Sori and C.W. Hamilton
University of Arizona, Tucson, USA (sori@lpl.arizona.edu)

1. Introduction

Effusive volcanism is a common geologic process in the inner solar system, and basalts cover the majority of the surfaces of Earth and Mars [e.g., 1, 2]. Volcanic activity has diverse styles of eruption, but cooling-limited, inflated, pāhoehoe-like sheet flows have been hypothesized to be the standard mechanism of lava emplacement on terrestrial planetary surfaces [3, 4]. Despite the significance of such lava flows, many aspects of flow behavior remain poorly quantified. Here, we address one such question: Under realistic discharge rates, cooling rates, and flow velocities, what is the maximum areal extent a single inflated, basaltic sheet flow can obtain?

To quantify flow behavior on Mars, we use numerical models to adapt parameters observed in the field or laboratories of terrestrial lava. We use a finite element method (FEM) flow model to estimate flow velocities of Martian basaltic lavas. These velocities are input into a model of the lateral spreading and crustal thickening of the inflating lava flow. We calculate the amount of lateral extent the feature can obtain before all lava is cooled into solid, brittle crust. We apply our results to Athabasca Valles, a lava-draped channel system on Mars whose formation remains debated [5–7].

2. Flow Models

We use the open-source FEM software package Elmer to solve the Stokes equations (which are conservation of mass and momentum equations) for a multi-rheological [8] lava flow. We choose a temperature-dependent rheology [9] and physical parameters appropriate for Martian flows [e.g., 10].

We find that for a set of nominal physical parameters (lava density 2500 kg/m^3, flow thickness 40 m), the maximum velocity of a Martian basaltic flow is 8 m/s. We note this velocity is consistent with estimates derived for Athabasca Valles from simple analytic approximations [4]. As expected, velocity increases with increasing lava density or flow thickness. Interestingly, the possibility of thicker flow units on Mars compared to Earth [10] do not lead to greater Martian flow velocities compared to terrestrial lava flows because of the counteracting effect of weaker Martian gravity. Our flow model results are described more extensively in a previous report [11].

3. Lateral Spreading

An inflated lava flow's multi-rheological structure limits the surface area to which the flow can extend over. A significant fraction of newly effused lava contributes to thickening of a brittle crust, removing volume that can spread laterally. If a lava flow is continuously sourced from a single point on the surface, it will grow large enough in areal extent such that new lava cools in the crustal thickening process before it reaches the terminus of the flow. Thus, under such assumptions, cooling of lava causes effusive flows to have maximum areal extents.

We model a parcel of lava as it flows through the molten core of an inflating basaltic flow. As the lava parcel travels through the core, at each time-step, we calculate the portion of that parcel that cools and solidifies, thereby thickening the brittle crust. The cooling rate is assumed to be 0.054 m hr^{-1}, calculated using cooling models [12]. Such a rate assumes no rainfall and thus is more applicable to Mars than the empirical values reported in [8] from high-rainfall terrestrial environments.

For Athabasca Valles, we assume a flow velocity through the molten core of 8 m/s, in accordance with our FEM model results. We assume lava flows radially outward from a single point source, either in a circle or in an angular sector. We consider the high

discharge rates (10^6–10^7 m^3/s) proposed in previous work specific to Athabasca Valles [4].

We find that under the assumptions described above, the Athabasca Valles flood lava cannot obtain an area >1000 km^2 in a single event (Fig. 1). The actual area covered by the lava, based on geologic mapping, is 2.5×10^5 km^2. A lava flow that grows outward in the plan-view shape of an angular sector can obtain a greater length compared to one that grows radially in all directions (Fig. 2). A Martian flow that grows in a narrow 1° angular sector obtains a maximum length of ~150 km, implying that multiple eruptive events from the same source could emplace a composite flow field with an area as high as $\sim 7 \times 10^4$ km^2.

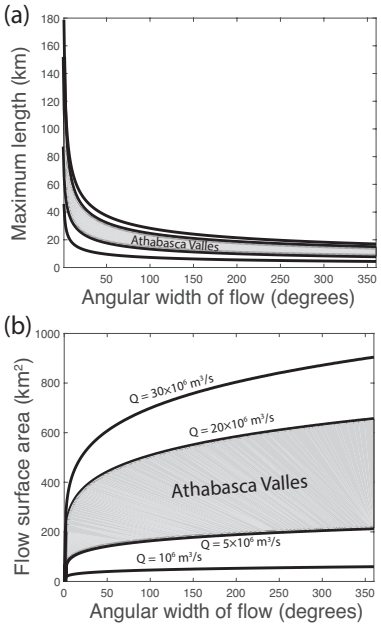

Figure 1. (a) Maximum lengths and (b) surface areas of pāhoehoe-like flood lavas on Mars for various discharge rates.

4. Conclusions

We find that a typical pāhoehoe-like inflated sheet flow of basalt cannot account for the observed shape and size of the Athabasca Valles flood lava on Mars, even for the highest allowable lava discharge rates. Therefore, the lava is unlikely to represent a standard pāhoehoe-like feature whose evolution is primarily governed by cooling and inflation.

Instead, we propose the Athabasca Valles lava likely experienced a significant degree of topographic control from preexisting structures. This result is supportive of the hypothesis that an aqueous flood carved out the valley before lava was subsequently emplaced and caused further erosion. This formation mechanism may also be supported by geologic analysis of the current topography [7].

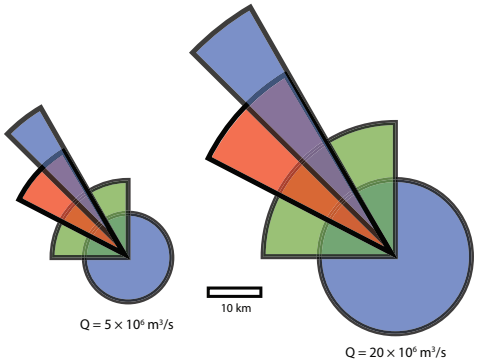

Figure 2. Scaled plan-view diagrams of the maximum surface areas covered by pāhoehoe-like flood lavas on Mars flowing radially outward from a point source.

References

[1] Self, S., Thordarson, T., and Leszthelyi, L., American Geophysical Union Monograph 100, pp. 381–410, 1997. [2] Keszthelyi, L. and McEwen, A.S., Cambridge Univ. Press, New York, USA, 2007. [3] Self, S., Keszthelyi, L., and Thordarson, T., Annu. Rev. Earth Planet. Sci. 26, pp. 81–110, 1998. [4] Thordarson, T. and Self, S., J. Geophys. Res. Solid Earth 103, pp 27411–27445, 1998. [5] Jaeger, W.L., Keszthelyi, L.P., McEwen, A.S., Dundas, C.M., and Russell, P.S., Science 317, 1709–1711, 2007. [6] Jaeger, W.L., et al., Icarus 205, pp. 230–243. [7] Keszthelyi, L., Jaeger, W.L., and Dundas, C.M., 48th LPSC, 20–24 March 2017, The Woodlands, TX, USA, 2017. [8] Hon, K., Kauahikaua, J., Denlinger, R., and Mackay, K., GSA Bull. 106, pp. 351–370, 1994. [9] Giordano, D., Russell, J., and Dingwell, D., Earth Planet. Sci. Lett. 271, pp. 123–134, 2008. [10] Hamilton, C.W., Fagents, S.A., and Thordarson, T., J. Geophys. Res. 116, E03004, 2011. [11] Sori, M.M., Hamilton, C.W., Lev, E., and Scheidt., S., 47th LPSC, 19–23 March 2016, The Woodlands, TX, USA, 2016. [12] Keszthelyi, L., Dundas, C., and Milazzo, M., J. Volcanol. Geotherm. Res., in revision, 2017.

EPSC Abstracts
Vol. 11, EPSC2017-417, 2017
European Planetary Science Congress 2017

TGO/CaSSIS – First in-orbit observations

N. Thomas(1), A. Pommerol(1), V. Roloff(1), G. Cremonese(2), M. Banaszkiewicz(3), J. Bridges(4), S. Byrne(5), V. da Deppo(6), S. Debei(7), M.R. El-Maarry(18), E. Hauber(8), C.J. Hansen(9), A. Ivanov(10), L. Keszthelyi (11), R. Kirk(11), R. Kuzmin(12), N. Mangold(13), L. Marinangeli(14), W. Markiewicz(15†), M. Massironi(16), A.S. McEwen(5), C. Okubo(11), P. Orleanski(3), P. Wajer(3), J. Wray(17), and R. Ziethe(1*).
(1)Physikalisches Inst., University of Bern, Sidlerstrasse 5, CH-3012 Bern, Switzerland (nicolas.thomas@space.unibe.ch), (2)INAF, National Institute for Astrophysics, Padova, Italy, (3)Space Research Center, Polish Academy of Science, Warsaw, Poland, (4)University of Leicester, Leicester, UK, (5)Lunar and Planetary Laboratory, Tucson AZ, USA, (6)CNR-IFN UOS Padova, Italy, (7)Centro Interdipartimentale di Studi e Attività Spaziali, Padova, Italy, (8)Deutsches Zentrum für Luft- und Raumfahrt, Institut für Planetenforschung, Berlin, Germany, (9)Planetary Science Institute, St. George, Utah, USA, (10)École polytechnique fédérale de Lausanne, Lausanne, Switzerland, (11)USGS, Astrogeology Science Center, Flagstaff AZ, USA, (12)Vernadsky Inst. of Geochemistry and Analytical Chemistry of Russian Academy of Science, Moscow, Russia, (13)Université de Nantes, Nantes, France, (14)IRSPS - Università "G.D'Annunzio", Pescara, Italy, (15)Max-Planck-Institut für Sonnensystemforschung, Göttingen, Germany, (16)Dep.Geosciences, University of Padova, Padova, Italy, (17) Georgia Inst. of Technology, School of Earth and Atmospheric Sciences, Atlanta GA, USA. (18) LASP, University of Colorado in Boulder, Boulder CO-80303, USA. *Now at Micro-Cameras and Space Exploration, Neuchatel, Switzerland.

Abstract

CaSSIS (Colour and Stereo Surface Imaging System) is the main imaging system for the ExoMars Trace Gas Orbiter (TGO) mission. A scientifically compelling instrument was completed in October 2015 and launched in March 2016 [1]. This abstract describes the current status of CaSSIS and provides a first assessment of its in-flight observations.

Observations

The scientific objectives of CaSSIS are to (1) characterize sites which have been identified as potential sources of trace gases, (2) investigate dynamic surface processes (e.g. sublimation, erosional processes, volcanism) which may help to constrain the atmospheric gas inventory, and (3) certify potential future landing sites by characterizing local (down to ~10 m) slopes.

The technical aims foreseen were to (1) acquire imaging observations at a scale of <5 m/px, (2) produce images in 4 broad-band colours optimized for Mars photometry, (3) acquire a swath width >8 km, and (4) obtain quasi-simultaneous stereo pairs over the full swath width for high res. digital terrain models. These technical aims combined with programmatic constraints drove the design. The concept was discussed at EPSC in 2014 [1]. A full instrument description is in review [2]. Details on the on-ground calibration of the instrument are provided in [3]. The full payload is described in [4].

CaSSIS was first switched-on on 7 April 2016 just over 3 weeks after launch and the first images of Mars in the Mars Capture Orbit (MCO) were acquired on 22 November 2016. An example from the first Mars sequence is shown in Figure 1.

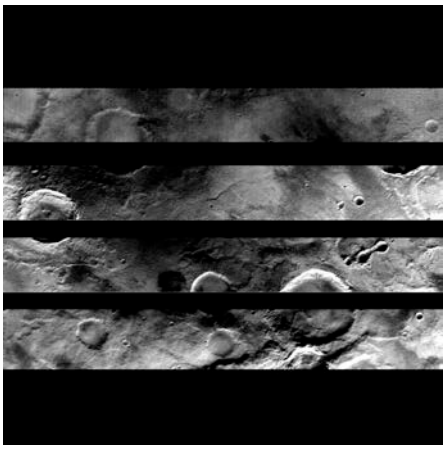

Figure 1 The first in-orbit observation of the surface of Mars with CaSSIS. This observation shows the image on the detector through the 4 filters. From the top, we see BLU, NIR, RED and PAN.

The timing of the push-frame images could be predicted well from the instrument geometry and the SPICE kernels generated by ESOC and ESAC. The test stereo pairs suggest that CaSSIS will perform stereo observations well [5,6]. Stereo reconstruction has already been performed [7]. Observations of Phobos [8] have been used to assess the photometric accuracy of the instrument and will be the subject of a publication. During the closest approach on 22 Nov. 2016, data at 2.7 m/px of Hebes Chasma was acquired with 700 µs exposure time with high signal to noise. Although the sites of the observations could not be targetted, scientifically interesting data could be acquired. The Hebes Chasma data show abundant slopes streaks and outcrops at high res (Figure 2).

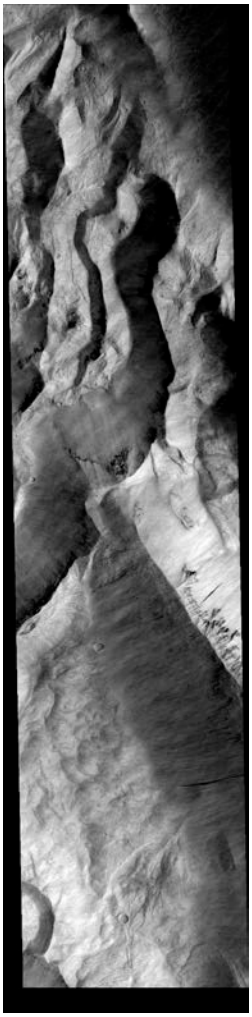

Figure 2 The reconstructed image of Hebes Chasma is 2237 x 9234 pixels in dimension at 2.7 m/px. Only one colour could be obtained in this case because of the very high ground-track velocity resulting from the close periapsis and the highly ellipitical orbit of TGO.

During the second test phase (March 2017), an invalid address in the memory caused the camera to re-boot shortly before the first periapsis pass. However, some data were acquired prior to this software error. An example is from Sisyphi Planum (Figure 3) which shows strong contrast.

The hardware appears to be working well. Future observations will test a new flight software version to be uploaded in August which incorporates compression algorithms in preparation for entry into the primary science phase in April 2018.

Figure 3 Sisyphi Planum (18W, 72S) showing dark surface material acquired at low resolution during the in-bound part of the periapsis pass on 5 March 2017.

Acknowledgements

The authors wish to thank the spacecraft and instrument engineering teams for the successful completion of the instrument. CaSSIS is a project of the University of Bern and funded through the Swiss Space Office via ESA's PRODEX programme. The instrument hardware development was also supported by the Italian Space Agency (ASI) (ASI-INAF agreement no.I/018/12/0), INAF/Astronomical Observatory of Padova, and the Space Research Center (CBK) in Warsaw. Support from SGF (Budapest), the University of Arizona (Lunar and Planetary Lab.) and NASA are also gratefully acknowledged.

References

[1] Thomas, N. et al. (2014), The Colour and Stereo Surface Imaging System (CaSSIS) for ESA's Trace Gas Orbiter, EPSC abstract Vol. 9, id. EPSC2014-100.
[2] Thomas, N. et al. (2017) Space Sci. Rev., submitted.
[3] Roloff, V. et al. (2017) Space Sci. Rev., submitted.
[4] Vago, J., et al. (2015), ESA ExoMars program: The next step in exploring Mars, Solar System Research, 49, 518-528.
[5] Cremonese et al., (2017) First Mars Surface Stereo Reconstruction with the CaSSIS Stereo Camera, LPSC (abstract)
[6] Re et al., (2017) this conference.
[7] Massironi et al. (2017) this conference.
[8] Pajola, M. et al. (2017) this conference.

EPSC Abstracts
Vol. 11, EPSC2017-418-1, 2017
European Planetary Science Congress 2017

Paleolakes of Northeastern Hellas Basin

N. H. Glines (1,2), H. I. Hargitai (2,3), and V. C. Gulick (1,2)
(1) NASA Ames Research Center, Moffett Field, CA, USA, (2) SETI Institute, Mountain View, CA, USA. (MS 239-20, NASA Ames, Moffett Field, CA, 94035, USA / natalie.glines@nasa.gov / virginia.c.gulick@nasa.gov) (3) Eötvös Loránd University, Budapest, Hungary, (1088 Budapest Muzeum krt 6-8 / hhargitai@gmail.com)

Abstract

We have identified 34 potential paleolakes in the Navua-Hadriacus-Ausonia region of northeastern Hellas, based on our previous mapping [1]. The presence of inflow and outflow channels, terracing, and sedimentary deposits such as delta-like landforms provide evidence for the formation of paleolakes. Although most recently resurfaced during the Amazonian, many paleolakes in this region formed during the Hesperian when Hadriaca Patera was active. Our study reveals a multi-source, episodic, lacustrine history for this region.

1. Introduction

Drainage systems of the Navua-Hadriacus-Ausonia region include outflow channels, valley networks, shallow valleys and channels, and wall valleys [1]. Water flowing in these drainages would have ponded in depressions produced by impact or other processes. Depressions with inlet and/or outlet channels or deposits are considered candidate paleolakes.

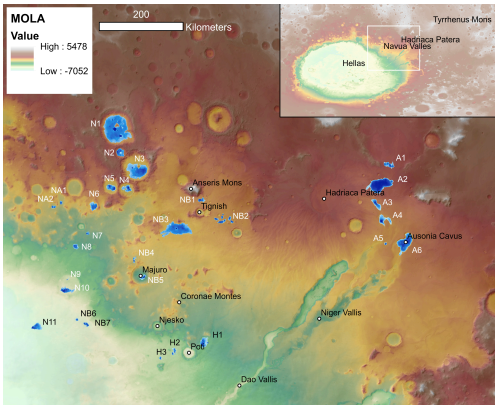

Figure 1: 34 Paleolakes identified, associated with the Navua Valles and surrounding channel systems of NE Hellas.

2. Paleolake Identification

Using a CTX mosaic and our previous drainage mapping [1], we have identified 34 individual paleolakes (Figure 1). Only one paleolake (N10; Figure 2) has been previously identified in any basin database. This lake is referred to as a "Hellas Group" lake by Cabrol and Grin [2], and more specifically as an open basin lake and deltaic deposit (Lake No. 128) by Fassett and Head [3] and Goudge et al., [4].

3. Paleolake Measurements

We delineated lake perimeters and water surface elevations in ArcGIS based on inlet/outlet or terrace elevations from MOLA. We used these elevations to determine water volumes with the 3D Analyst Surface Volume tool. 3 of the 34 lakes have two lake levels measured, and so the sum of all 34 lake volumes has a minimum and maximum, included in Table 1.

Table 1: Sum of 34 Paleolake Measurements

	Lake Area [km^2]	Lake Volume [km^3]	Lake Surface Elevation [m]	Water Depth [m]
MIN	~12,400	1,427	-1,055	9
MAX	~14,000	2,538	-6,345	1014

4. Paleolake Deposits and Floors

Approximately 60% of the basins in this region exhibit some form of terminal deposit. Most deposits are heavily eroded, revealing multiple layers (Fig. 2). About a third of these basins have light-toned deposits on their floor or margin. Patterned ground morphology is evident in several basins and may indicate the presence of periglacial processes. Knobby terrain is located within high elevation segments of the Navua Valles [5], and may be associated with channel activity, although it likely postdates the early major channel formation.

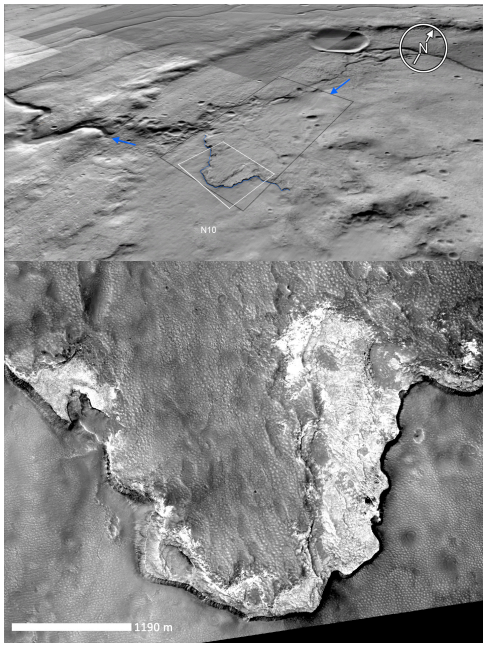

Figure 2: (above) CTX/MOLA perspective view of paleolake N10, deposit, and outlet, with flow direction (blue arrows), HiRISE footprint (black) and inset below (white). (below) HiRISE image ESP_040601_1460 of the eroded deposit margin, blanketed by a patterned material.

5. Timescales

Paleolake surface ages range from 0.5 to 3.75 Ga. Lakes near the floor of Hellas are younger than those in the highlands, consistent with Hellas' volcanic resurfacing at the Hesperian-Amazonian boundary (3.35 Ga). Lakes 3.54 Ga are consistent with the formation of Hadriaca Patera, and with the associated hydrothermal activity. The most common ages, ~3.54 and ~1.00 Ga, occur in all regions. While the oldest lakes are dated to the age of Martian valley networks, the youngest, Amazonian, ages indicate either transient flow, or a combination of periglacial reworking, aeolian modification, or blanketing processes postdating lacustrine episodes.

6. Astrobiological Significance

The Navua-Hadriaca-Ausonia region has a high density of paleolakes fed by channels active over a significant period. This has implications for our understanding of both global climate history and future paleolake identification elsewhere on Mars. It is unlikely that this highland region is unique in its high density of paleolakes, so studies elsewhere using CTX-resolution channel mapping (e.g. [1]) may uncover similar quantities of paleolakes. While liquid water paleolakes with deltaic deposits would be prime targets for astrobiological study (e.g. lake N10), lakes most proximal to hydrothermal centers have high potential for both sustaining and preserving life (e.g. lake A2) [6] even if they were frozen at the surface.

7. Summary and Conclusions

We have identified and measured 34 potential paleolakes within the Navua-Hadriacus-Ausonia region of NE Hellas Basin, Mars. These lakes were fed by channels active episodically throughout Mars' history, likely sourced from both local ground water and precipitation on upslope crater rims and mountain peaks.

Up to ~2,500 km^3 of water or ice would have filled these 34 paleolakes. While the state of the paleolakes as primarily ice or liquid water remains debatable (although our data suggests liquid), the potential volume of water, and potential duration of sustained presence of water on the surface, are significant, with implications for past climate and astrobiological value [6]. Evidence for hydrothermal activity from the local volcanic zone may be preserved in deposit layers throughout the drainage systems [6]. While we promote the region as a target of prime astrobiological investigation [6], we also propose an increased potential for paleolake identification throughout the highlands, following similar detailed CTX-resolution channel and deposit mapping.

Acknowledgements

Support was provided to H. Hargitai by the NASA Postdoctoral Program (NPP), and to V. Gulick and N. Glines by SETI Institute's NAI grant NNX15BB01A, and MRO HiRISE Co-I funds to Gulick.

References

[1] Hargitai, Gulick, and Glines: Icarus, 2017. [2] Cabrol and Grin: Icarus, Vol. 149, pp. 291-328, 2001. [3] Fassett and Head: Icarus, Vol. 198, pp. 37-56, 2008. [4] Goudge, Head, Mustard, Fassett: Icarus Vol. 219, pp. 211-229, 2012. [5] Hargitai and Gulick: LPSC, 20-24 March 2017, The Woodlands, TX, USA#1763. [6] Gulick, Hargitai, Glines, and Rodriguez: AbSciCon #3638, 2017.

EPSC Abstracts
Vol. 11, EPSC2017-425-1, 2017
European Planetary Science Congress 2017

Stability of Mid-Latitude Excess Ice on Mars over 10s of Millions of Years

A. Bramson, S. Byrne and J. Bapst
Lunar and Planetary Laboratory, University of Arizona, Tucson, Arizona, USA, (bramson@lpl.arizona.edu)

1. Introduction

Excess ice (higher water abundances than can fit into the pore spaces of the regolith) is now known to be common in the northern mid-latitudes of Mars. Thermokarstic features such as expanded craters [8] and scalloped depressions [3] point to the presence of high ice contents at these latitudes, and new impacts have directly exposed and excavated very pure water ice down to 38°N [2]. Radar sounding by the Shallow Radar (SHARAD) instrument onboard the Mars Reconnaissance Orbiter has detected dielectric interfaces that have been attributed to the bottom of excess ice sheets in both Arcadia Planitia [1] and Utopia Planitia [7]. Craters across Arcadia Planitia exhibit a terraced morphology due to layers in the subsurface that have been associated with the same ice layer detected by SHARAD [1].

Both Arcadia and Utopia deposits (Figure 1) each hold ice volumes on the order of 10s of thousands of km^3. Using independent measures of layer thicknesses from the terraced craters in Arcadia [1] and layered mesas in Utopia [7], the SHARAD studies were able to constrain the dielectric constants to ~2.5, consistent with excess ice and low dirt contents in the upper decameters of the surface. The thicknesses measured for the ice are 30-80 m across Arcadia Planitia and 80-170 m in Utopia Planitia.

Crater counting of expanded secondary craters in Arcadia Planitia suggests this ice is at least 10s of Myr old [8]. During this time, Mars has had many excursions through low obliquities, when low latitude ground ice is expected to be transported to the poles. Replenishment of this ice from the atmosphere in subsequent higher-obliquity epochs will only create pore-filling ice. Here, we model excess ice stability over 20 Myr of Martian orbital solutions [4] to investigate if it is reasonable to expect excess ice to be preserved for this long, and if so, the conditions necessary to reproduce the observed distribution, thicknesses and dielectric constants of these excess ice deposits.

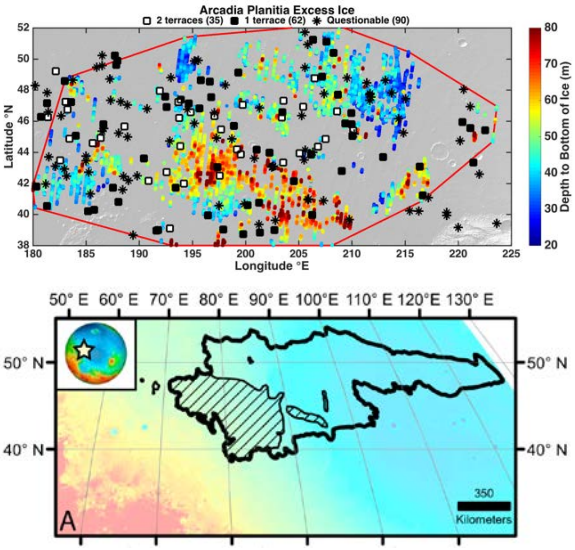

Figure 1: Maps of excess ice sheets in the mid-latitudes of Mars. The top plot is a modified map from [1] of radar reflectors (colored dots) and terraced craters (B/W markers) in Arcadia Planitia. The bottom map is from [7] and shows the extent of radar reflectors (diagonal lines) in Utopia Planitia.

2. Thermal Modeling

We model temperatures of the Martian subsurface using a 1D semi-implicit thermal conduction model that simulates surface energy balance and transfer of heat between subsurface layers. The model allows for subsurface layers of different thermophysical properties (e.g. conductivity, density, specific heat), which we use to model a surface porous regolith layer, which we assume is a sublimation lag deposit, atop excess ice. Within this lag deposit, we allow for the resupply of ice into the pore-spaces at and below its equilibrium depth (where $\rho_{vapor} \leq \rho_{atmos}$). We assume no retreat of the excess ice sheet when there is pore-filling ice in this lag as it can choke off diffusive exchange of vapor.

We calculate the annual-average saturation vapor densities at each depth and orbital solution. We model atmospheric water vapor conditions following the obliquity-dependent scheme of [6]. When $\rho_{vapor} > \rho_{atmos}$ at the excess-ice table, and there is no pore-filling ice within the lag deposit, ice is lost at a rate that is dependent on the vapor diffusivity of the regolith, the difference between the vapor density and atmospheric vapor content, and the depth of the ice table. When the excess ice retreats, it leaves behind any silicate material embedded within it, thus growing the lag deposit. We implement the growth of this regolith layer following the method described in [5].

We allow the ice sheet in the model to start infinitely thick to quantify the total ice retreat that could occur to the present-day. After the simulation, we introduce a bedrock layer at the depth observed [1,7] and calculate the dielectric constant of the material between that and the surface for comparison to observations (2.5 +/- 0.28 for Arcadia Plantia [1] and 2.8 +/- 0.8 for Utopia [7]).

3. Results

We find that there are final model stratigraphies consistent with the dielectric constants (Fig. 2a) of Arcadia Planitia and Utopia Planitia, while also yielding total ice retreats (Fig. 2b) on the same order of magnitude as the present-day thicknesses of ice. This suggests it is reasonable for the ice to be preserved over 10s of Myr. To match the dielectric constants, the ice likely needs to have maintained some porosity (~25-35%) and relatively low dirt contents (~3%). This ice is protected by its growing lag deposit, which our models predict reaches meters in thickness (Fig. 2c).

4. Summary and Conclusions

Excess ice is common across the Martian mid-latitudes. The ice sheets in Arcadia Planitia and Utopia Planitia have been observed to be widespread, clean (excess ice), and porous based on radar studies [1,7]. This is most consistent with buried snowfall. Here, we demonstrate that such ice could be on the order of 10s of Myr old, much older than obliquity cycles and possibly the North Polar Layered Deposits, and is consistent with the ages calculated by [8]. The ice must have formed thicker than currently observed to account for retreat during times of low obliquity and would be protected by a growing lag deposit containing transient pore-filling ice.

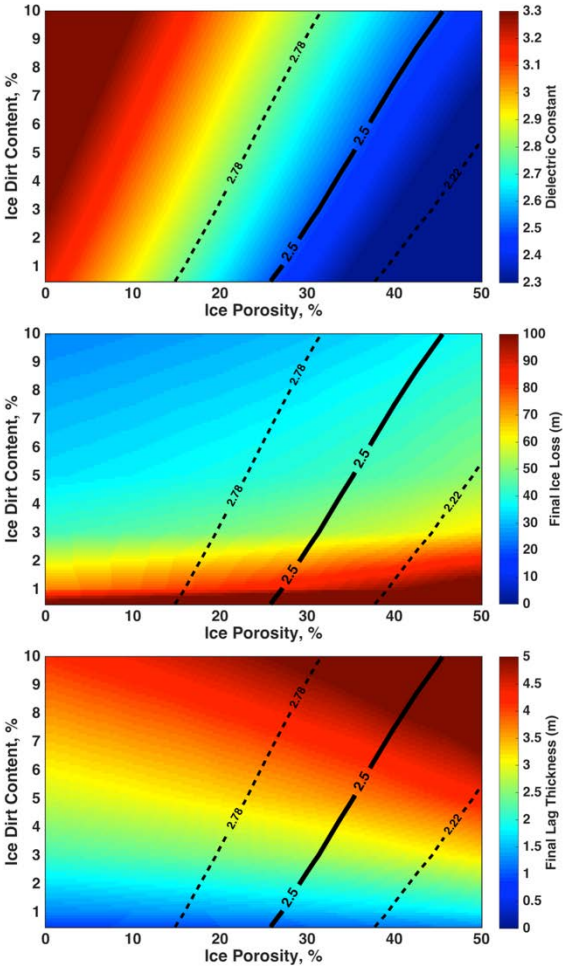

Figure 2: Results for 45°N in Arcadia Planitia (thermal inertia of 196 J m^{-2} K^{-1} $s^{-0.5}$ and albedo of 0.24). The top plot shows the dielectric constant associated with the final stratigraphy outputted by the models for a range of ice porosities and dirt contents. The final amount of ice loss and lag deposit thickness are shown in the middle and bottom plots.

References

[1] Bramson A. M. et al., GRL, 42, 6566, 2015.
[2] Dundas C. M. et al., JGR-Planets, 119, 109, 2014.
[3] Dundas C. M. et al., Icarus, 262, 154, 2015.
[4] Laskar, J. et al., Icarus, 170, 343–364, 2004.
[5] Schorghofer N., Icarus, 208, 598-607, 2010.
[6] Schorghofer N. and Forget F., Icarus, 220, 1112, 2012.
[7] Stuurman C. M. et al., GRL, 43, 2016.
[8] Viola D. et al., Icarus, 248, 190, 2015.

EPSC Abstracts
Vol. 11, EPSC2017-491, 2017
European Planetary Science Congress 2017

Physical state and temporal evolution of icy surfaces in the Mars South Pole

S. Douté(1) and C. Pilorget(2) (1) IPAG, Université Grenoble Alpes, Bât OSUG A CS 40700 38058 Grenoble Cedex 9 France (2) IAS Centre Universitaire d'Orsay, France

Abstract On Mars H_2O and CO_2 ices can be found as seasonal or perennial deposits notably in the polar regions. Their bidirectional reflectance factor (BRF) is a tracer of their evolution which is still not completely understood. It is a key parameter for characterizing the composition and the physical state, as well as for calculating the bolometric albedo, the energy balance of the icy surfaces, and thus their impact on the martian climate. The BRF is potentially accessible thanks to the near-simultaneous multi-angle, hyperspectral observations of the Compact Reconnaissance Imaging Spectrometer for Mars (CRISM) implying 11 viewing angles in visible and infrared ranges. In previous research [1, 2] we put forward the Multi-angle Approach for Retrieval of Surface Reflectance from CRISM Observations (MARS-ReCO), an algorithm that characterizes and corrects the aerosol scattering effects. The aerosol optical depth (AOD) and the BRF of surface materials are retrieved conjointly and coherently as a function of wavelength. In this work, we apply MARS-ReCO on time series of CRISM sequences over different regions of interest in the outskirts of the south permanent polar cap. The time series span from mid-spring to late summer (L_s=210-320°) during which the CO_2 ice sublimates sometimes revealing H_2O frost and defrosted terrains. Thanks to the atmospheric correction, we are able to identify various classes of spectrophotometric behavior. We also note a regular increase of the directional-hemispherical surface albedo during the period of the time.

Data In this paper we restrict the analysis to the visible channel (VIS) of the CRISM instrument (0.4-1.0 μm). The minimum solar incidence is 64° and the maximum is 75° implying varied but large ranges of phase angles (typically 40-115°) suitable for the use of MARS-ReCO and for the physical characterization of the icy materials. No ground truth is available for the region implying the calculation of quality criteria by the algorithm itself and a procedure of cross-validation.

Methods In order to facilitate the simultaneous processing of the multi-angle Top Of the Atmosphere (TOA) reflectance factor of one CRISM observation, the spectra corresponding to the eleven scans are rearranged in a common geographical grid of super-pixels (i.e., terrain units sensed at more than one geometry) to create a single data set which facilitates the access to photometric curves. Each spatial bin is $\approx$ 200 meters in size. Independently for each wavelength MARS-ReCO performs the processing of TOA photometric curves $\mathbf{R}^C = \left\{R_1^C, \ldots, R_{Ng}^C\right\}$ where Ng is the number of available angular measurements. MARS-ReCO retrieves conjointly the AOD and the BRF of surface materials. The inversion procedure exploits the spatial homogeneity of the atmosphere opacity relative to the surface. See [1] and [2] for a complete description of the processing. A first analysis of the retrieved surface BRF values consists of performing a non-supervised k-means classification of the phase curves extracted at a wavelength of 750 nm for each CRISM observation. Maps of the quasi nadir BRF and directional-hemispherical albedo are also computed and co-registered between observations allowing to extract the temporal evolution of these physical quantities at different locations.

Results MARS-ReCO gives results with good accuracy comparable to what is achieved for the processing of controlled synthetic data or real data acquired for moderately anisotropic mineral surfaces under usual incidence (40-60°). Even though the atmospheric conditions vary largely during the period of the time series we note a continuous increase of the directional hemispheric albedo of the icy surface ($\approx$ 20-50%) until $L_s \approx 270°$, followed by a decrease during the summer season (Fig. 1). Furthermore we note three to five classes of phase curves showing a good coherency between observations. The most prevalent class is dominantly forward scattering CO_2 ice but with a backscattering secondary lobe. When the defrosting is well advanced, as for observation FRT144E9 (Fig. 2), very distinct photometric behaviors become apparent. The "blue" class corresponds to parts of the CO_2 ice unit

that have a high concentration of sub-pixel topography (CO_2 type1). The phase curve presents a moderate and monotonic decrease of reflectance from the low to the high phase angles. It is likely controlled by the presence of extended shadows (sun low on the horizon) that are differently visible depending on the viewing geometry. The "magenta" class corresponds to parts of the CO_2 ice unit that is generally smoother (CO_2 type 2). The phase curve has a forward scattering lobe (large phase angles) and a backward scattering lobe (low phase angles). They are both modest, the former being linked with volume scattering and the latter being due to shadows. The "red" class is the unit of dust mixed with minute amount of water ice (mostly defrosted terrains). It is backscattering with a relatively strong monotonic decrease in reflectance from the low to the high phase angles (the dominant role of shadows). The "green" class corresponds to compositional transition zones with a high concentration of H_2O frost. It is the most anisotropic with two prominent diffusion lobes, a forward (volume scattering) and a backward (surface scattering), the latter being predominant.

Conclusions: In this study we recognize different classes of icy surface phase curves likely determined by their composition, grain micro-texture, and surface roughness that we will determine by modeling. Prior to sublimation, CO_2 ice shows a continuous increase of the nadir reflectance factor (≈20-50%) until $L_s \approx 270^o$, followed by a decrease during the summer season. Based on the mapping of the ice physical properties along with the examination of high resolution images, we will recognize in the near future the most relevant controlling processes: sublimation, structural modifications of perennial ice (e.g. cracks), dust settling and removal linked with atmospheric activity, etc.

Acknowledgements This research was funded conjointly by the Programme National de Planétologie and CNES.

References

[1] S. Doute et al. *JGR planets*, 118:1–20, 2013. doi: 10.1029/2012JE004195.

[2] S. Doute and X. Ceamanos. In *Geoscience and Remote Sensing Symposium (IGARSS), 2015 IEEE International*, pages 1–4, July 2015. doi: 10.1109/IGARSS.2015.7325682.

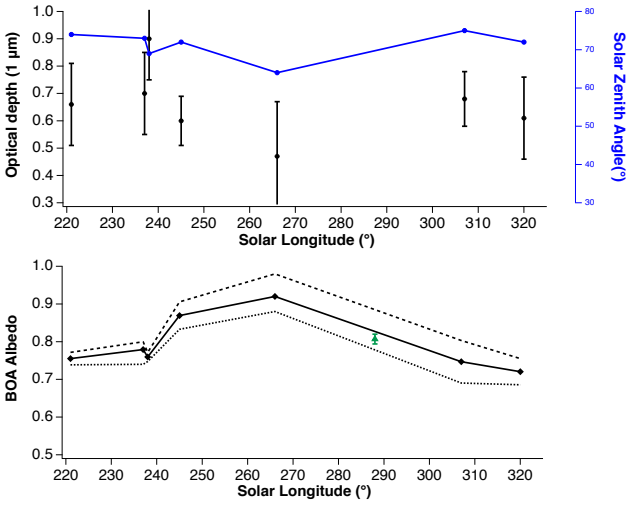

Figure 1: Time evolution for one of the sites. Top: incidence angle and AOD. Bottom: directional hemispheric albedo (mean behavior and standard deviation).

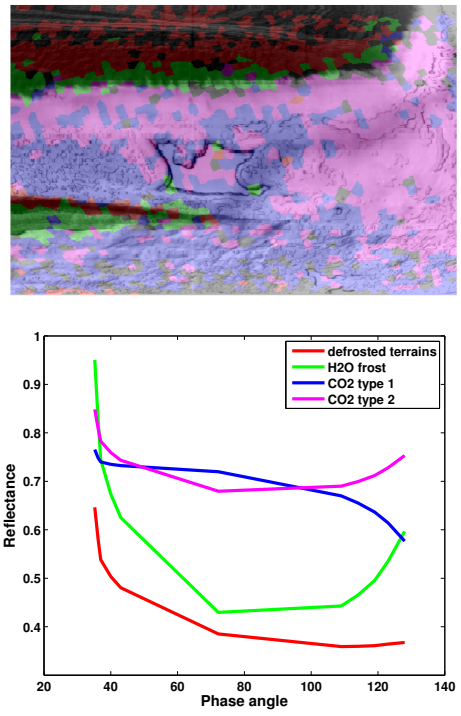

Figure 2: Classifying the phase curves at 750 nm for observation FRT144E9. Top: distribution of the color-coded photometric classes over the nadir full resolution CRISM scan. Bottom: mean phase curve of the classes.

EPSC Abstracts
Vol. 11, EPSC2017-541, 2017
European Planetary Science Congress 2017

The Martian crustal magnetic field: a global view as seen from MGS and MAVEN measurements

B. Langlais (1), E. Thébault (1) and A. Houliez (1)
(1) Laboratoire de Planétologie et Géodynamique, CNRS et Université de Nantes, France

Abstract

We present a new model of the Martian crustal magnetic field. This new model supersedes previously published models as it fully exploits the full wealth of available magnetic field measurements. The new model makes advances in four areas. (i) We apply a data selection scheme for MGS MAG Mapping Orbit (M0) measurements in order to reduce external field perturbations. (ii) We make use of MGS Electron Reflectometry (ER) indirect estimates of the total field to better constrain the model. (iii) We further consider MAVEN magnetic field measurements, until the most recent date. (iv) We improve the spatial resolution, down to ~100 km.

1. Introduction

Almost 20 years ago the Mars Global Surveyor revealed the striking magnetic figure of Mars [1]. While devoid of an active magnetic field today, Mars possesses a remanent magnetic field which may reach several thousands of nT locally. The processes which have shaped the crustal magnetization remain largely enigmatic. During almost 7 years MGS made magnetic field measurements, mainly at a constant altitude of 400 km and at only two local times. Low-altitude measurements (below 250 km) and at several local times are very sparse and may hamper the interpretation of magnetic field models in terms of planet history or of magnetic source properties.

The MAVEN mission [2] was inserted in orbit around Mars in Sept. 2014. It flies on a very elliptical orbit, with a periapsis as low as 125 km, and it will cover all local times. In this study we present a new model of the crustal Martian magnetic field built using both MGS and MAVEN measurements, using a technique we developed for MGS [3]. This new model uses MAG measurements by MGS and MAVEN, but also total field estimates at 185 km from MGS electron reflectometry (ER) measurements.

2. MAVEN measurements

MAVEN was inserted in orbit on 21 Sept. 2014. It flies on an elliptical orbit, between 150 and 6200 km, with periodical dip campaigns down to 125 km. The inclination is 74°, and the period is 4.5 hours. We use data up to the most recent available date. Data are night-time selected, and down-sampled to 0.05 Hz below 600 km and between 22:00 and 4:00. The external magnetic field activity is examined using the technique described below.

3. External field proxies and data selection

MGS flew over the same location, altitude and local time once a week during 7 years. This may be seen in a virtual observatory scheme. Every time the spacecraft flew over the same location it measured the same crustal field and a time varying external field. By isolating the time variable constituent it is therefore possible to estimate a temporal proxy which describe the level of external activity [4]. The scheme we follow is:

- night-side, median field measurement for each lat x lon= 0.8° x (0.8° cos(lat)) is found;
- individual differences to median value are computed for each bin and all data;
- Bx residual (mars Sun State system, X pointing towards the Sun) is found;
- L1 (mean) and associated L2 (rms) statistics are computed from differences on a Martian daily basis.

Results are compared to extrapolated magnetometer measurements from ACE spacecraft (close to the Earth). When Mars and the Earth are in adequate location, (anti)correlation is very good, close to -0.7. With this proxy it is easy to identify magnetic events (see Fig. 1), such as the occurrence of the well-documented Halloween 2003 magnetic super storm [5].

MO MGS night side data are selected accordingly, keeping only the 10% quietest Martian days (maximum L2 value of 4.8 nT). Earlier MGS data and recent MAVEN measurements are selected using the remote proxy, when appropriate.

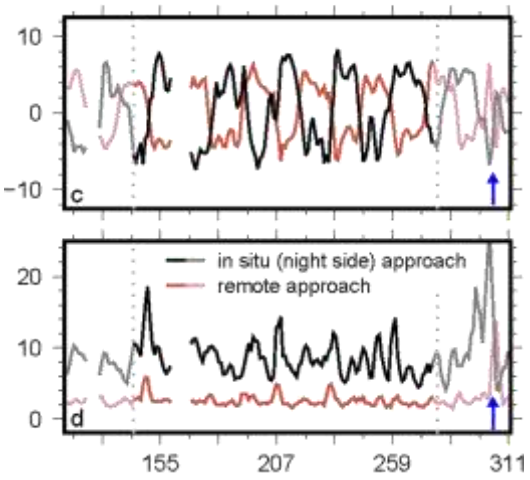

Figure 1: Comparison of in situ MGS proxy and remote (extrapolated) ACE one. Blue arrow indicates Halloween magnetic super storm in 2003. After [4]

4. Improved model resolution

We use Equivalent Source Dipoles: at each point, the magnetic field results from the contributions of sources located homogeneously below the Martian surface. A polar coordinates subdivision is chosen, with a mean distance between sources as low as 110 km. A L2 norm is used with a conjugate gradient approach (iterative scheme). The use of scalar (ER) data requires a priori knowledge of the magnetization vector and associated magnetic field vector at observation location (another iterative scheme).

5. Results

Globally the correlation coefficient between actual and model-predicted measurement exceeds 0.978. We can predict the magnetic field at altitudes as low as 125 km, which is below what was possible previously. The global picture of the magnetic field remains similar to [3], but the model has a better resolution (Fig. 2). The ESD model is converted into spherical harmonics and it converges up to SH degree 140. At a local scale, anomalies are better defined, which should ease the interpretation of the models in terms of magnetization properties.

Ideally actual magnetization and rock susceptibility measurements at the surface of Mars will bring the ultimate constraint on the nature and properties of the crustal Martian magnetic field. This is the main objective of the on-going NEWTON H2020 project, which aims at developing non-invasive in-situ magnetic characterization instrument suite [6].

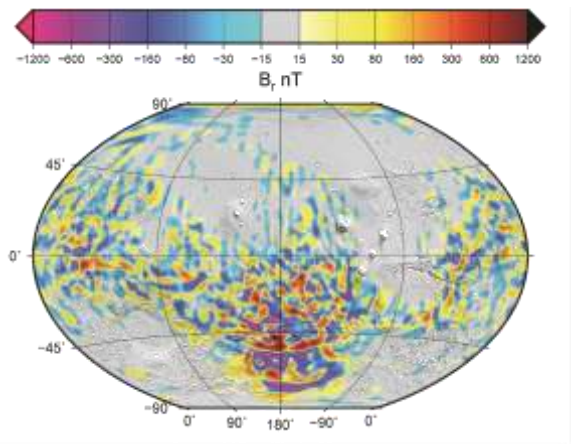

Figure 2: predicted radial field from the new model at 125-km altitude.

6. Acknowledgements

This work benefits from and contributes to the H2020 NEWTON project, which has received funding from the European Union's Horizon 2020 research and innovation program under grant agreement No 730041.

References

[1] Acuña, M., et al., 1999, Global distribution of crustal magnetization discovered by the MGS MAG/ER experiement, Science, 284, 1999. [2] Jakovsky, B., et al., Initial results from the MAVEN mission to Mars, Geophys. Res. Lett., 42, 2015. [3] Langlais, B., M. Purucker, and M. Mandea, the crustal magnetic field of Mars, J. Geophys. Res., 109, 2004. [4] Langlais, B., F. Civet, and E. Thébault, In situ and remote characterization of the external field temporal variations at Mars, J. Geophys. Res., 122, 2017. [5] Dyer, M., et al., Real-time shock arrival predictions during the Halloween 2003 epoch, Spa. Weather, 2, 2004. [6] NEWTON consortium, "NEWTON H2020 D2.1: Definition of instrument requirements and architecture. Design guidelines", 2017. http://www.h2020-newton.eu/index.php/deliverables.

EPSC Abstracts
Vol. 11, EPSC2017-550-4, 2017
European Planetary Science Congress 2017

In-flight performance and calibration of the ExoMars Trace Gas Orbiter CaSSIS imager: selected results

V. Roloff (1), S. Tulyakov (2), A. Pommerol (1), N. Thomas (1), A. Ivanov (2), J. Fernando (3), and the CaSSIS Science Team.
(1) Physikalisches Inst., University of Bern, Sidlerstrasse 5, CH-3012 Bern, Switzerland (victoria.roloff@space.unibe.ch), (2) École polytechnique fédérale de Lausanne, Lausanne, Switzerland, (3) Lunar and Planetary Laboratory, University of Arizona, Tucson, AZ 85721, USA.

1. Introduction

The ESA-led ExoMars Trace Gas Orbiter (TGO) was launched to Mars on 14 March 2016 [1]. The TGO will search for signs of past and present life on Mars, investigate its geochemical environment, and search for atmospheric trace gases and their sources. The TGO carries 4 scientific instruments in order to reach these goals: this includes the orbiter's high-resolution imager, CaSSIS (Colour and Stereo Surface Imaging System). We present selected results of CaSSIS in-flight calibration measurements. A full description of the instrument can be found in [2]. A detailed on-ground calibration campaign was performed [3], and a number of calibration products were gathered and utilised as part of the in-flight calibration campaigns.

2. Results

Near-Earth Commissioning and Mid-Cruise Check-out. On 7 April 2016, CaSSIS was first switched on, post-launch. A number of measurements were carried out in order to verify and confirm the status and response of the instrument. We developed an automated method to recognise stars in CaSSIS stellar calibration images using the Astrometry.net library. Stellar angular coordinates from the 2MASS catalogue were used to refine the focal length and lens distortion model of CaSSIS. The model was applied to ∼80 images, with ∼2000 recognised stars. As a result, the CaSSIS focal length was refined to 875.93 mm. By taking into account the refined parameters, we were able to improve the map-projected colour-filter alignment, and reduce colour fringes in colour images.

Mars Capture Orbit. Upon arrival at Mars, the first images of the surface were acquired on 22 November 2016. During this time the TGO was in a ∼4-sol orbit, with an angle of travel with respect to the equator of 7°. From two apoapses of the initial Mars Capture Orbit (MCO-1), CaSSIS observed the spectrophotometric reference stars π^2 Orionis and ξ^2 Cet, respectively. The spacecraft was slewed so that the images of the stars passed across the detector through all four colour filters. From the reduction of these datasets we have derived the Point Spread Function (PSF) of the instrument and its absolute calibration. We present here preliminary results on the reference star π^2 Orionis, obtained at apoapsis on 20 November 2016 during the first orbit of the MCO-1 campaign (Figure 1). All results analysed so far indicate a narrow PSF as well as excellent linearity of the detector (Figure 2). Both properties show the great potential of the instrument for Mars surface imaging. To evaluate the CaSSIS signal accuracy after calibration, we used the CaSSIS Phobos image that limits the atmospheric contamination and the diversity of the surface properties observed on Mars. Several spaceborne instruments have acquired Phobos images, which can be used to compare the measured signal to the CaSSIS Phobos colour images and evaluate the biases. One of them is the Observatoire pour la Minéralogie, l'Evolution, les Glaces et l'Activité (OMEGA) hyperspectral camera on board Mars Express. The instrument provides visible (V-detector) data that covers the CaSSIS spectral range. For the comparison, the selected OMEGA image has to have close photometric geometries (i.e. phase angle) to the CaSSIS image (phase angle of 35°) to minimise the photometric effect. OMEGA observation ORBD764_0 was selected for the study (phase angle of 35°). Figure 3 presents the comparison of the OMEGA and CaSSIS disc-integrated I/F reflectances at each CaSSIS filter. We note that the deviation from the OMEGA disc-integrated I/F reflectance is equal to 0% for the BLU and PAN filters. A deviation of 10% and 6.7% is observed for the RED and the NIR filters, respectively. However, these deviations can be explained by the extrapolation of OMEGA I/F reflectances made at high wavelengths to correct the OMEGA calibration issues.

This result shows the great potential of the instrument for Mars surface colour imaging.

CaSSIS data continues to provide compelling support for the instrument's scientific ability. The now 74°-inclined orbit of the TGO means that it rotates through all local times of day several times per Mars season, so CaSSIS will have the unique ability to monitor how surface processes change with time of day as well as season. As a result, CaSSIS will be able to complement existing datasets of the martian surface, significantly improve the global colour coverage, and provide support and a wider understanding of context to observations by other instruments on board the TGO.

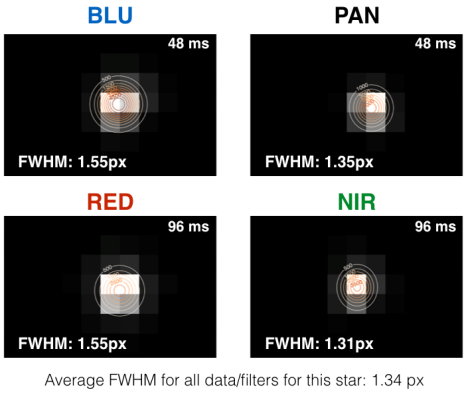

Figure 1: Images of π^2 Orionis in all four CaSSIS filters. Fitting these images with a 2D Gaussian function gives symmetric Point Spread Functions (PSF) with values of Full Width at Half Maximum (FWHM) in the range of 1.2 to 1.6 px, and an average value of 1.34 px. This indicates that the instrument is in good focus.

Acknowledgements

The authors wish to thank the spacecraft and instrument engineering teams for the successful completion of the instrument. CaSSIS is a project of the University of Bern and funded through the Swiss Space Office via ESA's PRODEX programme. The instrument hardware development was also supported by the Italian Space Agency (ASI) (ASI-INAF agreement no.I/018/12/0), INAF/Astronomical Observatory of Padova, and the Space Research Center (CBK) in Warsaw. Support from SGF (Budapest), the University of Arizona (Lunar and Planetary Lab.), the NCCR PlanetS, and NASA are also gratefully acknowledged.

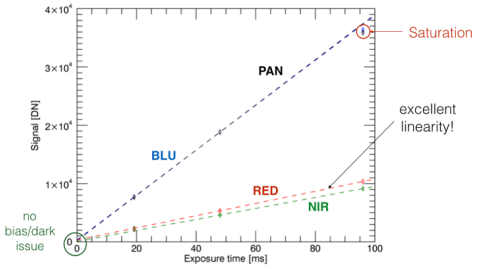

Figure 2: Plotting the integrated Point Spread Functions (PSF) intensity, as a function of the integration time, for all four colour filters shows the excellent linearity of the instrument response. This indicates that bias and dark signal behaviours are well under control, which should result in an accurate absolute calibration of the instrument.

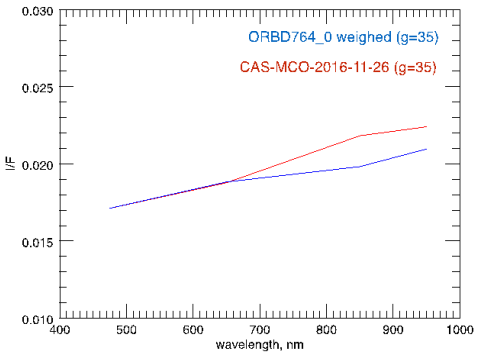

Figure 3: Comparison of the OMEGA (blue) and CaSSIS (red) Phobos disc-integrated reflectances. (BLU: centered to 475 nm, PAN: centered to 650 nm, RED: centered to 850 nm and NIR: centered to 950 nm). This result shows the great potential of the instrument for Mars surface colour imaging.

The authors would also like to thank the OMEGA team and Brigitte Gondet for providing the OMEGA Phobos calibrated data.

References

[1] Thomas, N. et al. (2014), EPSC abstract Vol. 9, id. EPSC2014-100.
[2] Thomas, N. et al. (2017), Space Sci. Rev., submitted.
[3] Roloff, V. et al. (2017), Space Sci. Rev., submitted.

EPSC Abstracts
Vol. 11, EPSC2017-551, 2017
European Planetary Science Congress 2017

Geomorphological assemblages in Arcadia Planitia: clues about a global scale event?

B. De Toffoli (1,2), R. Pozzobon (1), F. Mazzarini (3), M. Massironi (1,2) and G. Cremonese (2)
(1) Department of Geosciences, University of Padova, Padova, Italy (barbara.detoffoli@gmail.com), (2) OAPD, Istituto Nazionale di Astrofisica, Padova, Italy, (3) Istituto Nazionale di Geofisica e Vulcanologia, Pisa, Italy

Abstract

Mound-like features have been detected in the Arcadia Planitia region in the Northern hemisphere of Mars. Particularly, we investigated a surface covering ~100.000 Km^2 where three different landforms were observed. Due to their morphological characteristics and surface distribution we suggest that some of these mounds could be interpreted as water related features, such as mud volcanoes or spring vents.

1. Introduction

When unconsolidated materials are buried and confined in the subsurface in correspondence of a source of fluids, upwelling pulses occur when the buoyancy forces that push these sediment mixtures exceed the confining lithostatic pressure, such as in case of new fluid supply, increasing of pore pressures and a decrease of viscosity [1]. The northern lowlands are considered to have hosted large bodies of water in the Martian geological past that could have provided the conditions for deposition and storage of large quantities of sediments. Today these regions, and particularly Arcadia Planitia (centered at N47° E184°, ~4 Km below the mean elevation), show various assemblages of morphologies that could have recorded and contributed to these sediment and fluid resurgences [2].

2. Observations

The observations of the region of interest in central Arcadia Planitia were performed on 46 CTX (Context Camera onboard of Mars Reconnaissance Orbiter) images at 6 m/pixel resolution. Three different kinds of mound-like features were recognized according to morphological traits.

Low Light Features (LLF)
These features are the main constituent of the thumbprint terrain present in the area, consisting of circular mounds predominantly organized in the typical arcuate parallel chains. LLF are several hundred of meters in diameter and are defined by a bright albedo (compared to the surrounding plane), very low elevation, perimetral moats and swellings, rough surface and central pit surrounded by concentric ring-like features expressed as multiple apical incisions.

High Dark Features (HDF)
These mounds are rounded but irregular in shape, characterized by dark albedo, several kilometers wide and clearly elevated in respect of the surrounding plain, which trait is highlighted by blankets of debris covering the basal slopes. Their dark surfaces are rough and show one or multiple pits often recognizable in either apical or distal positions. HDF appear to be less densely distributed than the LLF in the study area. They are single or coalescent structures organized in clusters that can be associated in places to ghost crater rims, polygonal troughs and thumbprint terrain ridges.

Intermediate features between LLF and HDF can be also recognized in isolated contexts where LLF are superimposed to HDF either on apical or distal portions, or blended together alternating layers of light and dark materials showing mixed characteristics along ridges.

Circular Pitted Mounds (CPM)
Around 150 of these mounds have been detected within rim and floor of a degraded crater. Key traits are circular neat base, smooth surfaces, central pits surrounded by concentric ring-like features and multiple concentric crestal, distal and perimetral

incisions [3]. CPM are either single or coalescent structures organised in clusters or short alignments.

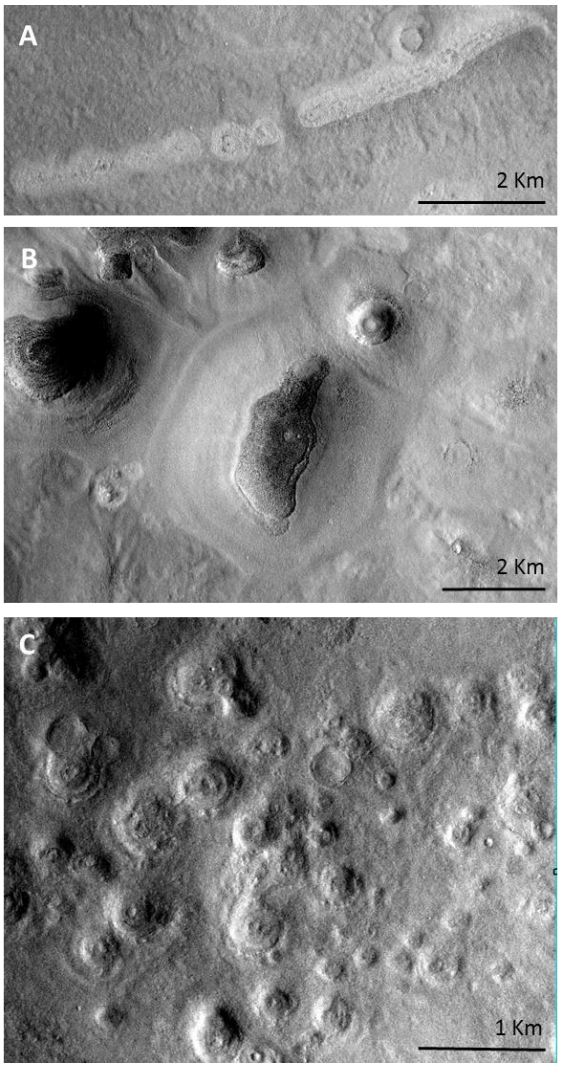

Figure 1: (a) chain of LLF; (b) cluster of HDF; (c) cluster of CPM.

3. Measurements and conclusions

Cluster and fractal analyses were performed on LLF and CPM to derive the thickness of the fractured medium that lays beneath the mound populations, which have acted as reservoir and pipeline for fluids and sediments [4]. The outcomes of this study mark a connection between these features and similar morphologies in the Northern Plains at comparable latitudes but on the opposite side of the planet, which are the surface expression of identical extents of networks of connected fractures and have been interpreted as mud-water resurgences [5]. Hence, such evidence suggests a putative common origin that could potentially be linked to a single triggering phenomenon that acted on global scale.

References

[1] Kopf A.: Significance of mud volcanism, Reviews of Geophysics, Vol. 40, pp. 1005. http://dx.doi.org/10.1029/2000RG000093, 2002.

[2] Tanaka K., Skinner J. Jr., Hare T.: Scientific Investigations Map 2888 Major Modification Events Province Elysium Province Widespread Materials Geologic Map of The Northern Palins of Mars, US Geological Survey, 2005.

[3] Orgel C., Hauber H., Skinner J.A., van Gasselt S., Ramsdale J., Blame M., Séjourné A., Kereszturi A.: Distribution, origin and evolution of hypothesized mud volcanoes, thumbprint terrain and giant polygons in Acidalia, Utopia and Arcadia Planitae: Implications for sedimentary processes in the northern lowlands of Mars, 46th Lunar and Planetary Science Conference, LPSC2015-1862, 2015.

[4] Mazzarini F. and Isola F.: Monogenetic vent self-similar clustering in extending continental crust: Examples from the East African Rift System, Geosphere, Vol. 6, issue 5, pp. 567-582, 2010.

[5] De Toffoli B., Pozzobon R., Mazzarini F., Massironi M. and Cremonese G.: Evidence of mud volcanism rooted in gas hydrate-rich cryosphere linking surface and subsurface for the search for life on Mars, Geophysical Research Abstract, Vol. 19, EGU2017-251, 2017.

EPSC Abstracts
Vol. 11, EPSC2017-555, 2017
European Planetary Science Congress 2017

ESKER-LIKE RING-SHAPED RIDGES IN PETA, NOVARA AND TWO OTHER UNNAMED CRATERS ON MARS: EVIDENCES OF ANCIENT GLACIERS?

L. Guallini (1), T. J. Parker (2), S. Sutton (3) and N. Thomas (1).
(1) Physics Institute, Space Research and Planetary Sciences, University of Bern, Sidlerstrasse 5, 3012 Bern, Switzerland; (2) Jet Propulsion Laboratory, California Institute of Technology, Pasadena, USA; (3) Lunar and Planetary Laboratory, University of Arizona, 1629 E University Blvd, Tucson, Arizona, USA (luca.guallini@space.unibe.ch).

Abstract

We found in Peta, Novara and two other unnamed craters south Meridiani Planum (Mars) ring-shaped ridges that shows morphology and morphometry possibly consistent with terrestrial eskers. On Earth, these latter are deposited by fluvio-glacial systems and are exposed when ices retreat. Further analyses are in progress.

1. Introduction

1.1 Background

Argyre Planitia and Dorsa Argentea Formation (early Hesperian) are in the southern emisphere of Mars, respectively in mid-latitudes and close to polar regions. Their terrains show well-developed and elongated ridges by the most interpreted as eskers ([1], [2], [3], [4]). On Earth, it is well known that these morphologic features (composed by poorly sorted consolidated sediments) are deposited by glaciers and are exposed when ices retreat. Their length follows the direction of movement of the ancient ice-tongues, and gives us an idea of their maximum extension during glaciations. However, on Mars similar ridges are not exclusive of mid-high latitudes, but can be found in some topographic basins, also close to the equator. In the present work, we focus on the Paraná/Loire Valles and Erythraeum Chaos quadrangle (south Meridiani Planum). We analyzed Peta Crater (Lat 21°S, Lon 351°E; Fig.1a), where sinuous ridges have been previously observed by [5]. We found that also Novara crater (Lat 24°S, Lon 350°E; Fig. 1b) and two other unnamed craters (UC1; Fig.1C, Lat 19°S, Lon 346°E and UC2; Fig. 1d, Lat 19°S, Lon 347°E) contain similar features.

1.2 Methodology

The region has been analyzed using high-resolution visible images (MRO CTX, 6.0 m/pix and HiRISE, 0.25 m/pix). Topographic basemaps are from HiRISE DEMs, obtained by stereo-pairs (1.0 m/pix). Images have been processed using the USGS ISIS 3 and georeferenced into ArcGIS 10.x. HiRISE DEMs have been obtained using NASA Stereo Pipeline and Bae Systems © Socet Set.

2. Observations

The studied craters have diameters comprised between ~40 and ~90 km. Peta crater, UC1 and UC2 are all characterized by one main impact basin plus a secondary crater. This latter is superimposed on the main one. Crater basins contains one or more circular ridges, following almost continuously (in the case of Peta) or discontinuously (in the case of UC1 and UC2) the crater perimeter. Radial ridges are also exposed in UC1. On the contrary, Novara crater has an elliptical shape and contains ridges only close to its south-western borders and in its middle toward northeast. In plan-view, ridges are occasionally branched and anastomosing. In cross-section view, ridges are up to several hundreds of meters wide and some tens of meters high. Their shape is usually asymmetric, characterized by one steep side toward the crater interior and one gentle side toward the crater exterior (Fig. 1e). The crest of the ridges is sharp or rounded and in several cases split in two parts by a trough (multiple crested; Fig. 2). Analyzing THEMIS-IR day and night images [6], the thermal inertia of these ridges is generally higher than surrounding terrains, suggesting they are well consolidated.

3. Preliminary Discussion and Conclusions

The ridges in all the considered craters do not appear to have any possible fluvial source channel. Thus, they probably formed by other mechanisms [5]. According to [5] one possibility is that the ridges in Peta crater are push moraines and barrier ridges that form and are modified as the ice cover freezes to the shore in colder months, then melts and moves around with changing winds in warmer months. A similar hypothesis could be extended to all the other observed craters in the present study. On the other hand, the progressive retreat/advance of the ice-sheets should make more than one order of moraines (i.e. cirque moraines). However, in the crater basins we observe only one main ring of ridges. Based on our preliminary analysis, we propose an alternative hypothesis to simple moraines. In fact, the branched/anastomosing plan-view elongation of the ridges and their occasional extension in the interior of the basins (as for example in Novara and UC1 craters) suggest that they could be related to fluvio-glacial processes. This hypothesis seems to be sup-ported by the morphology and morphometry of the ridges, that is consistent with terrestrial eskers (e.g. [7], [8]) and with the ones observed in the Dorsa Argentea and Argyre regions. Ring-shaped eskers in the craters could form by the progressive melting of the glaciers starting mainly from their thinner outer borders and creating water flows moving in function of the local topography. At the same time, the forming eskers are radially pushed outwards by the flowing/sliding ice.

Acknowledgements

Support from Swiss NCCR PlanetS is gratefully acknowledged.

References

[1] Head J.W. (2000a), Tests for ancient polar deposits on Mars: Origin of Esker-like sinous ridges (Dorsa Argentea) using MOLA data, *LPSC XXXI*, Abstract #1116.

[2] Head J.W. (2000b), Tests for ancient polar deposits on Mars: Morphology and topographic relationships of Esker-like sinuous ridges (Dorsa Argentea) using MOLA data, *LPSC XXXI*, Abstract #1117.

[3] Banks M.E. et al. (2009), An analysis of sinuous ridges in the southern Argyre Planitia, Mars using HiRISE and CTX images and MOLA data, *JGR, 114*, E09003.

[4] Tanaka K.L. et al. (2014), Geologic Map of Mars, *Map 3292, U.S Geological Survey.*

[5] Parker T.J. (2011), Sinuous ridges in Peta Crater, Mars, *LPSC XLII*, Abstract #2776.

[6] Christensen et al. (2004), The thermal emission imaging system (THEMIS) for the Mars 2001 Odyssey mission, *Space Science Reviews, 110*, 85-130.

[7] Shreve R.L. (1985), Esker characteristics in terms of glacier physics, Katahdin esker system, Maine, *GSA Bull., 96*, 639-646.

[8] Huddart D. et al. (1999), Morphology and sedimentology of high-artic esker systems: Vegbreen. Svalbard, *Boreas, 28*, 253-273.

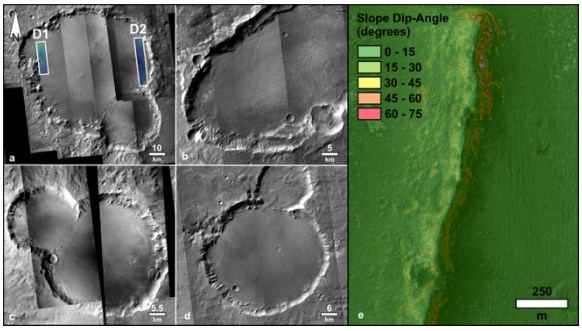

Figure 1. CTX images of Peta crater (a), Novara crater (b), UC1 (c) and UC2 (d). D1 and D2 are HiRISE stereo-pairs. In figure (e) is represented the slope dip-angle of one sample of the ridges inside Peta crater (calculated from HiRISE DEM D2). The crater center is toward left in the image.

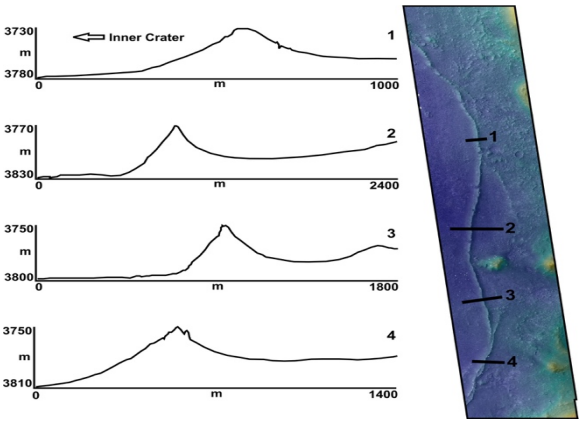

Figure 2. Cross-section profiles of one sample of the ridges inside Peta crater (calculated from HiRISE DEM D2).

EPSC Abstracts
Vol. 11, EPSC2017-566, 2017
European Planetary Science Congress 2017

Study of rootless cones on Olympus Mons Aureole, Mars

R.Parekh and N.Teanby
School of Earth Sciences, University of Bristol, UK (rp16119@bristol.ac.uk, n.teanby@bristol.ac.uk)

Abstract

Rootless cones, also known as pseudocraters, are the product of the interaction of lava with ground ice or near surface water. The study carried out on the north region of Olympus Mons Aureole where the cone structures identified. Large number of cones were analysed based on its morphological features, which will be compared with the cones of other region majorly comprised nearby the equator.

1. Introduction

The rootless cones forms due to continuous phreatomegmatic process where lava flows over water or ice rich surface/subsurface[1], [2]. It is known as rootless cones as there is no direct source which feed these cones but far from the location of cone construct[3]. First clear identification of cones were possible due to Viking data which imaged the Mars regions includes; Chryse Planitia[3], Deuteronimus Mensae, Acidalia Planitia[4], Islidis Planitia[5] and later Mars Orbiter Camera(MOC) acquired higher resolution images of Cerbus plains, Marte Valles, Amazonis Planitia, Olympus Mons[6] regions. In most of the cases, cones are modified by the geological erosion process; including impact process, mud flow, aeolian effect; however none of these able to explain the complete characteristics of cones[3].

2. Study region and geological settings

The survey area selected is located at north of Olympus Mons (between 34°-40° N and 215°-250°W). The region is characterized by rivers of lava flow and or mudflow, ridges and grabens[7]. During Amazonian period the volcanic flow might have descend from Tharsis region, Alba Patera, Amazonian Planitia and/or Olympus Mons itself which may have generated the deposit of aureole that covers more than 1.7million km^2 area[8]. The observed cones are scattered nearby the outer boarder of aureole deposits. Distinct termination between deposit and surroundings point towards the periodic process of eruption [7].The ridges and troughs are around 10-100km long and 5-10km wide[9] which are prominently visible in the center of the deposits, however from the center towards outward boundary the signature gets saturated due to erosion processes.

The rootless cones in this region was identified long ago[10] but detail study has not been carried out. Thus, the objectives to study cones of Olympus cones is to look for the cone features; measure morphometry of cones and analyse the frequency distribution of cones which will help us to understand the larger view of volcanic process and lava flow.

3. Observation

Total 2480 rootless cones identified using 12 ConTexT Camera (CTX)[11]images. The horizontal resolution of CTX images are 6 m/pixel and used to identify the locations of cones. However, for the morphological inspection High Resolution Imaging Science Experiment (HiRISE)[12] data were considered due to high spatial resolution of >0.25m/pixel. Nevertheless, due to limitation in coverage 8 images were found in study area. Based on HiRISE visual analysis the cones broadly divided into two categories: simple cones with smooth crater terrain; complex cones with rough crater terrain. The simple cones are usual structure that has already been identified in many regions of Mars[3], [6], [13]. Usually the cones have conical structure with depression and crater at the summit (Fig 1a).In case of complex cones, the crater present at the summit has rough terrain (Fig 1b). However, the process behind this has not understood yet. The major difference between these cones is in terms of diameters of crater. According to primary observation the complex cones seem to have higher average crater diameter than the simple ones.

4. Further Research

The motive behind analyzing rootless cones is to try to evaluate the volcanic activity on terrestrial planets. Further, author is trying to establish link between cones of various regions on Mars that may guide to different eruption process throughout the planet. This can lead us towards the better understanding of evolution of volatiles, past and current Martian climate condition, igneous processes and favourable locations for the biotic development.

References

[1] S. Thorarinsson, "The Crater groups in Iceland," Bull. Volcanol., vol. 14, no. l, pp. 3–44, 1953.

[2] S. A. Fagents and T. Thordarson, "Rootless volcanic cones in Iceland and on Mars," Geol. Mars Evid. from Earth-Based Analog., pp. 151–177, 2007.

[3] R. Greeley and S. A. Fagents, "Icelandic pseudocraters as analogs to some volcanic cones on Mars," J. Geophys. Res., vol. 106, no. E9, pp. 20527–20546, 2001.

[4] C. C. Allen, "Volcano-ice interactions on Mars," J. Geophys. Res., vol. 84, no. 9, pp. 8048–8059, 1979.

[5] H. Frey and M. Jarosewich, "Subkilometer martian volcanoes::properties and possible terrestial analogues," J. Geophys. Res., vol. 84, pp. 9867–9879, 1982.

[6] P. D. Lanagan, A. S. Mcewen, L. P. Keszthelyi, and T. Thordarson, "Rootless cones on Mars indicating the presence of shallow equatorial ground ice in recent times," Geophys. Res. Lett., vol. 28, no. 12, pp. 2365–2367, 2001.

[7] R. Lopes and J. E. Guest, "Further evidence for a mass movement origin of the Olympus Mons Aureole," J. Geophys. Res., vol. 87, no. B12, pp. 9917–9928, 1982.

[8] B. E. C. Morris and K. L. Tanaka, "Geologic maps on the Olympus Mons region of Mars," 1994.

[9] E. C. Morris, "Aureole deposits of the Martian volcano Olympus Mons," J. Geophys. Res., vol. 87, no. B2, pp. 1164–1178, 1982.

[10] C. Ann Hodges and H. J. Moore, "The subglacial birth of Olympus Mons and its aureoles," J. Geophys. Res., vol. 84, no. B14, pp. 8061–8073, 1979.

[11]M. C. Malin et al., "Context Camera Investigation on board the Mars Reconnaissance Orbiter," J. Geophys. Res. E Planets, vol. 112, no. 5, pp. 1–25, 2007.

[12]A. S. McEwen et al., "Mars reconnaissance orbiter's high resolution imaging science experiment (HiRISE)," J. Geophys. Res. E Planets, vol. 112, no. 5, pp. 1–40, 2007.

[13]S. A. Fagents, P. Lanagan, and R. Greeley, "Rootless cones on Mars: a consequence of lava-ground ice interaction," Geol. Soc. London, Spec. Publ. , vol. 202, no. 1, pp. 295–317, Jan. 2002.

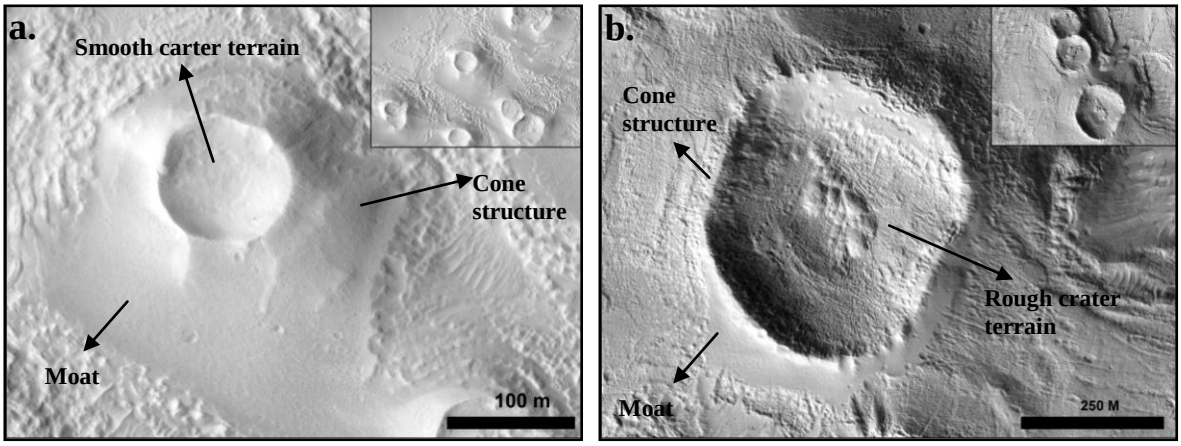

Figure 1 Typical example of simple cone(a) and complex cone(b) in Olympus Mons aureole (HiRISE image ID: ESP_034740_2145_RED and ESP_012363_2145_RED respectively).North upside

EPSC Abstracts
Vol. 11, EPSC2017-576, 2017
European Planetary Science Congress 2017

Ice-bearing deposits in the southern mid-latitude regions of Terra Cimmeria, Mars

S. Adeli (1), E. Hauber (1), R. Jaumann (1,2), G. Michael (2), and P. Fawdon (3)
(1) Deutsches Zentrum fuer Luft- und Raumfahrt (DLR), Institute fuer Planetenforschung, Rutherfordstr. 2, 12489 Berlin, Germany (Solmaz.Adeli@dlr.de) (2) Freie Universität Berlin, Institute of Geological Sciences, Malteserstr. 74-100, 12249 Berlin, Germany. (3) The Open University, Walton Hall, Milton Keynes MK7 6AA.

Abstract

In mid-latitude regions of Mars there is clear evidence of ground ice deposits whose formation has been assumed to be a result of Amazonian-aged climate changes, triggered by obliquity variations. We report here the presence of a new class of locally-observed deposits observed on the floor of an Amazonian-aged valley. These valley fill deposits (VFD) show evidence of shallow ice and are characterized by their convex-upward surface topography, crevasses, ablation moraines, sublimation pits, and ring-mold craters.

1. Introduction

Global circulation models (GCM) suggest that obliquity oscillations caused the mobilization of ice from polar regions and its re-deposition at lower latitudes [1, 2]. They show that during high obliquity periods, ice can be deposited almost anywhere in the mid-latitudes and during low obliquity ice is transported back to the poles [2-4]. Although the obliquity variations are not predictable for periods more than 20 Ma ago [5], it is likely that the surface of Mars, during Amazonian, has been repeatedly undergone such climate changes leading to deposition and sublimation/evaporation of ice-rich material [e.g., 3, 5, 6]. This study describes, for the first time, well-preserved glacial-like deposits in Terra Cimmeria, which are defined here as valley fill deposits (VFD) (Fig. 1-a). They are located on the floor of a valley system which bears a record of Amazonian-aged fluvial and glacial processes [7].

2. Morphological characteristics

Several deposits on the flat floors of S-N trending valleys south of Ariadnes Colles (34°S, 172°E) are characterized by (1) widths and lengths of a few kilometers, (2) convex-upward surface topography, and (3) pits and crevasses on their surfaces. These valley fill deposit (VFD) are located a few tens of kilometres east of the Tarq impact crater. Several of the VFDs are situated within the visible ejecta blanket of the Tarq Crater (Fig.1-a). The crater ejecta are clearly observable on the surface and surrounding area of those VFDs. Our crater size-frequency distribution results from the Tarq crater ejecta shows a model age ~μ410 (±60) Ma for the impact crater, which corresponds to middle Amazonian (epoch boundaries from [8]).

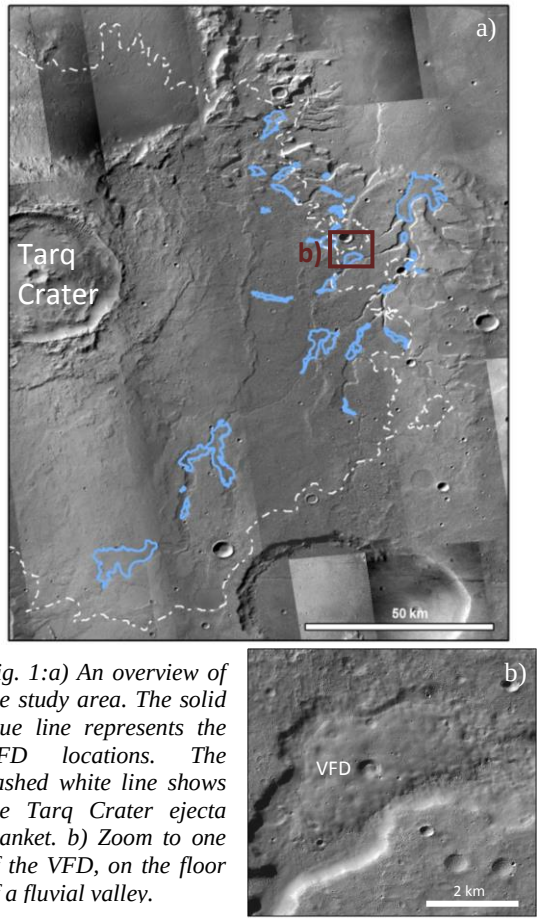

Fig. 1:a) An overview of the study area. The solid blue line represents the VFD locations. The dashed white line shows the Tarq Crater ejecta blanket. b) Zoom to one of the VFD, on the floor of a fluvial valley.

The VFDs have individual surface areas of a few km^2 to a few tens of km^2 (Fig1-b). In some cases they are located in the centre of the valley floor, whereas in other cases they cover the entire width of the host

valley, indicating their post-valley formation. The valley width could reach up to a few kilometres, in some areas. Using a HiRISE DEM, we observed that the VFD in the thickest part has a thickness of ~30 meters. The latitude dependent mantle (LDM) is also partly covering the VFD, and the surface of the VFD is outcropped where the LDM has been degraded or sublimated.

The surface of VFD shows only few impact craters, with diameters equal or smaller than ~700 m. Craters larger than 70 m are mostly degraded, their rims show almost no positive relief (at CTX resolution) and they have flat floors. Smaller modified craters have been observed, but there are also a few small fresh impact craters (smaller than 70 m in diameter) which do not show any modification of their rims and walls. On the surface of several VFD, we observed craters with a few hundred meters in diameter, bowl-shaped, and rimless, which have a flat floor. They have very similar characteristics to impact craters on LDA and LVF surfaces in mid-latitudes, which are termed ring-mold craters (RMC) by [9] and are thought to be a result of impacts into shallow buried ice.

Where higher resolution data are available, we can observe linear features, cracks, and crevasses on surface of VFD. Fig. 1-b shows one VFD which partly covers its host valley and display several crevasses at the surface as lateral or transverse crevasses. Transverse crevasses may indicate tensile stress caused by viscous flow of the deposit. In several cases, in front of the VFD margins, there is a zone up to 3 km of length, where the valley floors are rougher than further down the valley. We infer that this rough zone corresponds to sediment accumulation similar to moraine-like material in front of a glacier that moves down the valley. At the contact between the VFD and the valley walls, we observe several sublimation pits a few tens of meters wide and aligned along a preferential direction on the border of the VFD.

3. Discussion

The VFD have been observed on the floor of a valley system with traces of early to middle Amazonian fluvial activities [7] and our observations point to a post-valley formation for the VFD. The VFD is characterised by a convex-upward shape, transverse crevasses, sublimation pits, and association with moraine-like deposits. These characteristics, together with evidence of ring-mold craters, suggest that VFDs are ice-rich deposits with a thickness of a few tens of meters. The VFD has been later partly covered by LDM, which shows evidence of degradation, such as retreating boarders, sublimation pits, and scalloped surface.

The VFDs are partly distributed within the area covered by the Tarq Crater ejecta blanket. The superposition of the ejecta blanket on the VFD, points to the pre-ejecta distribution formation of these ice-bearing deposits, however, it is unclear whether the VFD formed prior to the impact event, or its deposition was contemporary with the impact and distribution of the ejecta blanket. In the former case, the ejecta blanket may have preserved the VFD by covering it. This ejecta cover had later been partly degraded, which led to the exposure of the currently present VFD in the area. On the other hand, in the latter case, the impact event may have occurred in ice-rich strata, which, subsequently, may have distributed a mixture of ejected material and ice, in other words, icy ejecta.

4. Implication:

The accumulation of ice/snow at mid-latitude regions cannot be explained by the current climatic condition of Mars, as the atmosphere does not sustain snow/ice accumulation and surface ice is unstable at mid-latitudes [10]. Therefore, the glaciation and deposition of VFD, regardless of the formation mechanism, should have taken place under different climatic conditions in the past. We conclude that the presence of ice-rich VFD underneath the young LDM is an evidence of an episodic and multi-event process of ice emplacement in the mid-latitude regions of Mars during the Amazonian period.

5. References

[1] Forget, F., et al. (2006), *Science. 311*, p. 368-371.
[2] Madeleine, J.-B., et al. (2009), *Icarus. 203*, p. 390-405.
[3] Smith, I.B., et al. (2016), *Science. 352*(*6289*), p. 1075-1078.
[4] Levrard, B., et al. (2007), *Journal of Geophysical Research: Planets. 112*(*E6*), p. E06012.
[5] Laskar, J., et al. (2004), *Icarus. 170*, p. 343-364.
[6] Head, J.W., et al. (2005), *Nature. 434*, p. 346-351.
[7] Adeli, S., et al. (2016), *Icarus. 277*, p. 286-299.
[8] Michael, G.G. (2013), *Icarus. 226*(*1*), p. 885-890.
[9] Kress, A.M. and J.W. Head. (2008), *Geophysical Research Letters. 35*.
[10] Mellon, M.T. and B.M. Jakosky. (1995), *Journal of Geophysical Research. 100*, p. 11781-11799.

EPSC Abstracts
Vol. 11, EPSC2017-584, 2017
European Planetary Science Congress 2017

Morphometric comparison and genetic implications of terrestrial, lunar and martian lava tubes

F. Sauro (1), R. Pozzobon (2) P. De Bernardinis (1) M. Massironi (2) and J. De Waele (1)

(1) Department of Biological, Geological and Environmental Sciences, Italian Institute of Speleology, University of Bologna, Bologna, Italy, (2) Department of Geosciences, University of Padova, Padova, Italy

Abstract

In this abstract we present a morphometric comparison between Terrestrial, Lunar and Martian lava tube collapses, based on high-resolution DTMs. The morphometric study allows identifying the depth of emplacement of the pyroducts in the different planetary bodies and sheds light on their formation processes, different sizes and ceiling stability due to the different planetary parameters and volcanism regimes.

1. Introduction

In the last twenty years pit craters, skylights, rills, and outflow channels on Lunar and Martian volcanic fields have been commonly interpreted as collapsed sections of lava tubes [1], although a clear understanding of their dimension, depth and formation processes in comparison to the Earth analogues remains elusive. As demonstrated by previous authors [2], not all pit crater chains can be directly related to lava tubes, but also other volcanic and tectonic processes are surely driving the formation of several of these pits. In order to identify the most promising lava tube candidates on Mars and the Moon we have adopted some main criteria that allows to distinguish lava tube pit chains on Earth not only from other volcanic pit features, but also between the two main different terrestrial morphotypes described (overcrusted and inflated) [3]. Following this necessary distinction, we present a morphometric comparison between lava tubes on Earth with some of the most prominent lava tube candidates identified on Mars and the Moon.

2. Lava tubes on Earth, Moon and Mars

Pit chains related to lava tubes on Earth present peculiar characters: 1) collapses are elongated ellipses with the minor axis representing the width of the tube; 2) their alignment is sinuous and can be braided; 3) the depth/width of the collapses represent the asymmetry ratio (ellipticity of the conduit), which is varying between inflated and overcrusted tubes. Taking these characters into account, we have performed morphometric analysis of terrestrial collapses and tubes dimension, focusing on Hawaii systems and in the Corona system of Lanzarote, which represents one of the most voluminous terrestrial tubes. On Mars, potential lava tube candidates have been proposed and measured on Hadriaca Patera, Arsia and Olympus Mons. On the Moon, we performed morphometric analysis in the area of Marius Hills, and specifically along the sinuous rills related to the Marius Hill skylight and along a pit chain in a parallel rill.

3. Methods

For all the morphometric analyses we relied on high-resolution DTMs. The lunar lava tube candidates have been measured on the Selene-Kaguya/LRO LOLA merged DTMs at ~59.22 meters/pixel gobal DTM, which is the result of merging and coregistration of stereo images from JAXA Selene-Kaguya mission with Lunar Reconnaissance Orbiter Laser Altimeter [4]. Martian DTMs were obtained by the stereo matching overlapping CTX (Context Camera, Mars Reconnaissane Orbiter) images at ~6 metrs/pixel with Ames Stereo Pipeline software [5]. The resulting DTMs at ~18 meters post spacing, were successively co-registered on validated HRSC DTMs provided by Mars Express mission and adjusted to the MOLA areoid. The collapses of the Corona Volcano lava tube, were measured on a 5 meters resolution DTM obtained from the interpolation of LIDAR shots provided by SGS.

4. Results and discussion

The data obtained are in agreement with recent modeling of lava tube stability on Mars and the Moon.

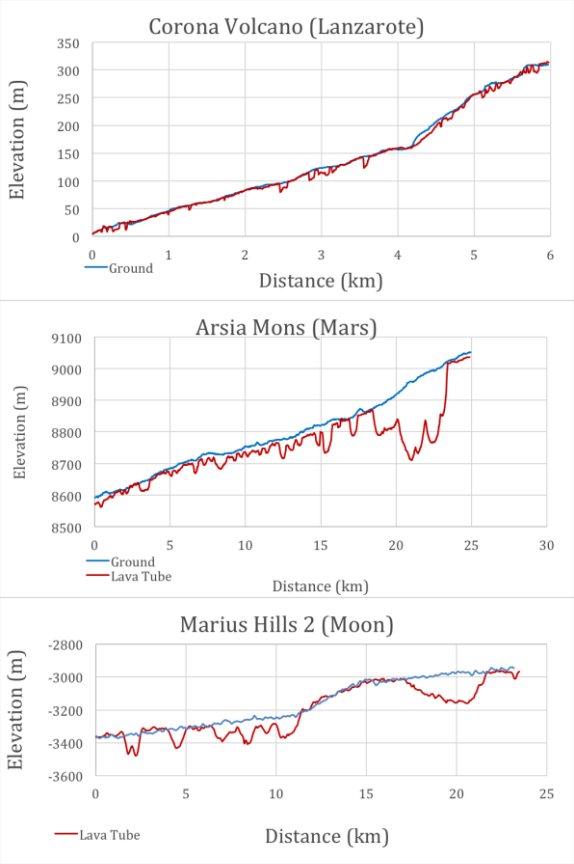

Figure 1: Examples of topographic profiles extracted along the tubes highlighting the collapses alignments and depths. In a) Marius Hills tubes b) Arsia Mons and c) Corona volcano

bodies [6] and sheds light on their formation processes and depth of emplacement. The depths of the collapses in each chain show a trend of maximum depth which correspond to the level of emplacement of the collapsed tube. While on Earth this is between 10 to a maximum of 30 meters, on the Moon the depth of the pit chain of Marius Hill is more than 100 m. On Mars this value is between 20 to 50 in Hardiaca Patera and between 30 to 80 in Arsia Mons. The minor axis analysis of the pit (which represent the witdth of the collapsed tube) shows a relevant increasing trend from Earth (20-30 m), to Mars (250 m), and to the Moon (0,8-1 km), suggesting that an increasing dimension of the conduits depending on gravity and effusion rates. However on the Moon pit chains are not so common suggesting that the most of the tubes have not been collapsed due to the higher stability of the ceilings, and are probably lying below deflated sinuous rills like where the Marius Skylight has opened to the surface. The asymmetry ratio (depth versus minor axis) is increasing from Earth to Mars and reach its maximum on the moon chains. This trend suggest that inflation processes are much more common and crucial in these planetary bodies compared to Earth.

References

[1] Cushing, G. E. (2012). Candidate cave entrances on Mars. Journal of Cave and Karst Studies, 74(1), 33-47.

[2] Wyrick, D., Ferrill, D. A., Morris, A. P., Colton, S. L., & Sims, D. W. (2004). Distribution, morphology, and origins of Martian pit crater chains. Journal of Geophysical Research: Planets, 109(E6).

[3] Kempe, S., Bauer, I., Bosted, P., Coons, D., & Elhard, R. (2010). Inflationary versus crusted-over roofs of pyroducts (lava tunnels). In Proceedings 14th International Symposium on Vulcanospeleology (p. 93).

[4] Barker, M.K., E. Mazarico, G.A. Neumann, M.T. Zuberc, J. Haruyama, D.E. Smith, (2016), A new lunar digital elevation model from the Lunar Orbiter Laser Altimeter and SELENE Terrain Camera, Icarus, Volume 273, Pages 346–355 doi:10.1016/j.icarus.2015.07.039.

[5] Shean, D. E., O. Alexandrov, Z. Moratto, B. E. Smith, I. R. Joughin, C. C. Porter, Morin, P. J. 2016. An automated, open-source pipeline for mass production of digital elevation models (DEMs) from very high-resolution commercial stereo satellite imagery. ISPRS Journal of Photogrammetry and Remote Sensing. **116**.

[6] Blair, D. M., Chappaz, L., Sood, R., Milbury, C., Bobet, A., Melosh, H. J., ... & Freed, A. M. (2017). The structural stability of lunar lava tubes. Icarus, 282, 47-55.

EPSC Abstracts
Vol. 11, EPSC2017-653-1, 2017
European Planetary Science Congress 2017

Delivery of organics to Mars through asteroid and comet impacts

K. Frantseva (1,2), M. Mueller (2,1), F.F.S. van der Tak (1,2), I.L. ten Kate (3) and S. Greenstreet (4,5)
(1) SRON Netherlands Institute for Space Research, Groningen, The Netherlands, (2) Kapteyn Astronomical Institute, University of Groningen, The Netherlands, (3) Department of Earth Sciences, Utrecht University, The Netherlands, (4) Las Cumbres Observatory, CA, USA, (5) University of California at Santa Barbara, CA, USA (k.frantseva@sron.nl)

Abstract

The recent discovery of methane in the Mars atmosphere and organic molecules in drill samples taken by Curiosity is surprising, as photodissociation and photodegradation would destroy most organics within hours. While burying in the subsurface will increase the lifetime, it is clear that organics must have been delivered in geologically recent times, presumably by impacts of asteroids, comets, and/or interplanetary dust particles (IDPs).

The IDP-borne organic flux on Mars was estimated to be 1.2×10^6 kg/yr by Flynn (1996) [**?**]. We calculate for the first time the flux from asteroids and comets.

We have performed numerical gravity simulations of impact rates on Mars within the past few Myr. We use the N-body integrator RMVS/Swifter to propagate the Sun and the eight planets from their current positions. Separately, we add comets and asteroids to the simulations as massless test particles, based on their current orbital distributions. In our asteroid simulations we focus on organic-rich (C-class), basing ourselves on the dynamical model by Greenstreet et al. (2012) [**?**] and on the measured distribution of taxonomic types across the Main Asteroid Belt. For the comets we assume a constant organic fraction.

We estimate the global carbon flux on Mars from cometary impacts to be $\sim 0.01 \times 10^6$ kg/yr within an order of magnitude, asteroid impacts deliver $\sim 0.042 \times 10^6$ kg/yr. Also, we find that organics from asteroids and comets will dominate over IDP-borne organics at distances up to 100 km from the crater center.

References

[1] Flynn, G. J.: The Delivery of Organic Matter from Asteroids and Comets to the Early Surface of Mars, Earth Moon and Planets, Vol. 72, pp. 469-474, 1996.

[2] Greenstreet, S., Ngo, H., Gladman, B.: The orbital distribution of Near-Earth Objects inside Earth's orbit, Icarus, V. 217, pp. 355-366, 2012.

EPSC Abstracts
Vol. 11, EPSC2017-660-1, 2017
European Planetary Science Congress 2017

Correlation of Radar and Visible Data of Mars' North Polar Layered Deposits

P. Becerra (1), I. Smith (2), D. Nunes (3), M.M. Sori (4), Y. Brouet (1), N. Thomas (1), and L. Guallini (1)
(1) Physikalisches Institut, Universität Bern, Switzerland (2) Planetary Science Institute, Tucson, AZ, USA. (3) Jet Propulsion Laboratory, Pasadena, California, USA (4) University of Arizona, Tucson, AZ, USA.

Abstract

We attempt to correlate two major datasets currently used to explore Mars' Polar Layered Deposits: Visible imagery and stereo-topography from HiRISE and sub-surface radar from SHARAD. The resulting stratigraphic columns can constrain formation models for the deposits and will be used to explore their connection to Mars' Amazonian climate evolution.

1. Introduction

A long-standing problem in Mars Polar Science is the interpretation of the stratigraphic record preserved in Mars' icy North Polar Layered Deposits (NPLD) [1] (Fig. 1a), whose accumulation patterns of ice and dust have long been associated with recent climatic changes due to temporal variations in the planet's astronomical parameters [2,3]. The internal layering of the NPLD is visible from orbit in exposures within a series of spiraling troughs that dissect the NPLD dome (Fig. 1a,b). Studies have relied on remote images of these troughs to map the stratigraphy [5-9] and search for a connection between NPLD accumulation and astronomical forcing [10-13]. Sub-surface sensing radar sounding has also proved invaluable in observing the internal structure of the deposits. The Shallow Radar (SHARAD) instrument [14] detects changes in dielectric properties with depth. As these vary for layers with different amounts of dust contamination, layering is observed in the radar data as "reflector" surfaces [15].

The optical and radar-based stratigraphies have predominantly been studied in isolation. In terrestrial climate science [17], orbital climate forcing was ultimately confirmed by the correlation of sedimentary, geochemical and paleo-magnetic records, suggesting that integration of datasets is necessary to build a complete climate record for the NPLD. In general, both radar and optical layers are assumed to result from varying amounts of silicic impurities in water ice [19]. Christian et al. [18] attempted the first quantitative correlation and found a general agreement between properties of radar reflectors and visible layers. This provided evidence that the same physical quantity (potentially dust fraction) controls the formation of both sub-surface radar reflectors and protruding strata. However, they were unable to achieve a unique correlation between one radar reflector and one visible layer or packet.

Here, we present our approach to this correlation by modeling the SHARAD propagation through permittivity profiles constrained by HiRISE-derived topographic profiles [9]. The objective is to combine the information from both datasets to obtain a dust-fraction-based NPLD stratigraphic profile at the finest resolution possible. These profiles can constrain orbitally-forced climate-accumulation models [20,21], thereby illuminating the connection between orbital history, climate, and polar accumulation during the formation of the NPLD.

2. Methods

The goal of the data integration is to obtain dust content vs. depth profiles that can be directly compared to the output of layer accumulation models. Our approach: (1) Model the radar wave propagation through synthetic permittivity profiles constrained by a relationship between the HiRISE-derived topographic expression of the layers, and permittivity (ε). (2) Correlate these profiles to real SHARAD data using spectral analysis and pattern-matching algorithms. This correlation results in HiRISE-SHARAD stratigraphic profiles of ε, which can be transformed to fractional dust-content [23] and thereby be used to constrain accumulation models.

We use the radar-propagation model of [19] and the HiRISE topography products of [9]. The layered medium through which we propagate the model radar wave is a ε profile constrained by the protrusion profiles of [9], which measure topographic expression of layers at the resolution of HiRISE Digital Terrain Models (DTMs) by calculating how much a layer deviates from an average linear fit to the trough slope [9] (e.g. fig. 2a,b).

3. Preliminary Results

Since we know that dust content affects the dielectric response of subsurface ice, and we assume that it affects protrusion [9,21] we make the change in ε with depth of the model profile depend on the

layer protrusion. The average fractional dust content within the NPLD is <5% [24], corresponding to an average ε = 3.1. Individual layers can have higher or lower values [25]. We search for an empirical model that relates protrusion to ε by varying the ε of layers between that of pure ice (3.0–3.15) and the highest values observed at the NPLD by [24] (~3.8), although this will vary to account for updated maximum values [25], and the possibility of high porosity [26]. The model radar profiles in Fig. 2c simulate the SHARAD pulse through a medium constrained by selected protruding layers from the profile at site N0 (known as "Marker Beds" [5]; Fig. 1a, 2b) corresponding to a depth of ~ 250 m, which were assigned a ε of 3.5 and a background ε of 3.15. Fig. 2c shows that thick protrusion peaks (>15 m) are resolvable, while thinner layers could be difficult to distinguish. A comparison with the observed radargram at site N0 (fig. 2d) shows that between 2.5 and 5 μs (~200 – 400 m in depth), there is a similar number of reflections in the observation (5-6) and the model (6-7), demonstrating that they are comparable.

4. Future Work

Our preliminary investigations have promising results. We will extend this study and generate synthetic radar profiles based on different empirical ε–protrusion relations at each site shown in fig. 1a. We will select 2–10 SHARAD observations to calculate average depth vs. power profiles (e.g. Fig. 2d) at locations near each trough wall, so that each site has a representative radar and protrusion profile. To correlate the synthetic radar profiles to SHARAD data, we will use two complementary methods: Wavelet analysis [13,27] and dynamic-time warping [9,28]. The first will estimate similarities between profiles by comparing their spectral properties, and the second will perform the direct correlation of profiles to select the best ε–protrusion empirical model. Further work involves comparing the integrated stratigraphy with formation models controlled by orbital cycles [e.g. 21].

5. Figures

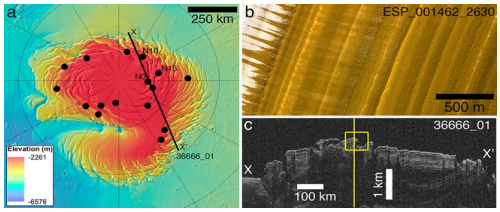

Figure 1. (a) Topographic map of the NPLD. Dots = locations of study sites and HiRISE DTMs from [9]. The line is the ground track of the SHARAD radargram shown in (c). (b) HiRISE image of exposed layers in an NPLD trough. (c) SHARAD radargram (X-X' in 1a). The square marks the approximate location of site N0. The line shows the position of the profile of Fig. 2d.

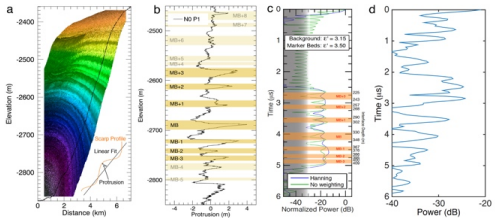

Figure 2. (a) HiRISE DTM and topographic profile of site N0. Inset is a schematic of the protrusion calculation [9]. (b) Protrusion profile of site N0. "Marker Beds" (MB) correlated to the stratigraphy of [7] are shown (c) Example synthetic radar profile produced by wave propagation through marker beds of 2b using a simple compressed pulse (green), and one weighted by a Hanning window (blue) [19]. (d) SHARAD radar profile near site N0. Delay times and power for both (c) and (d) are referenced to the first arrival of the surface reflection.

Acknowledgements

Part of this work is funded by the Swiss National Centre of Competence in Research (NCCR) PlanetS.

References

[1] Clifford, et al. *Icarus* 225 (2013) [2] Cutts *JGR* 78 (1973) [3] Cutts, et al. *Science* 194 (1976) [4] McEwen et al. *JGR* 112 (2007) [5] Fishbaugh et al. *JGR* 111 (2006) [6] Tanaka et al. *Icarus* 196 (2008) [7] Fishbaugh et al. *GRL* 37 (2010) [8] Limaye et al. *JGR* 117 (2012) [9] Becerra et al. *JGR* 121 (2016) [10] Laskar et al. *Nature* 419 (2002) [11] Milkovich and Head, *JGR* 110 (2005) [12] Perron and Huybers, *Geology* 37 (2009) [13] Becerra et al. *GRL* 44 (2017) [14] Seu et al. *JGR* 112 (2007) [15] Putzig et al. *Icarus* 204 (2009) [16] Smith et al. *Science* 352 (2016) [17] Imbrie, *Icarus* 50 (1982) [18] Christian, et al. *Icarus* 226 (2013). [19] Nunes & Phillips, *JGR* 111 (2006) [20] Levrard et al. JGR 112 (2007) [21] Hvidberg et al. *Icarus* 221 (2012) [23] Stillman, et al. *J.Phys.Chem.* 114 (2010) [24] Grima, et al. *GRL* 36 (2009) [25] Lalich and Holt, *GRL* 44 (2017) [26] Bramson et al. *GRL* 42 (2017) [27] Torrence and Compo, *Bull. Am. Met. Soc.* 79 (1998) [28] Sori et al. *Icarus* 235 (2014).

EPSC Abstracts
Vol. 11, EPSC2017-665-3, 2017
European Planetary Science Congress 2017

Subaqueous mass-flow deposits at Noachian Terby Crater, Mars: Decoding rheology and depositional style

P. Das, and A. Basu Sarbadhikari
Physical Research Laboratory, Ahmedabad, India (priyabrata@prl.res.in)

Abstract

Terby impact basin (~174 km diameter; 28.0°S, 74.1°E) is located at the northern rim of large Hellas basin of Mars (Fig. 1a), and represents an exposed Noachian lake sedimentary deposit [1, 2]. A detailed process based sedimentological study has been carried out to delineate the evolution of fluid flow process operative during Terby filling, using high resolution orbital images. The ~2 km thick layered succession is broadly classified into three different categories, i.e. slumps, debris flow and turbidites, and clubbed under subaqueous gravity flow deposits. The occurrence of large volume of semi-lithified clay-rich sediments suggests that the material were possibly transported from the northern slope and re-deposited in Terby crater.

1. Introduction

The submarine gravity induced flow is one of the most important sediment transport process across our planet, where water played a significant role to control the depositional properties [3]. Such underwater deposits are commonly referred as mass transport complex (MTC). Previous studies on Terby are mainly dealt with broad description and lithostratigraphic reconstruction [1, 2]. Based on stratal relationships and spectral mineralogy the basin has been descibed as a fluvio-lacustrine [1] and/or ice covered lake settings [2]. However, no attempt has been made so far to characterize the depositional flow process using specialized sedimentological approach. This study has been conducted from the fan-delta section of the basin and a systematic characterization of the sedimentary units has been done based on shape, size, geometry, internal fabrics and the mutual associations using HiRISE images.

2. Observations and interpretation

We have identified three major associations from the succession of Terby, i.e. mega-slump, debris flow and turbidity flow deposits. A well preserved kilometer long folded unit is occupied at the basal part of the succession that exhibits significant amount of bed rotation compared to overlying undeformed unit, and well preserved pinch-and-swell structure at the northern limb (Fig. 1b). The regional-scale structure suggests that a large volume of soft-sediment underwent compression related deformation (hydro-plastic), which resulted in extensional stretching during mass-failure. A ~750 m thick, flat based convex-up unit, composed large volume of debris avalanches with disharmonic folded to distorted-rafted-stratified multi-meter scale large beds indicates immediate disintegration of the deposited materials during propagation of slump (Fig. 1c).

The multi-meter scale thick, successive layers are composed of boulder conglomerate and bounded by planner to scoured decollement surface at the bottom and parallel layers at the top, exhibits overall thinning-up character (Fig. 1d). In places, foreset of the units are defined by large elliptical imbricated boulders separated by sigmoidal imbricated thrust duplex, suggests a compression driven propagation of debris during mass flows [4, 5]. The rheology of these units is ranging between cohesive debris flow to high density turbulent flow.

Sharp, concave-up, weakly-confined, multi-storied channels with broad slightly elevated levee-flood plain system developed sideways of the channels (Fig. 1e). However, these structures are not very prominent because of paucity of coarser clastic in the system. Along with this a thinning-up cycle of parallel bedded units is preserved in few restricted areas at the upper part, which suggests its distal/deeper water origin with the settlement rate of pelagic mud exceeded to the rate of fluvial fluxes. However, it is

difficult to over-rule the proximal origin, because such deposit type is also common in mass transport related sediment ponding [5]. The identified sequence of flow processes of Terby is shown in Figure 1f.

3. Summary and conclusions

Subaqueous mass flow deposits have wide spectrum of rheological character and commonly are accounted from hyperpycnal deltas and continental shelves, where accumulation of voluminous sediments is the most common triggering factor. Dominance of mega-slumps and voluminous debris flow deposits at the lower to middle half of Terby succession suggests sediment filling rate was very high at initial stages. Under such condition, chances of getting significant amount of phyllosilicates is very uncommon, unless the material was pre-deposited under stable aqueous condition and later reworked into the system. The imbrication direction of the debris thrusts and the rheology of the mega-slumps suggest a large volume of pre-deposited, semi-lithified sediments were transported from northern slope and re-deposited immediately after the depression created due to impact. Irrespective of over steepening of delta, such large volume of mass-transport deposits can also be triggered due to under-water impact and similar type of deposits are well studied from K-Pg boundary impact at the Gulf of Mexico [6, 7].

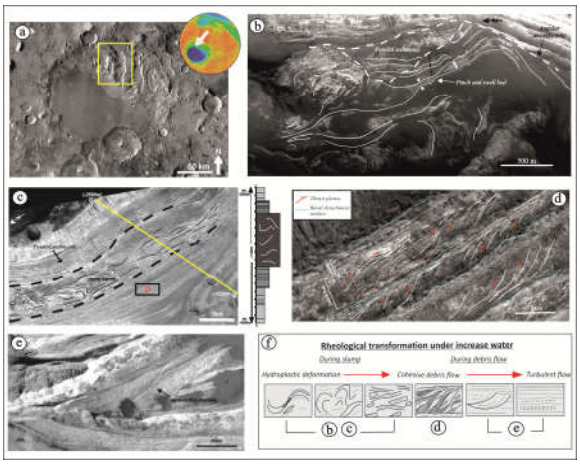

Figure 1: (a) Location of Terby impact crater at the north of Hellas basin, yellow box marked the study area. (b) Folded outcrop of mega-slump deposit located at the basal part of the succession. (c) Mega-slump deposit located at the middle of succession (marked by dashed line) sandwiched between layered rock strata. (d) Successive debris-flow units defined by basal erosional (sheared) surface, imbricated foreset and laterally continuous parallel bedded top. (e) Semi-confined, laterally accreted channel facies associated with thinly bedded units, upper part of the succession. (f) Interpreted mass-transport flow processes of Terby.

Acknowledgements

This work was funded by Department of Space, Government of India.

References

[1] Ansan, V., Loizeau, D., Mangold, N, Le Mouélic, S., Carter, J., Poulet, F., Dromart, G., Lucas, A., Bibring, J-P., Gendrin, A., Gondet, B., Langevin, Y., Masson, Ph., Murchie, S., Mustard, J.F., and Neukum, G.: Stratigraphy, mineralogy, and origin of layered deposits inside Terby crater, Mars, Icarus, Vol. 211, pp. 273-304, 2011.

[2] Wilson, S.A., Howard, A.D., Moore, J.M., and Grant, J.A.: Geomorphic and stratigraphic analysis of Crater Terby and layered deposits north of Hellas basin, Mars, Journal of Geophysical Research, Vol. 112, E08009, 2007.

[3] Telling, P.J., Charles, K. P., Piper, D.J.W: How are subaqueous sediment density flows triggered, what is their internal structure and how does it evolve? Direct observations from monitoring of active flows. Earth-Science Review, Vol. 125, pp. 244-287, 2013.

[4] Posamentier, H.W, and Walker, R.G.: Deep-water turbidites and submarine fans, in Walker, R.G., and Posamentier, H., eds., Facies Models Revisited, SEPM, Special Publication, Vol. 84, pp. 397–520, 2006.

[5] Kneller, B., Dykstra, M., Fairweather, L., and Pablo Milana, J.: Mass-transport and slope accommodation: Implications for turbidite sandstone reservoirs, AAPG Bulletin., Vol. 100, pp. 213-235, 2016.

[6] Sanford., J.C., Snedden, J.W., and Gulick, S.P.S.: The Cretaceous-Paleogene boundary deposit in the Gulf of Mexico: Large-scale oceanic basin response to the Chicxulub impact, Journal of Geophysical Research - Solid Earth, Vol. 121, pp. 1240–1261, 2016.

[7] Norris., R.D., and Frith, J.V.: Mass wasting of Atlantic continental margins following the Chicxulub impact event. Geological Society of America Special Papers, Vol. 356., pp. 79-95, 2002.

EPSC Abstracts
Vol. 11, EPSC2017-667-2, 2017
European Planetary Science Congress 2017

Revised coordinates of the Mars Orbiter Laser Altimeter (MOLA) footprints

Serena Annibali (1), Alexander Stark (1), Klaus Gwinner (1), Hauke Hussmann (1), Jürgen Oberst (1,2)
(1) Deutsches Zentrum für Luft- und Raumfahrt, Berlin, Germany (Alexander.Stark@dlr.de), (2) Technische Universität Berlin, Germany

Abstract

We revised the Mars Orbiter Laser Altimeter (MOLA) footprint locations (i.e. areocentric body-fixed latitude and longitude), using updated trajectory models for the Mars Global Surveyor and updated rotation parameters of Mars, including precession, nutation and length-of-day variation [1]. We assess the impact of these updates on the gridded MOLA maps. Ultimately, we aim at independent measurements of the rotation parameters of Mars. Using the method presented by Stark et al. [2], we co-register MOLA profiles to digital terrain models from stereo images (stereo DTMs) and measure offsets of the two data sets. At the same time we wish to assess the accuracy of the stereo DTMs and detect possible unidentified false returns in the MOLA data.

1. Introduction

The MOLA data greatly improved our knowledge about Mars morphology and became an extensively used reference for Mars. In the last decade, data from several space missions improved our knowledge on shape, gravity, and rotational state of the planet. With the improved knowledge of the gravity field of Mars, the trajectory of the Mars Global Surveyor (MGS) spacecraft has been reconstructed with better accuracy [3, 4]. However the MOLA data, released in 2003, remains to be based on an outdated spacecraft orbit and Mars rotation model (the so called IAU2000 Mars rotation model) neglecting the precession and nutation of the rotation axis as well as seasonal spin variations. The present work contains a comparison of the Mars parameters given in the IAU2000 reference frame [5] and in the more complete orientation model of Mars [3]. Assessing the discrepancy between old and new values of the planet's rotational parameters gives a first evaluation of the difference to be expected between old and recomputed MOLA footprint locations.

2. Data sources

2.1 MOLA measurements

The MOLA instrument on Mars Global Surveyor operated as an active altimeter from February 1999 until June 2001. Short Laser pulses at the Laser wavelength of 1.064 µm are sent to the surface [6]. From an average spacecraft altitude of 400 km the emitted pulse produces a footprint of about 75 m diameter [7]. A small portion of the reflected laser pulse is detected at the spacecraft and by measuring the time of flight of the laser pulses, precise measurements of spacecraft ranges are obtained. A single range measurement has a vertical precision in the order of 40 cm (over smooth terrain); the location of the laser footprints was corrected for spacecraft trajectory errors through an adjustment using height differences at cross-over points [8]. At the given shot frequency of 10 Hz, consecutive measurements are separated by 300 m and form topographic profiles, which ultimately yield global coverage. Interpolation is performed where data are missing and a gridded topographic model based on over 333 million surface measurements has been devised. Final registration of profiles and images are obtained with an uncertainty of < 100 m [9]. The complete data set is archived at the Planetary Data System [10].

2.2 Rotation parameters

The rotation parameters of Mars were recently improved based on all available tracking of spacecraft in orbit around Mars and of landers on the surface of Mars [1]. The model includes seasonal variations of the rotation rate, as well as precession and nutation terms of the rotation axis. A comparison of the Euler angles (right ascension, declination and prime meridian angle) of the previous IAU2000 rotation model and the new model from [1] is shown in Figure 1 over the time span of eight years.

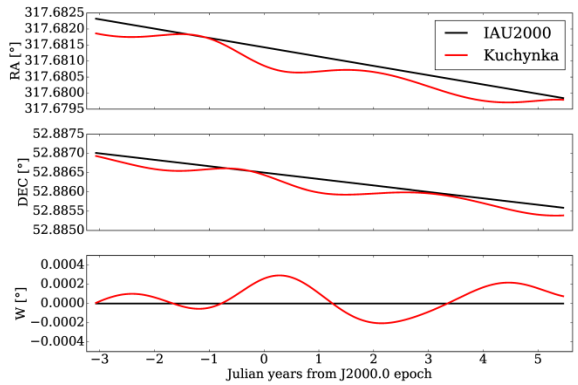

Figure 1: Variation of right ascension (RA), declination (DEC) and prime meridian (W) angles for the IAU2000 (black) and the Kuchynka et al. [1] (red) rotation models. For the prime meridian angle the rotation rate of the IAU2000 [5] model was subtracted from both models. Further, an offset of 0.0018° has been applied to the prime meridian angle of the Kuchynka et al. model in order to better notice its variations in time.

2.3 MGS orbit solutions

The accuracy of the laser altimeter profiles depends on the knowledge of the spacecraft position and attitude at the firing time. Any offset of the spacecraft directly translates to lateral and vertical offsets of the Laser spots on the ground. After completion of the MGS mission in November 2006, the Inner Planet Navigation and Gravity Group (IPNG) from JPL NASA performed an orbit determination for MGS using the complete set of available radio science observations based on the gravity model described by Konopliv et al. [3]. More recently, Genova et al. [4] determined the gravity field of Mars considering radio science data from MGS, Mars Odyssey and Mars Reconnaissance Orbiter. The orbits of the three spacecraft were updated in the process. However, the MOLA data itself was processed using the outdated MGS orbit solution by the Goddard Space Flight Center dating back to 2003.

3. Results

The locations of the MOLA footprints in the region within (337.5°, 360°) longitude and (15°, 30°) latitude have been recomputed according to the rotation model of Mars given by Kuchynka et al. [1] (Figure 2) and to the IAU2000 model. The obtained maps have been compared in terms of height differences (Figure 3).

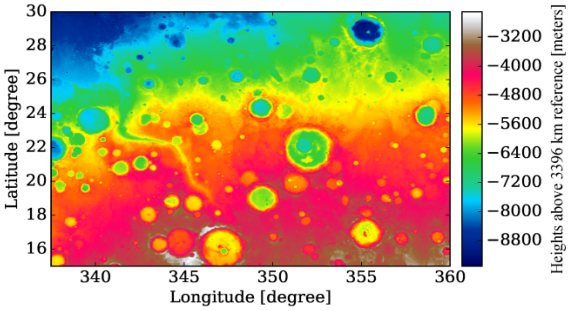

Figure 2: Example of a gridded terrain model for a small region of Mars from MOLA profiles computed using the Kuchynka et al. [1] rotation model. Interpolation was performed on regions without MOLA measurements.

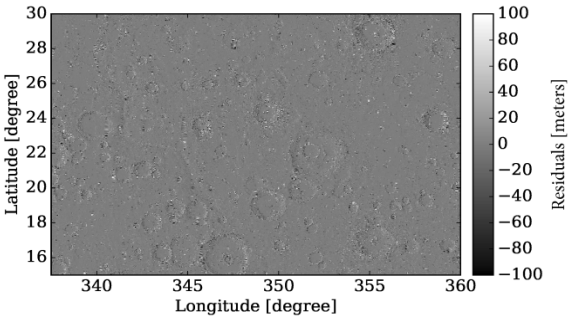

Figure 3: Difference between the nominal (IAU2000) MOLA data set and the terrain model computed using the Kuchynka et al. [1] rotation model.

The comparison reveals that even slight corrections to the rotational state of Mars can lead to height differences up to 100 m (in particular in regions with high slopes, where large interpolation effects are expected). Further work will assess the impact of the MGS orbit solutions on the MOLA data set.

Acknowledgements

This work was supported by a research grant from the Helmholtz Association and German Aerospace Center (DLR).

References

[1] Kuchynka et al. 2014, Icarus, 229, 340–347. **[2]** Stark et al. 2015, *GRL*, 42, 7881-7889. **[3]** Konopliv et al., 2006, *Icarus*, 182, 23-50. **[4]** Genova et al. 2016, *Icarus*, 272, 228-245. **[5]** Seidelmann et al. 2002, *Celest. Mech. Dyn. Astron.*, 82, 83-111. **[6]** Smith et al. 2001, *JGR-Planets*, 106, 23689-23722. **[7]** Neumann et al. 2003, *GRL* 30-11, 1561. **[8]** Neumann et al. 2001, *JGR-Planets*, 106, 23, 753-768. **[9]** Neumann et al. 2003, Lunar and Pl. Science XXXIV. **[10]** MOLA on *PDS* ftp://pds-geosciences.wustl.edu/mgs/mgs-m-mola-3-pedr-l1a-v1/mgsl_21xx/

EPSC Abstracts
Vol. 11, EPSC2017-670, 2017
European Planetary Science Congress 2017

The thermochemical structure of Mars - a seismological perspective on phase transitions, low-velocity layers and convection in the deep interior

S. Hempel (1,2), R. Myhill (3), A. Rivoldini (4) and R. F. Garcia (1)
(1) ISAE Supaéro, Toulouse, France, (2) Institut of Geophysics, University of Münster, Germany, (3) University of Bristol, United Kingdom, (4) Royal Observatory of Belgium, Brussels, Belgium

The deep thermal and chemical structure of Mars has been shaped by many processes, including impacts, core-mantle segregation, convection and volcanism. This structure is currently poorly constrained; improved constraints will help us better understand the planet's thermal, chemical, dynamic and magnetic evolution.

The InSight mission landing on Mars in 2018 will deploy a seismometer on Elysium Planitia, providing us with single-station three-component measurements of Martian seismicity, illuminating its interior structure. These measurements are subject to perturbations due to the significantly aspherical structure of the Martian crust, source location uncertainties, lander and environment noise, and due to waveform distortions due to yet unknown scattering properties of the Martian upper mantle and crust. In preparation for this mission, we build on earlier models of Mars structure (e.g. Mocquet et al, 1996; Sohl and Spohn, 1997; Gudkova and Zharkov, 2004; Khan and Connolly, 2008; Zharkov et al, 2009; Rivoldini et al, 2011) to investigate the effects of specific unknowns on seismic travel times and waveforms which we expect to be recorded during the mission (Nissen-Meyer et al., 2015; Hempel and Garcia, 2017).

In this study, we link model parameters such as average crustal thickness, mantle temperature, composition and convective vigour with seismic observables such as travel times and ray parameters. We discuss the trade-offs between the model parameters based on ray theoretical predictions, focusing on the effects of low-velocity layers in the uppermost and lowermost mantle, the absence or presence of triplications indicating the sharpness of phase transitions within the Martian mantle and the effects of core size and composition on seismic observables.

EPSC Abstracts
Vol. 11, EPSC2017-692-1, 2017
European Planetary Science Congress 2017

Detailed geological mapping of the fluvial deposits in Magong crater, Xanthe Terra, Mars

J. Knade (1,), **E. Hauber** (2), T. Platz (3,4), L. Le Deit (5) and K. Kinch (6)
(1) Beuth Hochschule für Technik, Berlin, Germany (s62756@beuth-hochschule.de), (2) Institute of Planetary Research, German Aerospace Center (DLR), Berlin, Germany (Ernst.Hauber@dlr.de), (3) Planetary Science Institute, Tucson, USA, (4) Max Planck Institute for Solar System Research, Göttingen, Germany, (5) Laboratoire de Planétologie et Géodynamique, University of Nantes, Nantes, France, (6) Niels Bohr Institute, University of Copenhagen, Copenhagen, Denmark.

Abstract

We present a detailed geological map of Magong Crater in Xanthe Terra, Mars. The ancient crater is situated at the terminus of Sabrina Vallis and hosts sedimentary deposits that were transported through this long and deeply incised valley. The sediments may represent a delta or, alternatively, an alluvial fan. Weak signatures of Fe/Mg-bearing phyllosilicates were detected in the central delta cliff section. A long and narrow, NE-trending topographic ridge is interpreted as a partially exhumed dyke. Numerous ~1 m-thick dark patches are distributed over the entire crater floor and may be remnants of a formerly continuous blanket of volcanic tephra or ash. The overall age of the aqueous sediments is dated to the Late Noachian/Early Hesperian epochs. This applies also to the surrounding highland materials. High-resolution images of the crater floor show a heterogeneous morphology, featuring a large variety of degraded craters and ejecta blankets, honeycomb-like depressions and polygonal fractures similar to mud cracks. Apart from the sedimentary deposits, the crater floor is very flat and meets the geological and technical criteria for a future possible landing site.

1. Introduction

Magong Crater has a diameter of ~40 km and is located in the north of Xanthe Terra at 11.9°N, 313.4°E. Its degraded rim and the flat floor suggest that it has formed in the Noachian. Sabrina Vallis is a deeply incised valley with few tributaries which extends for about 250 km in W-E direction through Middle Noachian highland material [1] and terminates in Magong Crater. Layered sedimentary deposits [2,3] at the mouth of Sabrina Vallis may be a promising target for in situ investigations by a future rover [4]. We performed detailed geological mapping of Magong Crater to distinguish between a deltaic and alluvial fan scenario for the origin of these sediments. Previous studies focused mainly on criteria for a possible landing site [5] and showed a simplified geological map featuring age determinations based on crater counts. The goal of this study is to clarify stratigraphic relationships, determine layer geometries, refine the sedimentary characteristics of the layers, improve the knowledge of the crater history by obtaining additional crater retention ages, and establish the crater floor resurfacing history.

2. Data and Methods

Morphological mapping (Fig. 1) was performed on HRSC (12.5 m/px), CTX (5-6 m/px) and HiRISE (0.25 m/px) images in a GIS environment. For age determination we used the CraterTools [6] and Craterstats [7] software packages. Digital Elevation Models (DEM) based on stereo images were used for topographic measurements.

3. Observations

The sedimentary deposit extends from the apex at the terminus of Sabrina Vallis to the center of Magong crater, covering ~220 km² (~19% of the crater floor). The sedimentary deposits are subhorizontally layered (Fig. 2a) and can be traced for >1km along the eroded cliffs at the distal part of the sediments. The main body of the sediments is covered with eolian deposits, which fill small craters and tend to form transverse aeolian ridges (TAR). The deltaic deposit is partly surrounded by a shallow topographic moat, which is flat-floored and dissected by polygonal fractures (Fig. 2b). Faint traces of polygonal fractures can also be found near the northern crater rim and outside of the moat in southern parts of the crater.

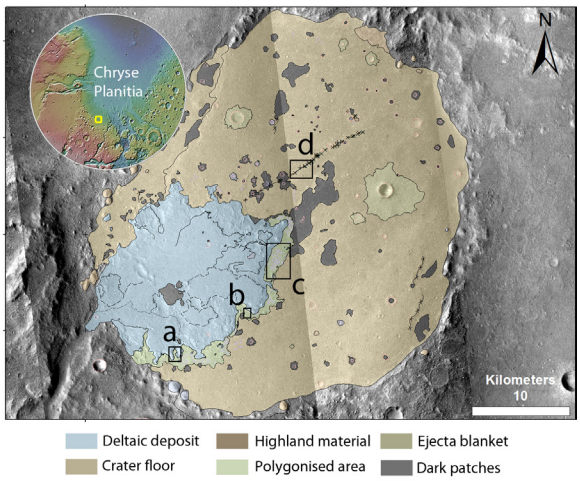

Figure 1: Refined geological map of Magong Crater and the sedimentary features. Boxes mark the locations of Figs. 2a-d. The geology of the sedimentary body is still mapped in preliminary form.

Circular depressions surrounded by concentric fractures are locally observed (Fig. 2c) and resemble "honeycomb" terrain identified in western Hellas Planitia [8], although at a smaller scale. The crater floor shows various heterogeneous morphological features. The most striking feature is a NE-trending ridge (Fig. 2d). Two similar small ridges are located near the western crater rim and are oriented in E-W direction. The crater floor appears dust-free and exhibits a rough texture with a variety of degraded craters. Aeolian bed forms can be found in some larger craters. Fresh craters exposed dark-toned underlying strata. Patches of dark deposits overlie the crater floor and can also be locally observed on top of the delta.

4. Discussion

Sabrina Vallis and the surrounding highland terrains show characteristics for periods of extensive fluvial activity. The Sabrina valley system was formed at about 3.8 Ga (all ages relate to the Neukum chronology), whereas the delta represents the last stage of fluvial activity at 3.4 Ga [3-5]. The dark patches are hypothesized to be remnants of a tephra blanket emplaced through eruptions in nearby Lederberg crater [9], although it is not possible to unambiguously confirm this. The topographic ridge is interpreted to be a partially exhumed dyke. It is unclear if the similar ridges elsewhere in the crater are also associated with igneous activity. The polygonal features are possibly mud or desiccation cracks. It is unknown whether the circular depressions near the deltaic deposits represent diapiric processes as in the Hellas basin floor [9].

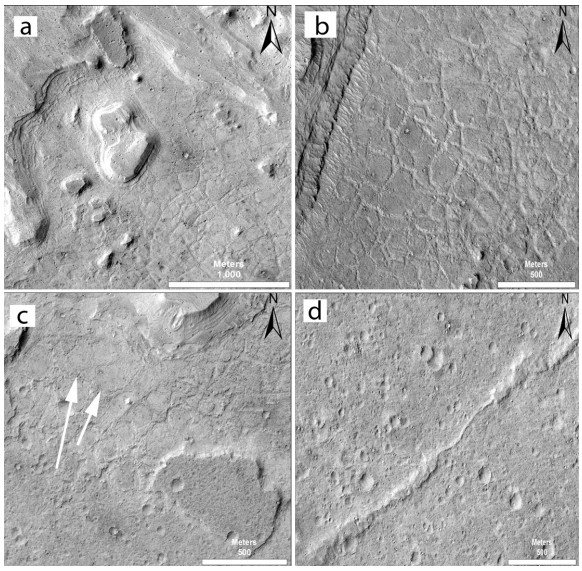

Figure 2: Close-up HiRISE views of (a) the layered sediments, (b) polygonally fractured floor of the moat surrounding the eroded margin of the sedimentary body, (c) the *miniature* "honeycomb" terrain (arrows), and (d) the NE-trending topographic ridge.

References

[1] Tanaka, K.L., et al.: USGS Scientific Inv. Map, SIM 3292, 2014; [2] Hauber, E., et al.: Planet. Space Sci., 57, 944-957, 2009; [3] Hauber, E., et al.: JGR, 118, 1529–1544, 2013; [4] Platz, T., et al.: EPSC Abstracts, 9, EPSC2014-811, 2014; [5] Hauber, E., et al.: EPSC Abstracts Vol. 10, EPSC2015-862, 2015; [6] Kneissl, T., et al.: Planet. Space Sci., 59, 1243–1254, 2011. [7] Michael, G. & Neukum, G.: Earth Planet. Sci. Lett., 294, 223–229, 2010. [8] Bernhardt, H., et al.: JGR, 121,714–738, 2016. [9] Brož, P. & Hauber, E.: JGR, 118, 1656-167, 2013.

EPSC Abstracts
Vol. 11, EPSC2017-703-2, 2017
European Planetary Science Congress 2017

Origin of Bright Dust Devil Track on Mars

K.Hamada (1), S. Nishizawa (2) and **K.Kurita** (1)
(1) ERI,Univ. of Tokyo,Japan USA, (2) Riken Advanced Institute for Computational Science, Japan

Abstract

Bright Dust Devil Tracks(BDDT) on Mars are an enigmatic surface signature on Mars. Although several mechanisms have been proposed why the bright albedo is formed there still exist inconsistent observed features and they are still enigmatic. The biggest enigma would be coexistence of BrightDDT(BDDT) and DarkDDT(DDDT) in regional scale and in some cases they are cross-cutting. This requires an specific explanation for the formation of both BDDT and DDDT during the short life time(several Earth months). In this study we performed detailed investigation on DDT in two regions where BDDT are abundantly observed; in and around Schiaparelli Crater and Amazonis Planitia by using CTX images. We found 1) BDDT are confined to localized regions while DDDT are distributed broadly in these regions, 2) in 10km scale both BDDT and DDDT exhibit dominant orientations, and 3) existence of banded DDT. By using these observed signatures as constraints we propose diurnal variation of local wind system such as wind direction and speed would control the formation of BDDT and DDDT.

1. Introduction

On the martian surface dust devil tracks are globally distributed ubiquitous features and this means the dust devil activity is one of the general atmospheric activity on Mars. The activity can be traced by linear tracks on the surface. The most common type has lower albedo than the surrounding areas, thus called as dark dust devil track. The dark-looking feature is interpreted as exposure of coarse grained substrate by removal of the surface fine-grained dust during dust devil activity.
There exist, however, brighter dust devil tracks though the number is quite few. Several mechanisms for the bright albedo have been proposed such as the existence of highly reflective substrate, rearrangement of the surface grains and compaction ([1],[3],[**?**]). Particularly [5]proposed a physical mechanism of modification of the arrangement of surface grains through field surveys of terrestrial BDDT, But all these mechanisms can not fully explain the coexistence of BDDT and DDDT in the same region.In this study we performed detailed investigation on DDT in two regions where BDDT are abundantly observed.

2. Analysis

We selected two regions for the analysis of BDDT; Region A in and around Schiaparelli Crater and Amazoni Planitia. Both regions are known to have higher density of BDDT([3],[**?**]). Relatively uniform coverage of CTX/MRO in these regions with the average resolution of 5m made homogeneous survey possible. Fine structure of the DDT is analysed in HiRISE/MRO images. We constructed population density map for DDT in the bin size of 0.125°.

3. Results

Here we report selected results in Schiaparelli regions about population density for BDDT and DDDT, orientation distribution of BDDT and DDDT.

3.1. Distribution

Most of BDDT are concentrated in the south regions of the crater while DDDT are distributed homogeneously. The distribution of BDDT corresponds to the dark region in THEMIS Day IR map. This trend is clearly recognized in Figure 1. The upper figure is THEMIS Day IR map and the middle exhibits the population density of BDDT, the lower exhibits that of DDDT. The region designated as A is an island of dark region where localized distribution of BDDT can be seen clearly. This strongly suggests the formation of BDDT is controlled by the surface characteristics but the important feature is not only BDDT but also large numbers of DDDT are observed in this region. Simple exposure mechanism can not explain this coexistence.

3.2. Orientations

Figure 2 shows one of the presentative images in Region A. Both BDDT and DDDT can be seen. The most

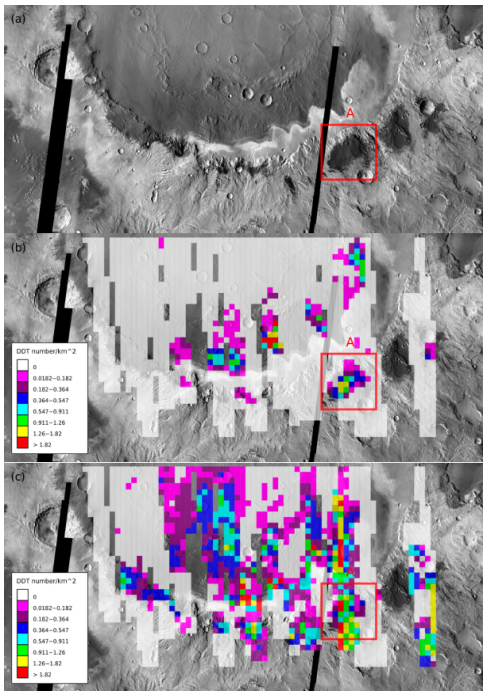

Figure 1: Distributions of BDDT(middle) and DDDT(lower).

remarkable feature is the orientation of DDT; most BDDT are aligned in NW-SE direction while DDDT are in NE-SW. This feature is particularly prominet in Region A.

Figure 3 summarizes the histogram of the orientation for BDDT and DDDT.

4. Probable Formation Mechanism for BDDT

The coexistence of BDDT and DDDT would be constraint for the formation mechanism of BDDT. Several models are proposed such as the existence of bright substrate such as ice and salts just below the surface. But the coexistence requires further explanation. The model of preferred orientation of the disturbed surface grains also requires further explanation. The key would be preferred orientations of BDDT and DDDT. This suggests difference in the formation time in the diurnal wind cycle.

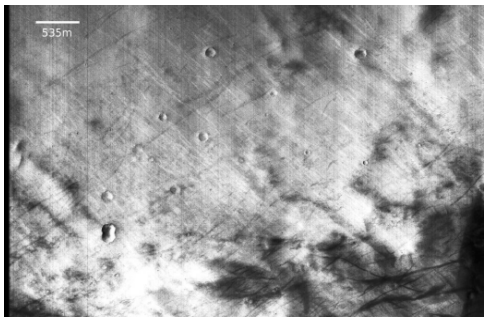

Figure 2: Coexistence of BDDT and DDDT

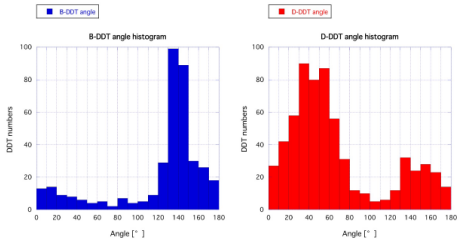

Figure 3: Orientation histograms for BDDT and DDDT in SE of Schiaparelli Crater.

References

[1] Balme,M.and Greeley,R.: Dust devils on Earth and Mars, Rev.Geophys.,44,RG3003,2006.

[2] Balme,M. et al: Field measurements of horizontal forward motion velocities of terrestrial dust devils, towards a proxy for ambient winds on Mars and Earth, Icarus 221,632-645,2012.

[3] Cantor,B.,Kanak,K., and Edgett,K.: Mars Orbiter Camera observations of Martian dust devils and their tracks and evaluation of theoretical vortex models, J.Geophys.Res.,111,E12002,2006.

[4] Fenton,L.,Toigo,A.,and Richardson,M.: Aeolian processes in Proctor Crater on Mars,J.Geophys.Res. 110,E06005,2005.

[5] Reiss,D.,Raack,H.,and Hiesinger,H.: Bright dust devil tracks on Earth, implications for their formation on Mars, Icarus 211,917-920,2011.

[6] Whelley,P. and Greeley,R.: The distribution of dust devil activity on Mars, J.Geophys.Res. 113,E07002, 2008.

EPSC Abstracts
Vol. 11, EPSC2017-848-1, 2017
European Planetary Science Congress 2017

Holuhraun 2014−2015 Eruption Site in Iceland: A Flood Lava Analogue for Mars

Joana Voigt (1), Christopher W. Hamilton (2), Stephen P. Scheidt (2), Léa E. Bonnefoy, (2), Ingibjörg Jónsdóttir (3), Ármann Höskuldsson (3), and Thorvaldur Thordarson (3)
(1) Institute of Planetary Research, German Aerospace Center (DLR), Berlin, Germany (joana.voigt@dlr.de), (2) Lunar and Planetary Laboratory, University of Arizona, Tucson, USA, (3) Faculty and Institute of Earth Sciences, University of Iceland, Reykjavík, Iceland

1. Introduction

The surface of Mars includes enormous flow fields produced by lava and/or fluvial events [e.g., 1, 2, 3]. The origin of the surface is mainly inferred from morphological and topographical observations based on high-resolution images. Therefore, flow textures (e.g., facies), and topographical relationships can be used as a key tool in reconstructing the evolution of the emplacement and provide information on physical parameter, such as viscosity and effusion rate. The Holuhraun 2014−2015 eruption, with an area of 83.5 km^2, is the largest flood lava flow in Iceland since the Laki eruption in 1783–1784 [4, 5]. Studying the products of such a large and recent eruption provides unique insights into the emplacement of flood lavas on Earth and other planetary bodies. Large effusive eruption on Earth are infrequent in the modern geologic record and therefore the 2014–2015 lava flow at Holuhraun offers an ideal study area for examining lava flow textures (i.e. facies) that are unaffected by modification processes induced by running water, aeolian sedimentation, and vegetation. We here present the first facies map of the whole Holuhraun lava flow, which we linked to the chronological emplacement history [5]. Furthermore, we present strong analogues to Martian flow fields, especially within the youngest volcanic province on Mars, Elysium Planitia [1].

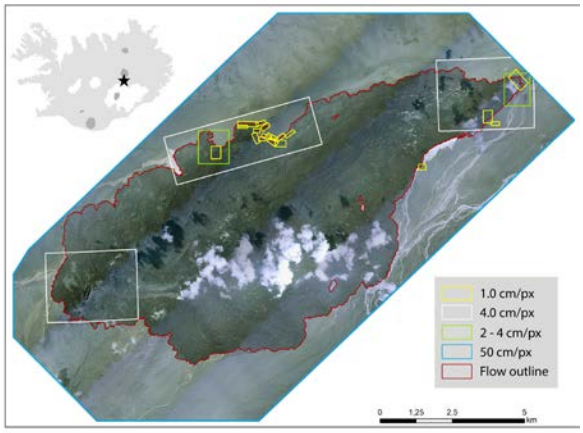

Figure 1: Location of Holuhraun eruption side on Iceland. Boxes represent used remote sensing data in respect to their resolution.

2. Data and Method

To map the facies at the Holuhraun lava flow we used an orthomosaic (50 cm/pixel) to generate a facies map of the whole lava flow field with a digitalizing scale of 1:800. Detailed analyses are based on remote sensing data obtained using Unmanned Aerial Vehicles (UAVs) at resolutions of 1–4 cm per pixel and used to generate 4–20 cm per pixel Digital Terrain Models (DTMs). In-situ field observations establish detailed descriptions of the different facies and their relationships to one and another. For a compilation of this information we generated a geospatial database in ArcGIS to compare the known eruption chronology to the different facies. Investigations in Rahway Valles and Marte Vallis on Mars were supported by the Context (CTX) camera (6 m/pixel) [6], High Resolution Imaging Science Experiment (HiRISE) camera (0.3 m/pixel) [7] and topographic constraints from the Mars Global Surveyor (MGS) Mars Orbiter Laser Altimeter (MOLA).

3. Results

The facies map of the whole Holuhraun lava flow field contains six main spatial facies, including the two endmembers of lava flow morphologies, ‘a‘ā and pāhoehoe types, as well as “transitional” morphological types—including spiny/rubbly, shelly pāhoehoe, and platy/shelly types—and vent-type material (Figure 2). Within these main facies we identify structures specific to individual lava types, such as lava channel rims, linear compressional ridges and extensional rifts, platy-ridged pattern,

spirals and inflation features including lava rise pits and wedges. Comparing our results of the main morphological units with the chronological emplacement map from Pedersen et al. (2017) [5] shows that the main facies are strongly linked to different emplacement episodes. Furthermore the facies we identify at Holuhraun are common on Martian surface. In particular, we observe that flow units in Rahway Valles and Marte Vallis regions of Mars commonly exhibit surface morphologies that closely resemble the “transitional” lava flow types observed in association with the 2014–2015 Holuhraun eruption in Iceland and we infer that they are similarly the products of large fissure-fed eruptions, rather than the products of aqueous flooding events.

4. Conclusions

Our results show that there is indeed a link between main facies and the emplacement time. Due to the fact that the chemical composition of the Holuhraun 2014−2015 event was constant over the eruption period the facies map provides a great opportunity in studying the controlling factors of the morphologies. Further work will concentrate on links to the topographic variations, effusion rate, rheology and emplacement chronology of flow units.

Acknowledgements

The authors want to thank the Faculty and Institute of Earth Sciences of the University of Iceland in providing assistance and the Vatnajökull National Park (Vatnajökulsþjóðgarður) Service for providing permission and support for the fieldwork. Joana Voigt acknowledges the Geological Society of America (GSA) for supporting the field trip with a Graduate Student Research Grand 2016 and the GSA Lipman Research Award. Christopher Hamilton acknowledges funding support from NASA PGG Grant # NNX13AQ05G and MDAP Grant # NNX13AK62G.

References

[1] Vaucher, J. et al. (2009), Icarus 204. [2] Jaeger, W. L. et al. (2010), Icarus 205. [3] Tanaka, K. et al. (2014), pamphlet 43 p. [4] Gudmundsson et al. 2016 Science. [5] Pedersen et al. 2017 (in press) Journal of Volcanology and Geothermal Research. [6] Malin, M. C. et al. (2007), J. Geophys. Res. Planets 112. [7] McEwen, A. S. et al. (2007), J. Geophys. Res. Planets 112.

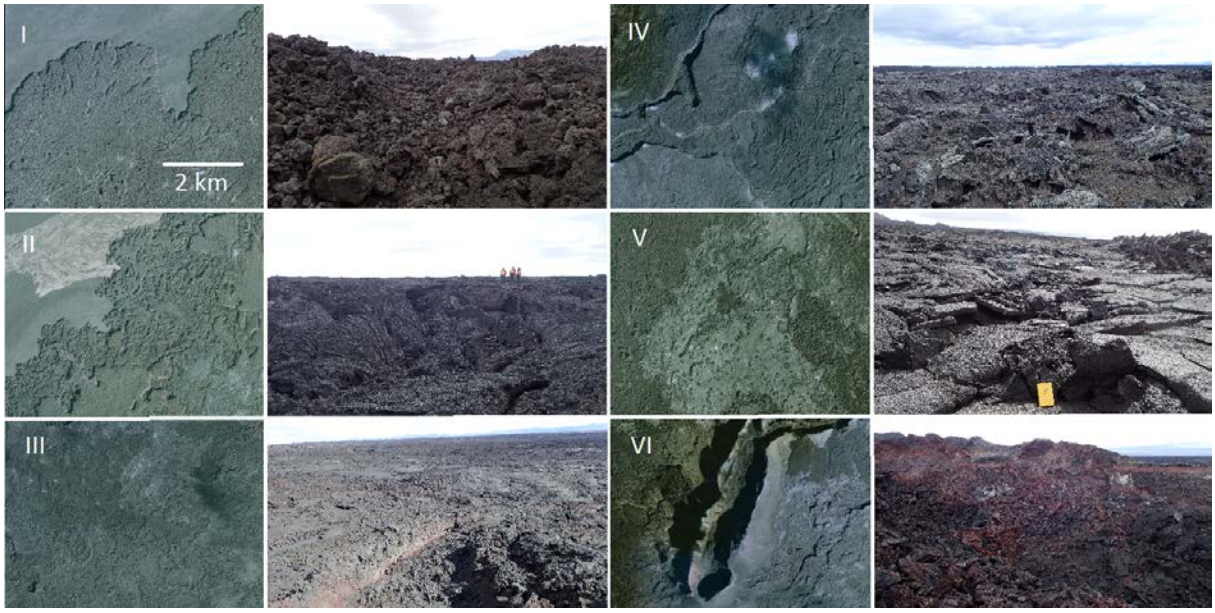

Figure 2: Overview of each facies of the Holuhraun lava flow field based on a mapping scale of 1:800. Left-hand side shows the surface structure seen by remote sensing data with 50 cm per pixel. Right-hand side are examples from the field observations of the relevant facies. I. ‘A‘ā-type, II. Spiny/Rubbly-type III. Pāhoehoe-type, IV. Shelly Pāhoehoe-type, V. Platy/Shelly-type, VI. Vent-type.

EPSC Abstracts
Vol. 11, EPSC2017-852, 2017
European Planetary Science Congress 2017

ExoMars Lander Radioscience LaRa, a Space Geodesy Experiment to Mars.

V. Dehant (1), S. Le Maistre (1), **R.M. Baland** (1), M. Yseboodt (1), M.J. Péters (1), Ö. Karatekin (1), A. Rivoldini (1), and T. Van Hoolst (1)
(1) Royal Observatory of Belgium, Brussels, Belgium (v.dehant@oma.be)

Abstract

The LaRa (Lander Radioscience) experiment is designed to obtain coherent two-way Doppler measurements from the radio link between the ExoMars lander and Earth over at least one Martian year. The instrument lifetime is larger than the one Earth year of nominal mission duration. The Doppler measurements will be used to observe the orientation and rotation of Mars in space (precession, nutations, and length-of-day variations), as well as polar motion. The ultimate objective is to obtain information / constraints on the Martian interior, and on the sublimation / condensation cycle of atmospheric CO_2.

The LaRa instrument consists of a coherent transponder with up- and downlinks at X-band radio frequencies. The signals will be generated and received by Earth-based giant antennas belonging either to the NASA deep space network (DSN), the ESA tracking network, or the Russian ground stations network.

We will describe the experiment and discuss important aspects of the radio tracking data analysis, which uses dedicated software developed for determining the variations in the ExoMars lander position relative to the Earth, as a function of time.

1. Introduction

The X-band transponder LaRa is designed to obtain two-way Doppler measurements at the instrument accuracy level of 0.05 mm/s @ 60 second integration time (0.02 mm/s @ 60 second integration time for the instrumental contribution) from the radio link between the ExoMars lander and the Earth over at least one Martian year.

These Doppler measurements will be used to obtain the orientation and rotation of Mars in space (precession and nutations, polar motion, and length-of-day variations). The ultimate objectives are to obtain information on Mars' interior and on the sublimation/condensation process of CO_2. This is possible since one will be able to obtain the moment of inertia of the whole planet that includes the mantle and the core, the moment of inertia of the core, as well as the seasonal mass transfer between the atmosphere and ice caps.

The LaRa experiment will be used jointly with the other experiments of the ESA ExoMars Payload, as well as the InSight (Interior exploration using Seismic Investigations, Geodesy, and Heat Transport) NASA mission, in order to obtain the maximum amount of information about the interior of Mars and consequently about its formation and evolution. These objectives are in compliance with the ExoMars objective "To investigate the planet's deep interior to better understand Mars's evolution and habitability".

2. The instrument

The LaRa instrument is a coherent transponder using one uplink and one downlink at X-band. There is a corresponding ground segment of the experiment since the signal is observed by the NASA Deep Space Network (DSN), Roscosmos (NPOL) Ground Stations (GS), or the ESA tracking stations (ESTRACK).

The LaRa transponder will be switched-on for receiving the uplink signal from the Earth ground station. It will re-transmit the signal coherently for one hour towards the ground station. This sequence will be repeated twice per week. The longer the mission lifetime, the best it is for reaching the LaRa objectives. The minimum guaranteed mission is one Earth year. This period will be followed by an

extended operation period as long as the available power allows it.

3. Ground segment operation

The ground operations of LaRa are crucial for the realization of the experiment. The LaRa transponder receives the signal from the Earth ground station directly and transmits it back to Earth coherently. The operation of LaRa from the lander point of view corresponds to a simple switch on-off command. The timing of this command is determined and coordinated by the ground segment. The operation of LaRa from the ground segment point of view depends mainly on the availability of the ground station, the position of Mars in the ground station sky, and on the position of the Earth in the lander sky. There are other constraints that will be detailed in the next paragraphs.

The role of the ground segment is to transmit from Earth an uplink signal to LaRa on the surface of Mars and receiving a signal back from LaRa, in X-band (see Figure 1).

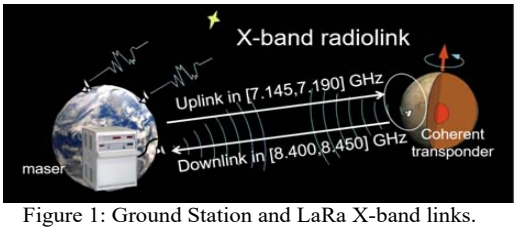

Figure 1: Ground Station and LaRa X-band links.

Knowing a priori a first high-precision approximation of the Doppler between the ground station at the emitting time and the lander at the receiving time, the ground station can emit a signal pre-compensated for this Doppler so that LaRa receives at Mars a frequency near 7.16 GHz (in [7.145, 7.190] GHz). At the ground station, a very precise uplink signal computation will be necessary for the initial sent signal so that the signal arriving at the lander is in the lock-in bandwidth of LaRa, i.e. so that the signal is "pre-compensated". This is a key feature of the ground station necessary to achieve successful acquisition lock with the LaRa receiver; this is a procedure well known by the ESTRACK and DSN ground stations.

The LaRa experiment planning consists of 2 sessions/week during the minimum guaranteed period of the mission, and 1 or 2 sessions/week during the rest of the mission. These sessions are planned according to the geometry of the Earth and Mars relative position, the position and orientation of the lander, the day/night successive situation, the solar activity, the operation of the other Surface Platform payload instruments, and the ground station availability.

4. Objectives

Rotational variations will allow us to constrain the moment of inertia of the entire planet, including its mantle and core, the moment of inertia of the core, and seasonal mass transfer between the atmosphere and the ice caps. The LaRa experiment will be combined with other ExoMars experiments, in order to retrieve a maximum amount of information on the interior of Mars. Specifically, combining LaRa Doppler measurements with similar data from the Viking landers, Mars Pathfinder, Mars Exploration Rovers landers, and the forthcoming InSight-RISE lander missions, will allow us to improve our knowledge on the interior of Mars with unprecedented accuracy, hereby providing crucial information on the formation and evolution of the red planet.

Acknowledgements

This work is financially supported by the Belgian PRODEX program managed by the European Space Agency in collaboration with the Belgian Federal Science Policy Office.

EPSC Abstracts
Vol. 11, EPSC2017-937-2, 2017
European Planetary Science Congress 2017

Coregistration of Mars South Polar CTX Images to HRSC Base Images

A. R. D. Putri, P. Sidiropoulos, J-P. Muller
Imaging Group, Mullard Space Science Laboratory (MSSL), University College London, Department of Space & Climate Physics, Holmbury St Mary, Dorking, Surrey, RH5 6NT, United Kingdom
(alfiah.putri.15@ucl.ac.uk)

1. Introduction

Large number of changes have been observed on the south polar region of Mars, as well as in the north polar region and globally, signing that even though pretty static, Mars surface is dynamic. Especially in the south polar region, changes such as seasonal and interannual changes have been observed, with the growth and recession of ice caps and features such as so-called "spiders" and "swiss-cheese terrains". There is a need of quantitative research on these changes, which is difficult to be done manually because of the increase of the number and size of image data available and the currently non-uniform reference between Mars image datasets.

2. HRSC Base Images

We have produced 33 single-strip HRSC DTMs over the south pole [1] to fill the gaps between MOLA DTMs with higher resolution images such as CTX, MOC-NA, and HiRISE. The HRSC DTMs with resolution of 50 m/pixel with mean average difference of 1.08 m to MOLA South Polar MEGDR and 2.20 (up to 0.04 m) to MOLA PEDR, and until half after correction. The full resolution DTMs are produced using a NASA-VICAR-based pipeline developed by DLR (German Aerospace Centre), with Kim and Muller [2] modified method in image matching based on (Gruen-Otto-Chau) algorithm [3]. The setup has also been modified for the polar region. Orthorectified (ORI) images have been produced to be used in further research, including change detection research and as base images for coregistration.

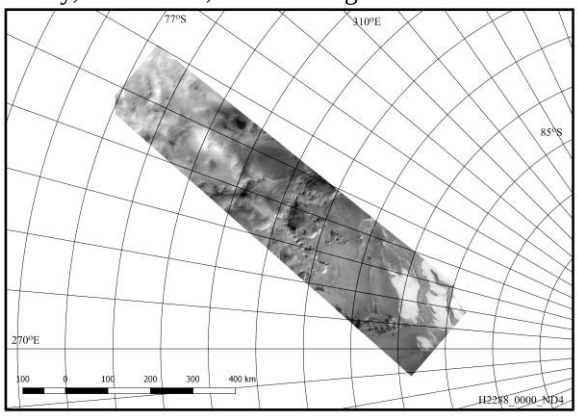

Figure 1: HRSC ORI H2288 0000 (25-10-2005, MY27, Ls 312.46) produced

3. Coregistration of CTX Images

As previously over the south pole the images are coregistered to MOLA baseline, coregistered dataset of Mars south polar high-resolution images are currently unavailable. As the information obtained for SPICE kernels as NASA-supplied areoreference information is unsatisfactory to produce coregistered dataset, autocoregistration and orthorectification (ACRO) programme has previously been developed to fulfill this objective.

The previously developed ACRO programme mentioned has been successfully coregistered highresolution images from CTX, MOC-NA, THEMIS VIS, and Viking to MC11 Quadrangle and to Mars global dataset by utilizing DLR-produced HRSC ORI images. For this research the programme is modified to receive the HRSC base images input and to produce the result in polar stereographic projection.

4. Result

The example of the coregistration result can be seen in Figure 2. We could see that CTX images with 2 MY difference could be orthorectified to HRSC orthorectified images. Further results and their statistics in regards of the south pole and comparison to global Mars coregistration will be presented during the congress.

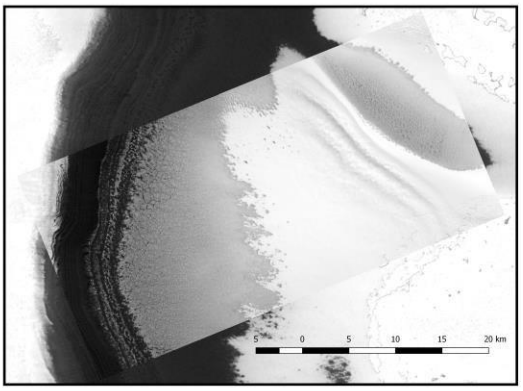

Figure 2: Example of result, back: level-4 HRSC ORI H2288 0000 (25-10-2005, MY27, Ls 312.46), front: B11 013813 0955 XN 84S078W (07-07-2009, MY29, Ls 299.19)

5. Summary and Conclusions

In this paper we have been able to present the work regarding coregistration on Mars South Polar images. We have successfully applied the pipeline previously used to MC11 and to Mars global images to Mars South Polar images. Currently ongoing work is being done to coregistered more than 5000 CTX images in polar stereographic projection to HRSC orthorectified base images. Coregistration of other South Polar high-resolution images will follow.

Acknowledgements

Part of the research leading to these results has received partial funding from the European Union's Seventh Framework Programme (FP7/2007-2013) under iMars grant agreement n˚ 607379; MSSL STFC Consolidated grant no. ST/K000977/1 and the first author is supported by the Indonesian Endowment Fund for Education.

References

[1] A. R. D. Putri, P. Sidiropoulos, and J.P-Muller. A New South Polar Digital Terrain Model of Mars from the High Resolution Stereo Camera (HRSC) onboard of the ESA Mars Express for tracking changes over the SPRC. Icarus, under review, 2017.

[2] J.R. Kim and J.-P. Muller. Multi-resolution topographic data extraction from Martian stereo imagery. Planetary and Space Science, 57(14-15):2095 2112, 2009.

[3] D. Shin and J.-P. Muller. Progressively weighted aadaptive correlation matching for quasi-dense 3d reconstruction. Pattern Recognition, 45(10):3795{3809, 2012.

[4] P. Sidiropoulos and J.-P. Muller. A systematic solution to multi-instrument co-registration of high-resolution planetary images to an orthorectied baseline. IEEE Transactions on Geoscience and Remote Sensing, under review, 2017.